

AN INVESTIGATION OF BEAM SCANNING OF ARRAYS ON
CYLINDRICAL, CONICAL AND SPHERICAL SURFACES

A THESIS SUBMITTED TO
THE GRADUATE SCHOOL OF NATURAL AND APPLIED SCIENCES
OF
MIDDLE EAST TECHNICAL UNIVERSITY

BY

YÜCEL TAKAK

IN PARTIAL FULFILLMENT OF THE REQUIREMENTS
FOR
THE DEGREE OF MASTER OF SCIENCE
IN
ELECTRICAL AND ELECTRONICS ENGINEERING

APRIL 2015

Approval of the thesis:

**AN INVESTIGATION OF BEAM SCANNING OF ARRAYS ON
CYLINDRICAL, CONICAL AND SPHERICAL SURFACES**

submitted by **YÜCEL TAKAK** in partial fulfillment of the requirements for the degree of **Master of Science in Electrical and Electronics Engineering Department, Middle East Technical University** by,

Prof. Dr. Gülbin Dural Ünver
Dean, Graduate School of **Natural and Applied Sciences** _____

Prof. Dr. Gönül Turhan Sayan
Head of Department, **Electrical and Electronics Engineering** _____

Prof. Dr. Özlem Aydın Çivi
Supervisor, **Electrical and Electronics Engineering Dept., METU** _____

Examining Committee Members:

Prof. Dr. Gülbin Dural Ünver
Electrical and Electronics Engineering Dept., METU _____

Prof. Dr. Özlem Aydın Çivi
Electrical and Electronics Engineering Dept., METU _____

Prof. Dr. Sencer Koç
Electrical and Electronics Engineering Dept., METU _____

Assoc. Prof. Dr. Lale Alatan
Electrical and Electronics Engineering Dept., METU _____

Assoc. Prof. Dr. Vakur B. Ertürk
Electrical and Electronics Engineering Dept., Bilkent Uni. _____

Date: 28/04/2015

I hereby declare that all information in this document has been obtained and presented in accordance with academic rules and ethical conduct. I also declare that, as required by these rules and conduct, I have fully cited and referenced all material and results that are not original to this work.

Name, Last name : Yücel TAKAK

Signature :

ABSTRACT

AN INVESTIGATION OF BEAM SCANNING OF ARRAYS ON CYLINDRICAL, CONICAL AND SPHERICAL SURFACES

Takak, Yücel

M.S., Department of Electrical and Electronics Engineering

Supervisor: Prof. Dr. Özlem Aydın Çivi

April 2015, 133 pages

Recently, wide angle scanning antennas are often required especially in many radar applications. It is known that planar arrays have limited scan range without beam deformation. In this study design and production steps for wide angle scanning antenna arrays conformed on cylindrical, conical and spherical surfaces that operate at X-Band are investigated. Antenna elements used in these conformal arrays are designed using full wave electromagnetic solver tool HFSS. A MATLAB code for obtaining array patterns in principal planes using active element pattern is developed and it is verified by comparing the results with the ones obtained by HFSS for arrays with small number of elements. Fabricated antenna elements are produced and their conformability on desired surfaces is investigated. Non-planar surfaces where antenna located are produced using 3D printer. Designed antennas are conformed on the produced surfaces and their radiation patterns are measured for some scan angles. Obtained radiation patterns are in good agreement with simulation results.

Keywords: Wide Angle Scanning, Conical Array, Cylindrical Array, Spherical Array

ÖZ

SİLİNDİRİK, KONİK VE KÜRESEL YÜZEYLER ÜZERİNE YERLEŞTİRİLMİŞ ANTEN DİZİLERİNDE HUZME TARAMASI ÜZERİNE BİR İNCELEME

Takak, Yücel

Yüksek Lisans, Elektrik ve Elektronik Mühendisliği Bölümü

Tez Yöneticisi: Prof. Dr. Özlem Aydın Çivi

Nisan 2015, 133 sayfa

Son zamanlarda, özellikle radar uygulamalarında, geniş açılara tarama yapabilen antenler önem kazanmıştır. Düzlemsel anten dizilerinde belirli bir açıdan sonra yönlendirilen huzmenin bozulmaya başladığı bilinmektedir. Bu çalışmada X-Bandda çalışan, silindirik, konik ve küresel yüzeyler üzerine kaplanmış, geniş açı taramalı anten dizilerine yönelik tasarım ve üretim çalışmaları sunulmaktadır. Anten dizilerinde kullanılan elemanlar HFSS yazılımı kullanılarak tasarlanmıştır. Aktif eleman örüntüsü kullanılarak anten dizisinin örüntüsünü hesaplayan bir yazılım MATLAB ortamında geliştirilmiştir. Bu programın doğruluğu kısıtlı sayıda eleman içeren anten dizilerinin HFSS benzetimleri ile karşılaştırılarak gösterilmiştir. Tasarlanan anten dizileri üretilmiş ve geometrilere uygunlukları incelenmiştir. Antenlerin kaplanacağı düzlemsel olmayan yüzeyler üç boyutlu yazıcı kullanılarak üretilmiş ve anten dizilerinin bu yüzeyler üzerine kaplanabilirliği incelenmiştir. Tasarlanan anten örüntüleri ölçülmüş ve sonuçların benzetim sonuçları ile uyumlu olduğu görülmüştür.

Anahtar Kelimeler: Geniş Açı Tarama, Silindirik Anten Dizileri, Konik Anten Dizileri, Küresel Anten Dizileri.

To my family

ACKNOWLEDGEMENTS

I sincerely thank my supervisor Prof. Dr. Özlem Aydın Çivi for all her guidance and support throughout my study. I would like to thank to Dr. Can Barış Top and Akın Dalkılıç for their guidance. I also thank to Arda Özgen and Uğur Kaya for their help in production of non-planar surfaces. I sincerely thank Ömer Öçal and Murat Sertkaya for their help during production of antenna elements. I would like to thank ASELSAN Inc. for financing and providing resources during my study.

TABLE OF CONTENTS

ABSTRACT	V
ÖZ.....	VI
ACKNOWLEDGEMENTS.....	VIII
TABLE OF CONTENTS.....	IX
LIST OF TABLES	XI
CHAPTERS	
1 INTRODUCTION.....	1
2 DESIGN OF X-BAND PROBE FED PATCH ANTENNA AND APERTURE COUPLED PATCH ANTENNA	9
2.1 DESIGN OF PROBE FED PATCH ANTENNA	10
2.2 DESIGN OF APERTURE COUPLED PATCH ANTENNA.....	15
3 ARRAY RADIATION PATTERN CALCULATION BY ACTIVE ELEMENT PATTERN.....	21
3.1 ARRAY RADIATION PATTERN CALCULATION FOR LINEAR ANTENNA ARRAYS	21
3.2 RADIATION PATTERN CALCULATION OF ARRAYS ON NON-PLANAR SURFACES	29
3.2.1 Radiation Pattern Calculation without Phase Correction.....	31
3.2.2 Radiation Pattern Calculation with Phase Correction.....	33
4 ANTENNA ARRAYS ON CYLINDRICAL SURFACE.....	35
4.1 FABRICATION OF CYLINDRICAL ANTENNA BASE	35
4.2 APERTURE COUPLED PATCH ANTENNA ARRAY	36
4.2.1 Fabrication of Aperture Coupled Patch Antenna Array.....	37

4.2.2 Simulation Results for Aperture Coupled Patch Antenna.....	38
4.3 PROBE-FED PATCH ANTENNA ARRAY	41
4.3.1 Fabrication of Probe-Fed Patch Antenna Array	41
4.3.2 Simulation and Measurement Results for Probe-Fed Patch Antenna Array	44
5 ANTENNA ARRAYS ON CONICAL SURFACE.....	57
5.1 FABRICATION OF CONICAL ANTENNA ARRAY	57
5.2 SIMULATION AND MEASUREMENT RESULTS.....	59
6 ANTENNA ARRAYS ON SPHERICAL SURFACE	69
6.1 FABRICATION OF SPHERICAL ANTENNA ARRAY	69
6.2 SIMULATION AND MEASUREMENT RESULTS.....	71
7 CONCLUSIONS.....	83
REFERENCES	85
APPENDICES	
A. MODELLING CONFORMAL ANTENNA ARRAYS USING HFSS.....	89

LIST OF TABLES

TABLES

Table 2-1 RO5880 properties.....	10
Table 2-2 Coaxial fed patch antenna parameters	11
Table 2-3 Aperture coupled patch antenna dimensions	16
Table 4-1 Electrical properties of ABSPlus P430.....	36
Table 4-2 Coordinates, rotation angles and phase values for $5\lambda_0$ cylinder	47
Table 4-3 Measured and ideal phase values exported from HFSS	50
Table 4-4 Beam properties on cylinder for 0° scan	51
Table 4-5 Beam properties on cylinder for 15° scan	52
Table 4-6 Beam properties on cylinder for -15° scan	53
Table 5-1 Coordinates, rotation angles and phase values for conical array.....	61
Table 5-2 Measured and ideal phase values exported from HFSS	62
Table 5-3 Beam properties on cone for 0° scan on $\theta=50^\circ$ plane	63
Table 5-4 Beam properties on cone for 15° scan on $\theta=50^\circ$ plane	64
Table 5-5 Beam properties on cone for -15° scan on $\theta=50^\circ$ plane.....	65
Table 6-1 Coordinates, rotation angles and calculated phase values for spherical array.....	72
Table 6-2 Measured and ideal phase values exported from HFSS for spherical array	75
Table 6-3 Beam properties on sphere for 0° scan on $\phi=0^\circ$ plane	76
Table 6-4 Beam properties on sphere for 0° scan on $\phi=90^\circ$ plane	77
Table 6-5 Beam properties on sphere for 15° scan on $\phi=90^\circ$ plane	78
Table 6-6 Beam properties on sphere for 15° scan on $\phi=0^\circ$ plane	79

LIST OF FIGURES

FIGURES

Figure 1-1 Geometrical shapes for wide angle scanning	2
Figure 1-2 Pyramid and pyramid frustum [3]	2
Figure 1-3 Two different element placement geometries [4].....	3
Figure 1-4 Faceted and smoothly curved cylindrical antenna arrays [5]	4
Figure 1-5 Circumferential and meridian spherical array	5
Figure 1-6 Faceted hemispherical dome [7].....	6
Figure 2-1 Coaxial fed patch antenna [11].....	10
Figure 2-2 HFSS model for probe fed patch antenna.....	12
Figure 2-3 Antenna element on a cylinder of $5 \lambda_0$ radius.....	12
Figure 2-4 S_{11} for different radius values.....	13
Figure 2-5 H-Plane radiation pattern of the antenna on $\varnothing=90^\circ$ plane	14
Figure 2-6 E-Plane radiation pattern of the antenna on $\varnothing=0^\circ$ plane	14
Figure 2-7 Aperture coupled patch antenna geometry [14]	15
Figure 2-8 HFSS model for aperture coupled patch antenna	17
Figure 2-9 Impedance variation with stub length between 9.3-9.7GHz	17
Figure 2-10: Impedance variation with slot length between 9.3-9.7GHz	18
Figure 2-11 H-Plane radiation pattern of aperture coupled patch antenna on $\varnothing=90^\circ$ plane.....	19
Figure 2-12 E-Plane radiation pattern of aperture coupled patch antenna on $\varnothing=0^\circ$ plane.....	19
Figure 3-1 Geometry of a linear array.....	21
Figure 3-2 HFSS model for 5x1 planar antenna array	23
Figure 3-3 Pattern from HFSS and calculated pattern from active element patterns	24

Figure 3-4 Measurement setup for 5x1 linear antenna array	24
Figure 3-5 Measured active element patterns on $\phi = 90^\circ$ plane	25
Figure 3-6 H-Plane radiation pattern for 5x1 linear array on $\phi = 90^\circ$ plane	25
Figure 3-7 H-Plane active element pattern for the center element for 5x1 planar array	28
Figure 3-8 H-Plane radiation patterns for 5x1 array with $0.475\lambda_0$ element spacing.	29
Figure 3-9 A cylindrical antenna array with phase center common for all elements	32
Figure 3-10 A cylindrical antenna array with phase center on the face.....	33
Figure 3-11 Coordinate systems for conical, cylindrical and spherical surfaces	34
Figure 4-1 Fabricated cylindrical antenna geometry using 3D printer	36
Figure 4-2 Aperture coupled patch antenna ground layer and aperture.....	37
Figure 4-3 Produced aperture coupled patch antenna array.....	37
Figure 4-4 Cylindrical antenna array switch schematic.....	39
Figure 4-5 13x1 antenna array with different scan angles	41
Figure 4-6 Probe fed patch antenna	42
Figure 4-7 Active S_{11} values for 5 elements on cylinder with $5\lambda_0$ curvature.....	43
Figure 4-8 Produced cylindrical antenna	43
Figure 4-9 HFSS model for 5 element probe fed antenna array	44
Figure 4-10 Radiation pattern measurement setup for probe-fed cylindrical antenna array.....	45
Figure 4-11 Measured ϕ (H-Plane) and θ (E-Plane) polarized active element patterns	46
Figure 4-12 Measured S matrix phase values	48
Figure 4-13 Measured S matrix amplitude values	49
Figure 4-14 H-Plane array radiation pattern directed to 0° on cylinder.....	51
Figure 4-15 H-Plane array radiation pattern directed to 15° on cylinder.....	52
Figure 4-16 H-Plane array radiation pattern directed to -15° on cylinder	53
Figure 4-17 E-Plane radiation pattern of cylindrical array on $\phi=0^\circ$	54

Figure 4-18 H-Plane radiation patterns for 5x1 antenna array with 12° separation..	55
Figure 5-1 Produced conical antenna	58
Figure 5-2 S_{11} for conical array	58
Figure 5-3 Conical antenna array switching schematic.....	59
Figure 5-4 HFSS model for faceted conical array.....	59
Figure 5-5 Conical antenna array measurement setup	60
Figure 5-6 Measured active element radiation patterns on cone.....	61
Figure 5-7 E-Plane array radiation pattern directed to 0° on cone on $\theta=50^\circ$ plane ..	63
Figure 5-8 E-Plane array radiation pattern directed to 15° on cone on $\theta=50^\circ$ plane	64
Figure 5-9 E-Plane array radiation pattern directed to -15° on cone on $\theta=50^\circ$ plane	65
Figure 5-10 Mutual coupling between antenna elements on cone	66
Figure 6-1 Element placement for spherical array block	70
Figure 6-2 Produced spherical antenna array	70
Figure 6-3 Active S_{11} values for spherical antenna elements.....	71
Figure 6-4 HFSS model and measurement setup for spherical antenna.....	73
Figure 6-5 Measured active element patterns on $\phi=90^\circ$ (a) and $\phi=0^\circ$ (b) plane	73
Figure 6-6 E-Plane array radiation pattern directed to 0° on sphere $\phi=0^\circ$ plane.....	76
Figure 6-7 H-Plane array radiation pattern directed to 0° on sphere $\phi=90^\circ$ plane ...	77
Figure 6-8 H-Plane array radiation pattern directed to 15° on sphere $\phi=90^\circ$ plane .	78
Figure 6-9 E-Plane array radiation pattern directed to 15° on $\phi=0^\circ$ plane	79
Figure 6-10 19 elements spherical array	80
Figure 6-11 H-Plane radiation pattern for 19 element array conformed on sphere ..	81
Figure 6-12 E-Plane radiation pattern for 19 element array conformed on sphere...	81

CHAPTER 1

INTRODUCTION

Recently, especially in radar applications, it is crucial to steer antenna beam in various directions without deformation in beam shape. Planar phased array antennas are widely used for electronic scanning applications. Due to antenna element characteristics and geometry of planar surface, it is not possible to scan wide angles with planar antenna arrays [1]. To overcome these problems, several methods have been proposed. One method is mechanically rotating planar array to desired direction. In most of the applications, beam is steered mechanically in one plane e.g. azimuth plane (or elevation plane), whereas in the orthogonal plane electronic beam steering is preferred. Although this solution seems very attractive, it has some disadvantages. Mechanical systems are bulky and slow. Also maintenance in short intervals is required, which increases cost of the system. In mechanical steering, due to inertia of the antenna, response of the system is slower compared to electronic steering. Therefore, it is necessary to develop electronically scanning antenna arrays that can scan wide angles. Another method to obtain wide angle scanning is using faceted antenna structures [2]. A faceted antenna is the combination of planar antennas to simulate the surface of the nonplanar antenna. Depending on the number of planar antennas, maximum scan angle of each antenna may vary for full hemispherical or azimuthal coverage. In Figure 1-1, some examples of possible faceted antenna structures and maximum scan angle for each face to cover 360° in azimuth are given.

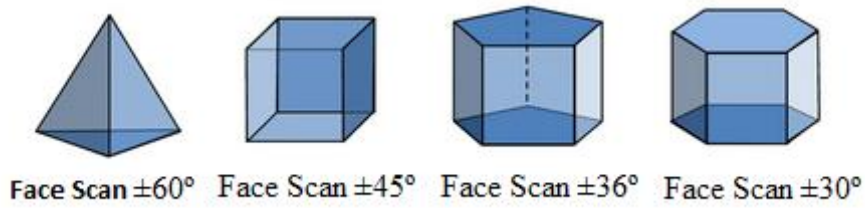


Figure 1-1 Geometrical shapes for wide angle scanning

Increasing the number of faces on a multifaceted structure reduces maximum scan angle required by each planar array surface. It is well known that antenna directivity is proportional to the antenna size. Therefore, keeping antenna diameter constant and increasing face number, reduces directivity of each sub array on the antenna. In literature there are several research papers available about optimizing the number of faces of a multi face antenna. In [3], optimization of faceted pyramid and pyramid frusta are studied in detail. Pyramid and pyramid frusta arrays are shown in Figure 1-2. [3] mainly covers optimizing maximum scan angle, reducing the number of elements on each planar sub array and optimizing cone angle. It is shown that pyramid frustum with total 6-7 faces has the optimal array geometry for hemispherical scan coverage.

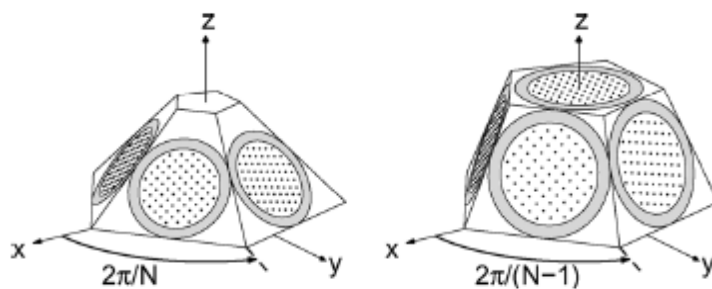


Figure 1-2 Pyramid and pyramid frustum [3]

Similarly in [3], it is shown that in a faceted pyramid, increasing number of faces above 6 have only small effect on maximum scan angle and scan loss. It is also mentioned in [3] that pyramid of 4 faces provides maximum directivity with an acceptable scan loss. Another geometric structure which is similar to a pyramid is a conical surface. A conical antenna can fit on a nosecone of an aircraft without extra covering. There are lots of research papers on conical conformal antennas and their optimization. Reduction of grating lobes, achieving narrower beams and reducing antenna diameter are the main concerns of interest. In [4], detailed study about conical antenna arrays has been presented. Basically two array topologies have been proposed. In the first approach, element separation on each row is constant. This means moving from base of the cone to the apex, the number of elements decreases. In the second approach, the number of elements in each row is constant. This means that moving from base of the cone to the apex, element separation decreases. To increase the number of rows on a conical surface, it is necessary to place bottom elements with a larger spacing by also taking into account grating lobes. To place an equal number of elements, it is necessary to reduce element number on the large diameter region. Both configurations are shown in Figure 1-3.

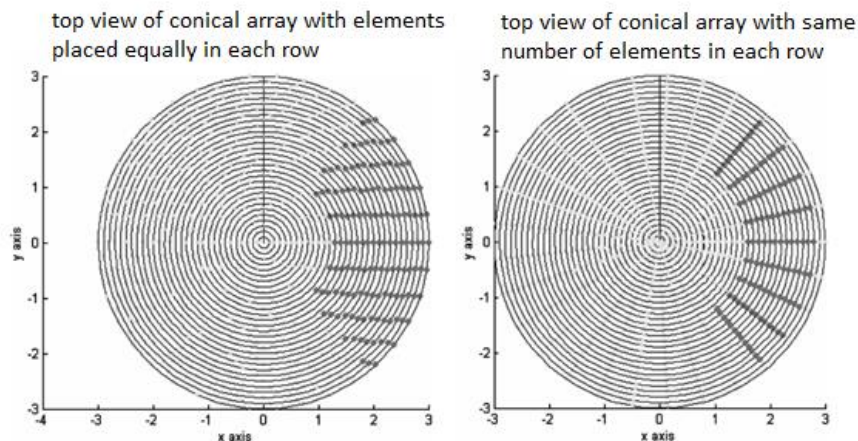


Figure 1-3 Two different element placement geometries [4].

Another important point focused in [4] is unpredictable grating lobe locations. It will not be sufficient to analyse radiation patterns in principle planes only. Due to geometry of cone, grating lobe in radiation pattern can occur somewhere in 3D space which is not visible in the principle planes. In this thesis only single row of conical antenna array is studied. So these concerns should be considered in future studies.

Cylindrical surface is another important geometry widely studied and used in conformal antenna applications. This geometry is simpler compared to cone due to its symmetrical surface. Cylindrical antennas can be modelled as faceted or smoothly curved. In [5], two different antennas are produced using faceted antenna modelling. In Figure 1-4 antennas fabricated in [5] are given.

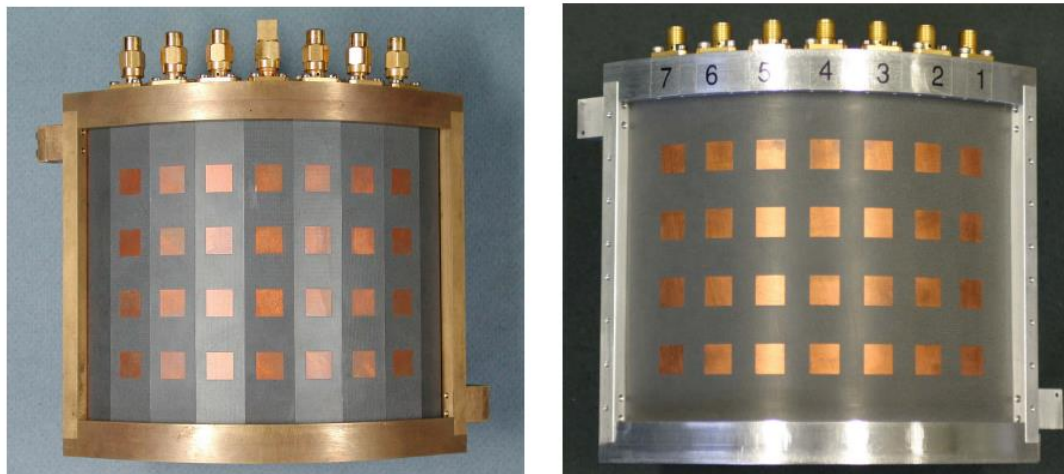


Figure 1-4 Faceted and smoothly curved cylindrical antenna arrays [5]

These two antennas are designed to operate at 9.4GHz. It is shown that there is almost no difference in the performance of both antennas up to 9.5 GHz. This information is important for this study because antenna arrays are modelled as faceted geometries in simulation programs. But face angle is very small compared with the one mentioned in [5]. In this thesis cylindrical and conical antennas are divided into 180 small segments. This means two faces are separated by 2° .

Another array structure investigated for its beam steering property is spherical antenna array. There are different element placement and beam steering topologies available for spherical arrays. If antenna elements are intended to be placed individually, there are two possible configurations as described in [6]. One is circumferential spherical array and other is meridian spherical array. These two configurations are shown in Figure 1-5.

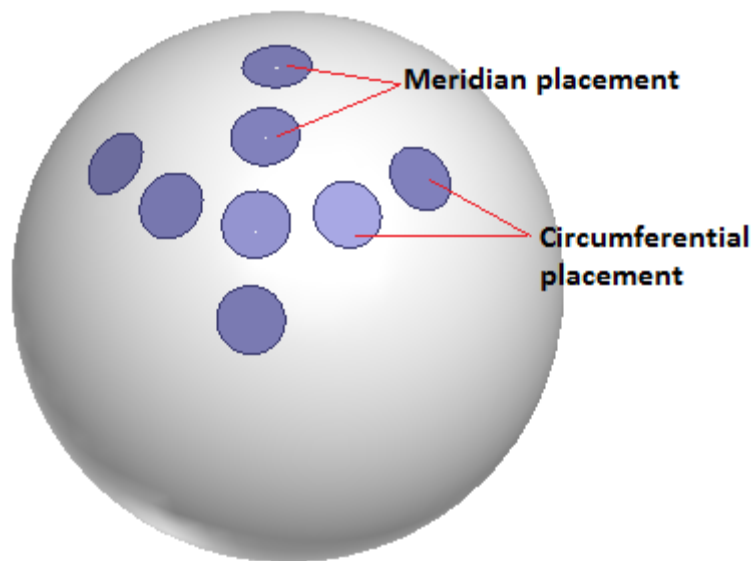


Figure 1-5 Circumferential and meridian spherical array

Additionally, some spherical surfaces are covered with planar antenna arrays to approximate surface of sphere geometrically. An example is an array consisting of triangular planar sub arrays. In these antennas each planar sub block can steer the beam up to a certain limit. Then for wide angle scanning, corresponding sub array is switched. It is also possible to combine 6 triangular blocks and obtain a hexagonal structure. In Figure 1-6 triangular faceted spherical dome is shown. In this study, spherical surface is covered with hexagonal non-planar blocks.

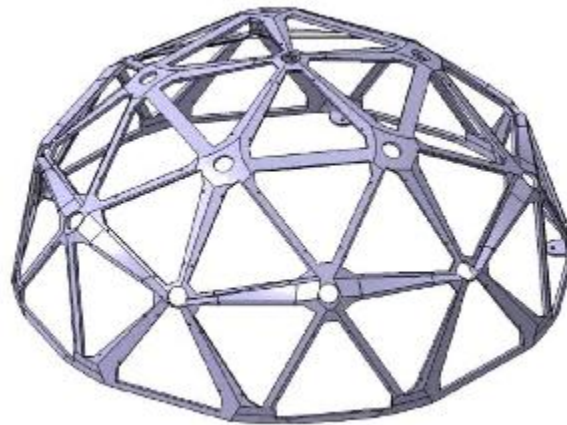


Figure 1-6 Faceted hemispherical dome [7]

Antennas that cover the surface of a cylinder, cone or sphere are also named as conformal antenna arrays [8]. This type of antenna has advantages mentioned before compared with planar antennas. First of all, as they cover shape of non-planar surface they cause no extra aerodynamic load. Especially in air platforms this is an important advantage. Moreover, as they wrap surface of the platforms they are installed on, no extra space is required for placement. This is a great advantage for platforms containing large number of antennas.

The purpose of this thesis is to investigate electronically scanning arrays of microstrip patches on cylindrical, spherical and conical surfaces for applications that require wide angle scanning. For these geometries beam scanning is possible by a single switched beam that directs in desired angle or multiple beams directed to different angles. Single beam is synthesized by exciting a sub array on the sphere. In this case, element phase and amplitudes on the sub array are not uniform. For the multiple beams case, two or more sub arrays are excited at the same time using two or more feed networks. In the following chapters, steering of a single beam for wide angle scan is investigated.

In chapter 2, design of aperture coupled microstrip patch antenna and probe fed microstrip patch antenna are presented. The effect of curvature on the antenna radiation characteristics is also discussed.

In chapter 3, calculation of radiation patterns of arrays by using active element patterns is given. Antenna radiation pattern calculation using S matrix of the array is discussed. The concepts of active element pattern and array factor calculation for non-planar arrays are presented for cylindrical, conical and spherical geometries. Concept of phase center is introduced. Effect of phase center in the array pattern calculation is discussed.

In chapter 4, first fabrication steps for cylindrical antenna array are presented. Problems encountered during fabrication process are discussed. Then simulation and measurement results of the designed antennas are compared. Array radiation patterns obtained using developed MATLAB [9] code based on active element pattern, HFSS [10] simulations and measurements are compared for some scan angles.

In chapter 5 steps in chapter 4 are repeated for conical antenna array and in chapter 6 same steps are repeated for spherical antenna array.

Chapter 7 includes concluding remarks, some possible improvements and future work.

Guidelines for modelling conformal antenna structures in HFSS is prepared and given in the Appendix of this thesis.

CHAPTER 2

DESIGN OF X-BAND PROBE FED PATCH ANTENNA AND APERTURE COUPLED PATCH ANTENNA

Conformal arrays consisting of probe fed microstrip patch antennas and aperture coupled patch antennas are investigated in the frame of this thesis study. Therefore, as a first step these antennas operating at X-Band at 9.5 GHz are designed. Since the scope of this study is to investigate beam scanning properties of non-planar antenna arrays, bandwidth and polarization of the elements are not considered in detail. The design process for the antenna elements is started with selection of the dielectric substrate. Rogers Duroid 5880 is used as dielectric substrate for the designed antennas. In Table 2-1 parameters for RO5880 are given. RO5880 is a low loss PTFE material frequently used in antenna applications. It is a relatively flexible substrate that can be conformed on non-planar surfaces. RO5880 plates can easily cut and shaped. Proto Laser PL200 machine is used to fabricate the antennas. It is also resistant to chemical processes so fabrication by chemical processes such as lithography is also possible. But it requires more time and work so that laser process is selected to fabricate designed antennas.

Table 2-1 RO5880 properties

Property	Frequency	Value
Dielectric Constant	10 GHz	2.2±0.02
Dissipation Factor	10 GHz	0.0009
Permeability	10 GHz	1
Copper Cladding	-	35μm

In the following sections, design and simulations of the probe fed and aperture coupled patch antennas are presented.

2.1 Design of Probe Fed Patch Antenna

First antenna type designed for this thesis is a probe fed patch antenna. Geometry of a simple probe fed patch antenna is given in Figure 2-1. It is easier to design and produce a probe fed patch antenna compared to an aperture coupled patch antenna. On the other hand, this antenna has higher cross polarization ratio relative to the centered slot aperture coupled patch due to non-symmetric feed position.

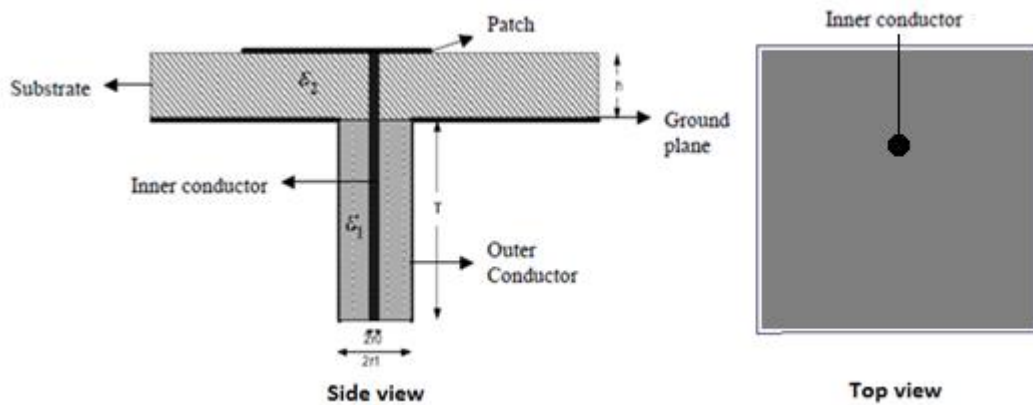


Figure 2-1 Coaxial fed patch antenna [11]

In a probe fed patch antenna, design variables are patch length, patch width and feed offset. Patch length affects the operation frequency of the antenna, while patch width and feed offset affect resonant resistance of the antenna. A commercially available coaxial cable is used as coaxial probe. Used cable has 0.5mm inner conductor diameter and 1.5mm outer conductor diameter. Dielectric substrate of coaxial cable is Teflon based PFTE. Dimensions of designed antenna are given in Table 2-2. For beam steering purposes all the elements on the array need to be excited separately. It is easier to feed antennas on curved surfaces with a probe compared to feeding by a microstrip transmission line. Design of the antenna is realized using HFSS. Antenna ground plate dimensions are reduced to 13.5mm in both directions in order to have a flexibility to increase the number of elements on curved geometry.

Table 2-2 Coaxial fed patch antenna parameters

Parameter	Value
Coaxial cable operation frequency	Up to 18 GHz
Coaxial probe inner conductor diameter	0.5mm
Coaxial probe dielectric layer diameter	1.5mm
Coaxial dielectric constant	2.08
Dielectric Substrate	RO5880
Dielectric thickness	0.508mm
Patch width	10.05mm
Patch length	10.05mm
Feed offset	1.5mm

Planar antenna modeled in HFSS for dimensions given in Table 2-2 is given in Figure 2-2.

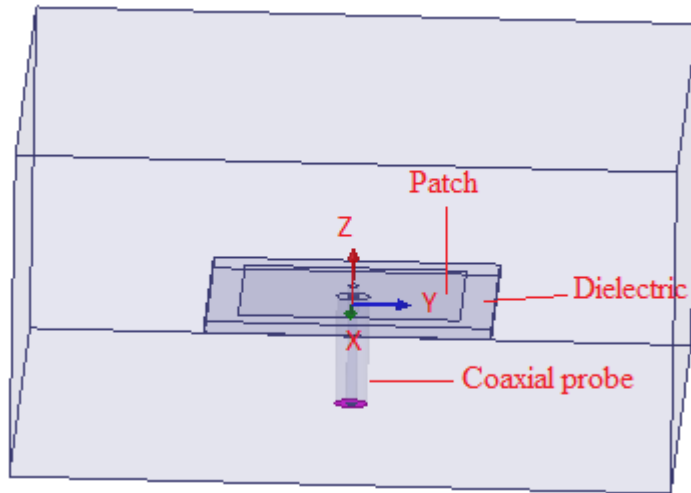


Figure 2-2 HFSS model for probe fed patch antenna

Designed patch antenna is conformed on a curved surface. The effect of curvature on radiation pattern and S_{11} are investigated by modeling various curved antennas on HFSS. For this purpose probe fed patch antennas are modeled on cylinders of radius $2.5 \lambda_0$, $3 \lambda_0$, $4 \lambda_0$ and $5 \lambda_0$. Where λ_0 is the free space wavelength at 9.5 GHz. Side view of an antenna on a cylinder of $5 \lambda_0$ radius in HFSS is given in Figure 2-3. Details of the modeling of this antenna by HFSS are given in Appendix A.

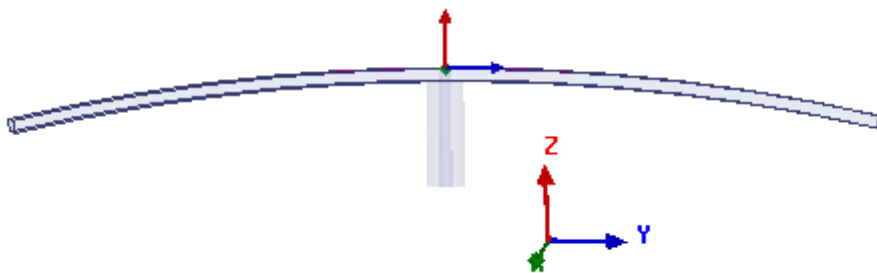


Figure 2-3 Antenna element on a cylinder of $5 \lambda_0$ radius

S_{11} values of antennas on cylinders with different radius are given in Figure 2-4.

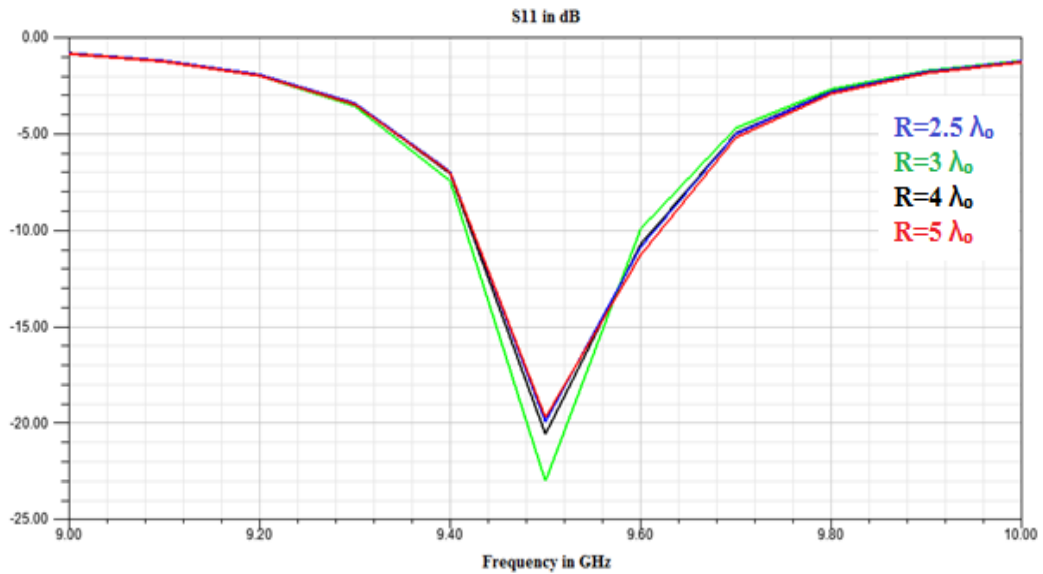


Figure 2-4 S_{11} for different radius values

It is observed from Figure 2-4 that, S_{11} does not change significantly with the radius of curvature. Radiation patterns of these antennas are plotted in Figure 2-5 and Figure 2-6. It is obvious that radiation pattern also does not change considerably with radius. It is known that S_{11} and radiation pattern of antenna on curved surface changes slightly when the radius of curvature is larger than $2\lambda_0$. Deformation in these properties become considerable when radius of curvature is below $2\lambda_0$ [12]. Since the main objective of this study is to investigate arrays, cylinders of such a small radius have not been considered.

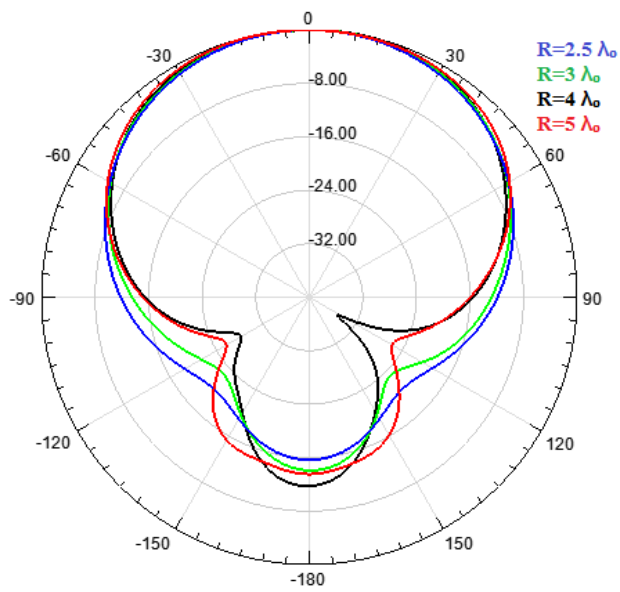


Figure 2-5 H-Plane radiation pattern of the antenna on $\theta=90^\circ$ plane

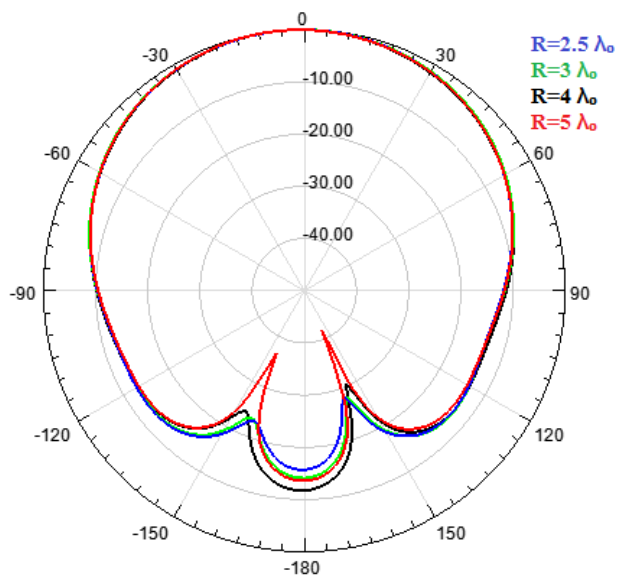


Figure 2-6 E-Plane radiation pattern of the antenna on $\theta=0^\circ$ plane

From simulation results in both planes, it can be concluded that there is more deformation on the radiation pattern in bending plane which is H plane. Expectedly, radiation pattern has less deformation in E plane. These results are similar with the ones obtained for proximity coupled patch antenna in [13].

2.2 Design of Aperture Coupled Patch Antenna

Second antenna designed in this study is an aperture coupled patch antenna. Geometrical structure of this antenna is given in Figure 2-7. A simple aperture coupled patch antenna consists of the following five layers:

1. Feed Layer
2. Feed Dielectric Layer
3. Ground Layer
4. Patch Dielectric Layer
5. Patch Layer

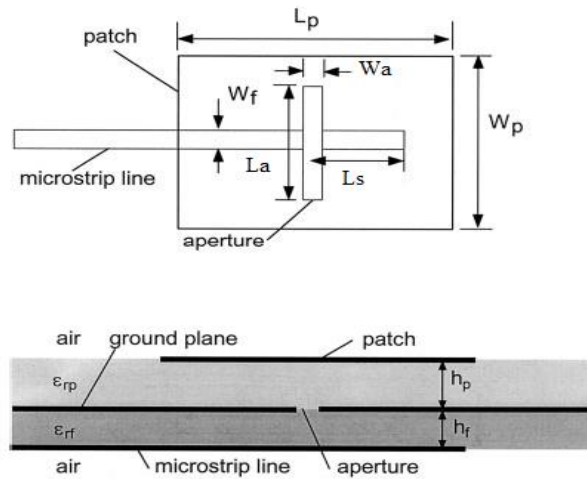


Figure 2-7 Aperture coupled patch antenna geometry [14]

Aperture coupled patch antenna has two dielectric layers separated with a common ground plane. The feed of this antenna is an open ended microstrip line located on the bottom of feed dielectric layer. Under feed line there is a dielectric layer with dielectric constant 2.5. This is the dielectric constant of the material that this patch antenna will cover. Patch antenna is located on the top of patch dielectric layer. The feed line and the patch are electromagnetically coupled through an electrically small aperture placed on ground plane. Dimensions of the designed antenna are given in Table 2-3.

Table 2-3 Aperture coupled patch antenna dimensions

Parameter	Value
Patch Length, L_p	8mm
Patch Width, W_p	7.5mm
Patch Dielectric Thickness, h_p	0.508mm
Feed Dielectric Thickness, h_f	0.254mm
Feed/Patch Diel. Constant, $\epsilon_{rp}/\epsilon_{rf}$	2.2
Feed Width, W_f	0.75mm
Stub Length, L_s	0.9mm
Aperture Length, L_a	5.05 mm
Aperture Width, W_a	0.7mm

Length of the antenna is first selected as a half of the free space wavelength at 9.5 GHz as an initial design step. Patch width is selected equal to patch length. Slot length is selected half of the patch width and slot width is selected $1/10^{\text{th}}$ of the slot length. Feed line width is calculated using feed dielectric thickness. The characteristic impedance of the feed line should be 50 Ω . For 0.128mm dielectric thickness, the feed width is calculated as 0.75mm. HFSS model for the designed

antenna is given in Figure 2-8. After these initial settings using optimetrics option of the HFSS, optimum values given in Table 2-3 are obtained.

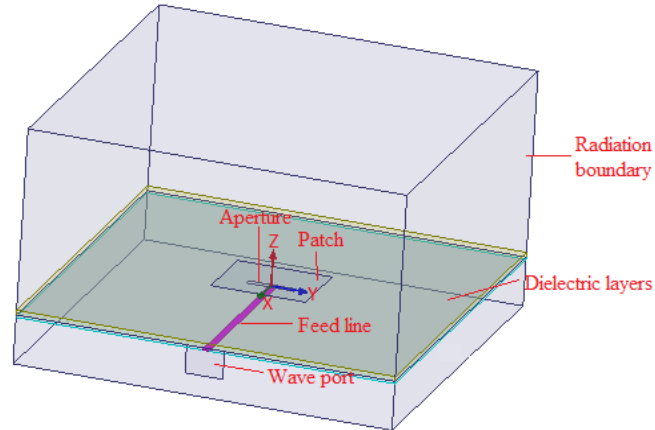


Figure 2-8 HFSS model for aperture coupled patch antenna

For the aperture coupled patch antenna, effects of the aperture length and the stub length have been investigated in detail to give insight for future works on similar topics. From Figure 2-9 it is obvious that increasing the stub length L_s decreases input impedance of the antenna. On Smith chart input impedance line moves from open circuit point to short circuit point.

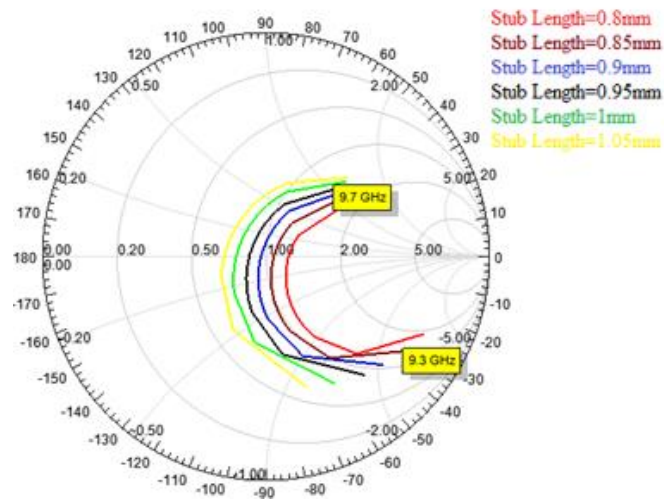


Figure 2-9 Impedance variation with stub length between 9.3-9.7GHz

In Figure 2-10, impedance variation of aperture coupled patch antenna with slot length is given. It is observed that as the slot length increases input impedance line moves on a constant resistance circle on Smith chart from capacitive region to inductive region. Simulations are performed from 9.3-9.7GHz band.

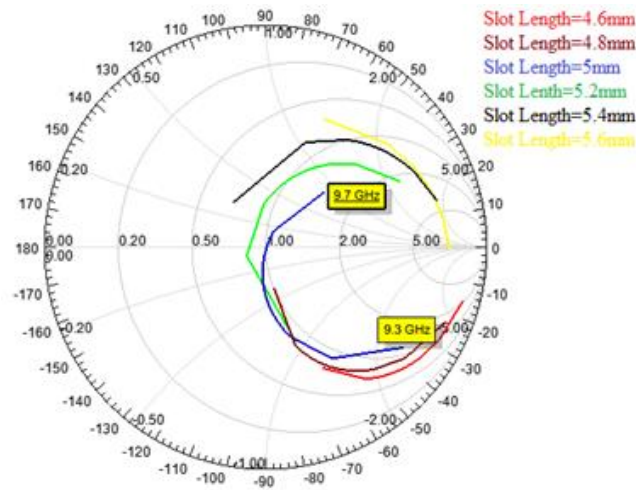


Figure 2-10: Impedance variation with slot length between 9.3-9.7GHz

As observed from Figure 2-9 and Figure 2-10, stub length and slot length provide flexibility to match antenna input impedance. Effects of these parameters were investigated in [15] analytically and similar graphical results were obtained. Simulated and measured patterns for this antenna in two principal planes are plotted in Figure 2-11 and Figure 2-12. Measurements are carried out in SATIMO [16] spherical near field antenna measurement system. A good agreement is observed between measurement and simulation results.

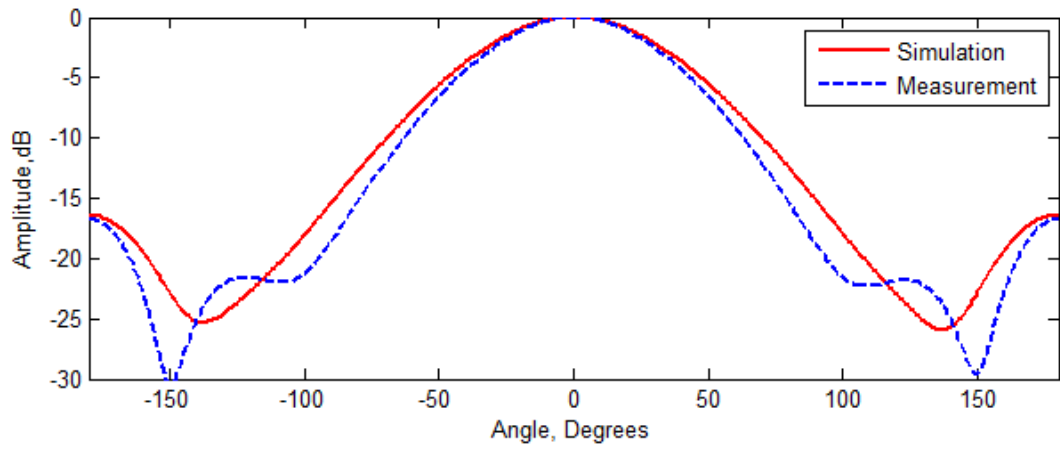


Figure 2-11 H-Plane radiation pattern of aperture coupled patch antenna on $\Theta=90^\circ$ plane

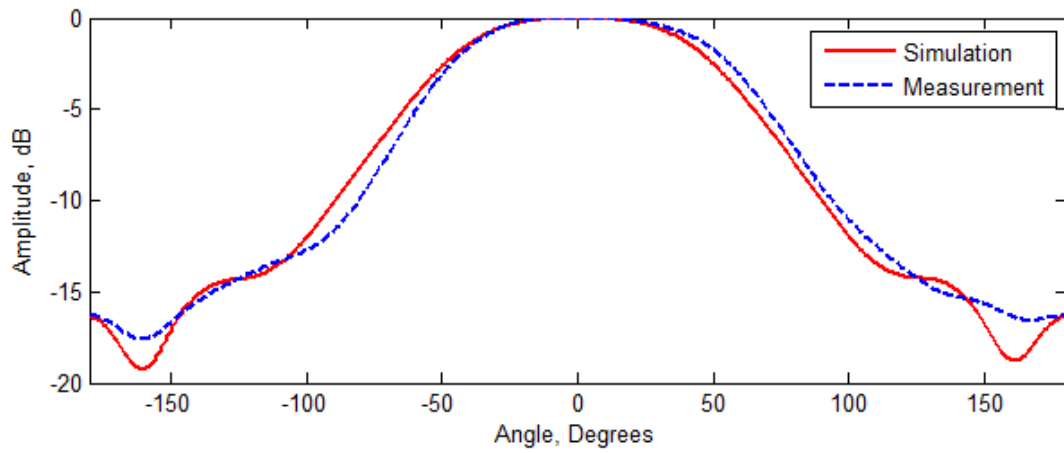


Figure 2-12 E-Plane radiation pattern of aperture coupled patch antenna on $\Theta=0^\circ$ plane

In addition to parameters studied in this chapter, aperture coupled patch antenna has more than a dozen material and dimensional parameters. Behaviour of electrical properties of the antenna with variation in these parameters are described in detail in [17]. Dielectric constant of the substrate beneath patch affects the bandwidth. Lower dielectric constant increases bandwidth of the antenna. Although increase in the thickness of the dielectric increases bandwidth of the antenna, it decreases radiation efficiency of the antenna. Patch length determines radiation frequency of the antenna, the smaller the patch antenna, the higher the resonant frequency. Patch width of the antenna determines resonant resistance of the antenna. Wider antennas have lower input resistance. Aperture length and width of the antenna determine coupling level of the antenna. Longer and wider aperture increases back radiation from the antenna.

CHAPTER 3

ARRAY RADIATION PATTERN CALCULATION BY ACTIVE ELEMENT PATTERN

An antenna array is an arrangement of two or more antenna elements to obtain required radiation characteristic. It is used to increase directivity, minimize interferences from undesired directions and steer antenna beam to desired direction. In this chapter initially array radiation pattern calculation methods for linear antenna arrays are described then array radiation pattern calculation methods for non-planar antenna arrays are given.

3.1 Array Radiation Pattern Calculation for Linear Antenna Arrays

In linear antenna arrays radiated beam can be directed to a specified direction by controlling the excitation phase of the antenna elements. As seen from Figure 3-1 to direct the main beam to an angle θ measured from array axis, a progressive phase shift of amount $k d \cos \theta$ should be applied to array elements.

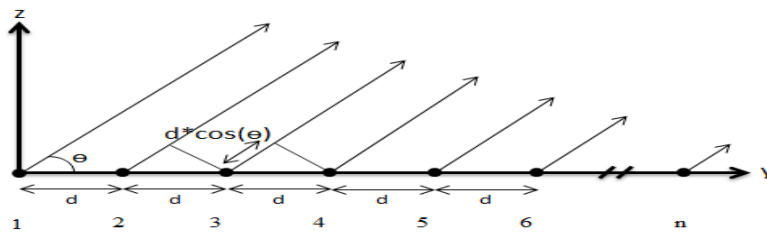


Figure 3-1 Geometry of a linear array

For the antenna array given in Figure 3-1, array factor AF is calculated using formula given in (3-1).

$$AF = \sum_{n=1}^N e^{j(n-1)(kd \cos \theta + \beta)} \quad (3-1)$$

Here d is the distance between elements, β is the required phase value to steer beam in desired direction θ . For calculation of array radiation pattern AP, array factor is multiplied by isolated element pattern EP.

$$AP = AF \times EP \quad (3-2)$$

Formulation given in (3-2) assumes that all elements in the array have radiation patterns identical to the isolated antenna element. However in reality this is not the case. When an antenna element is placed in an array environment its characteristic changes due to mutual coupling from surrounding elements [18]. If coupling level between antenna elements is high, difference between array pattern calculated using (3-2) and real pattern increases. To obtain an array pattern in a fast and accurate way, active element pattern method can be used. Active element pattern is a combination of element's own pattern together with effects of radiation from surrounding elements. Active element pattern of an antenna element is measured in array environment. To obtain an active element pattern, corresponding element in the array is excited and other elements in the array are terminated in matched loads [18]. Active element pattern in an array depends on the position of the element. The center element in an antenna array sees a different environment than the edge element. If antenna array is infinitely large then active element patterns are identical for each element. In infinitely large antenna arrays, equation (3-2) can be used

effectively by substituting active element pattern instead of isolated element pattern. For small antenna arrays, array pattern can be calculated most efficiently by taking into account all active element patterns.

$$E(\theta, \phi) = \sum_{n=1}^N a_n E_n^{act}(\theta, \phi) \quad (3-3)$$

In (3-3) a_n is complex excitation coefficient for the n^{th} antenna element, E_n^{act} is the active element pattern for the n^{th} element and $E(\theta, \phi)$ is the overall array pattern. Similarly, excitation coefficients required to obtain desired beam shape can be investigated using active element patterns. Actually simulation program HFSS used in this study also uses active element pattern method to compute array pattern. An antenna array consists of 5x1 probe-fed patch antenna with dimensions given in Table 2-2 is designed in HFSS. Antenna elements are placed $0.6329 \lambda_0$ (20mm) apart. Where λ_0 is the free space wavelength at 9.5 GHz. The HFSS model for the designed antenna is given in Figure 3-2.

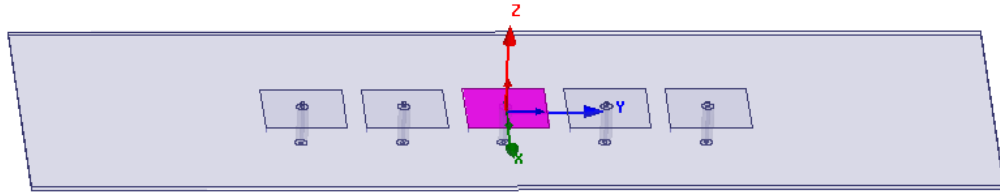


Figure 3-2 HFSS model for 5x1 planar antenna array

Active element pattern of each element is exported from HFSS. These patterns are substituted in equation (3-3) and array pattern directed to 0° on $\phi=90^\circ$ plane is computed. In Figure 3-3 array pattern from HFSS and calculated pattern using active element patterns from HFSS are given on the same graph. These two patterns are perfectly matched.

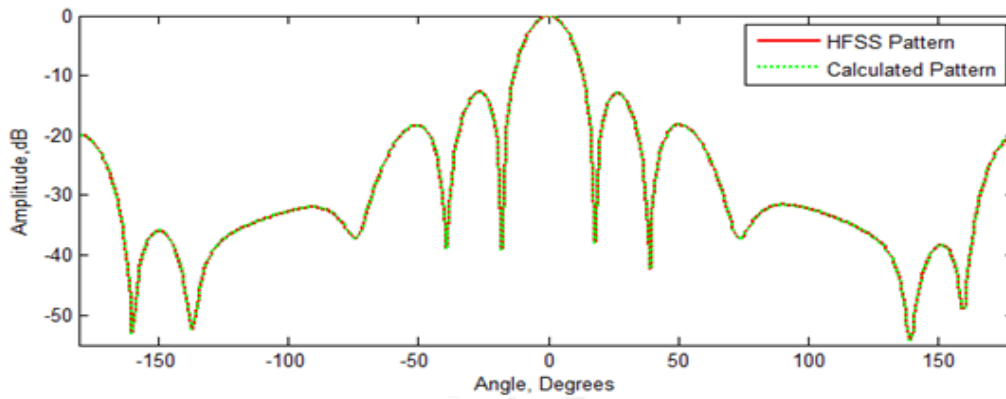


Figure 3-3 Pattern from HFSS and calculated pattern from active element patterns

Simulated antenna array is produced and measured to verify the method described. Measurement is carried out in SATIMO spherical near field measurement system. Produced antenna array is fed with a commercially available 8-way power divider using equal length cables. Five ports of this power divider are used and other three ports are terminated in matched loads. Active element pattern measurement setup is shown in Figure 3-4.

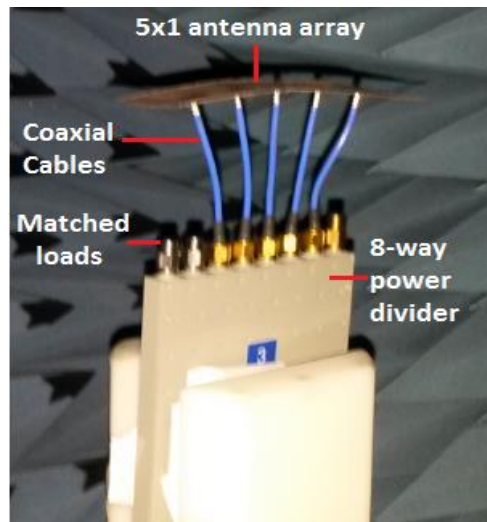


Figure 3-4 Measurement setup for 5x1 linear antenna array

Measured patterns are given in Figure 3-5. From these patterns a beam directed to 0° is synthesised.

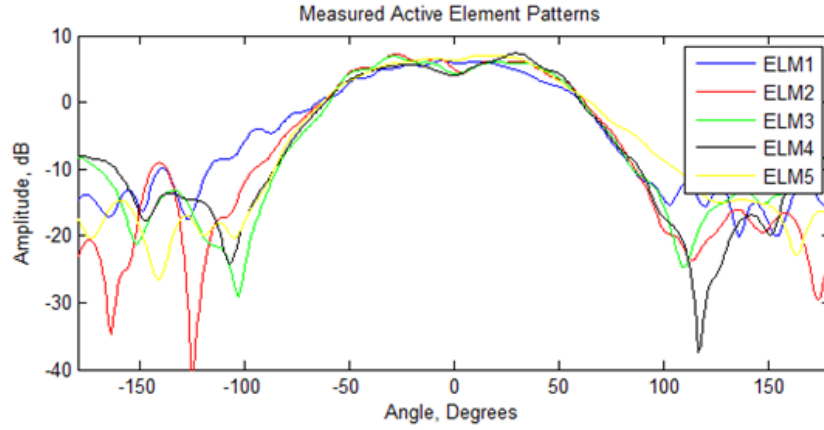


Figure 3-5 Measured active element patterns on $\phi = 90^\circ$ plane

In Figure 3-6 array pattern synthesised from measured active element patterns, array pattern exported from HFSS and measured array pattern from measurement setup are plotted on the same graph.

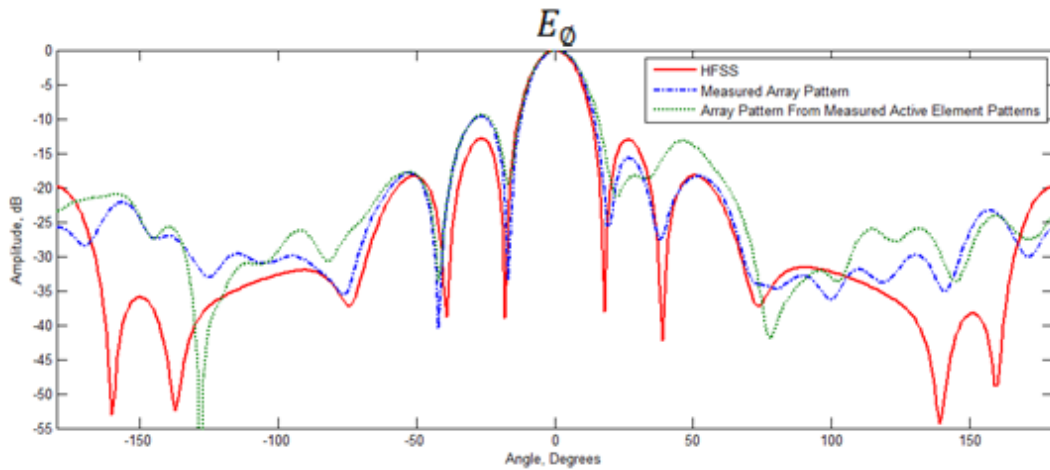


Figure 3-6 H-Plane radiation pattern for 5x1 linear array on $\phi = 90^\circ$ plane

It is obvious from Figure 3-6 that all three patterns coincide on main beam. Differences between measured and simulated patterns are due to production and measurement tolerances. Also it can be observed that measured array pattern and array pattern calculated from active element patterns are almost same even at far angles from the boresight. Slight difference between these two patterns is due to switching elements while measuring active element patterns. In this thesis active element pattern measurement is carried out by connecting excitation probe to active element and terminating other elements in matched loads. During this step cable and antenna orientations may change slightly and this can lead difference in array patterns. If an RF switch which can switch excitation probe could have been used, this difference would be minimized.

It is also possible to obtain an approximate antenna active element pattern in a small antenna array using isolated element pattern. For this purpose two different methods are described in [19]. First method is using Fourier decomposition of measured antenna active element pattern. To realize this method complex voltage patterns $g_m(u)$ of the antenna elements should be measured in the array environment.

$$g_m(u) = f^i(u) \sum_n c_{mn} e^{jkn dsin(u)} \quad (3-4)$$

In (3-4) $f^i(u)$ is isolated element pattern, u is observation angle and c_{mn} are the Fourier coefficients of the patterns. The coefficients can be calculated using equation (3-5).

$$c_{mn} = \frac{1}{2\pi} \int_{-\frac{\pi}{kd}}^{\frac{\pi}{kd}} \frac{g_m(u)}{f^i(u)} e^{-jkn du} du \quad (3-5)$$

In order to use equation (3-5) $f^i(u)$ must not have a null in the integration interval. But since the beam width of an isolated element pattern is usually very large this

would not be a problem. Using Fourier coefficients it is possible to compensate effect of mutual coupling by exciting array elements with the obtained coefficients.

Second method for antenna active element calculation is using array S (scattering) matrix. Radiation pattern of an antenna element in an array can be obtained using formulation given in (3-6).

$$E_m = a_m f^i(u) \frac{e^{-jkr_0}}{r_0} \sum_n (\delta_{nm} + s_{nm}) e^{jnkdu} \quad (3-6)$$

In this equation E_m is the element pattern of element m in an array environment. r_0 is far field observation point, a_m is the excitation coefficient of element m, s_{nm} is S parameter between n^{th} and m^{th} element in the array. Kronecker delta δ_{nm} is 1 if $n=m$ and 0 else. Using this formulation active element patterns of all elements in an array can be calculated by using S matrix of the antenna array.

In Figure 3-7 isolated element pattern of an probe fed patch antenna with dimensions given in Table 2-2, active element pattern of the same antenna located in 5x1 antenna array as given in Figure 3-2 and active element pattern of the antenna element in the same array calculated using equation (3-6) are given. From these plots it can be concluded that an approximate active element pattern can be obtained using S matrix of the antenna array.

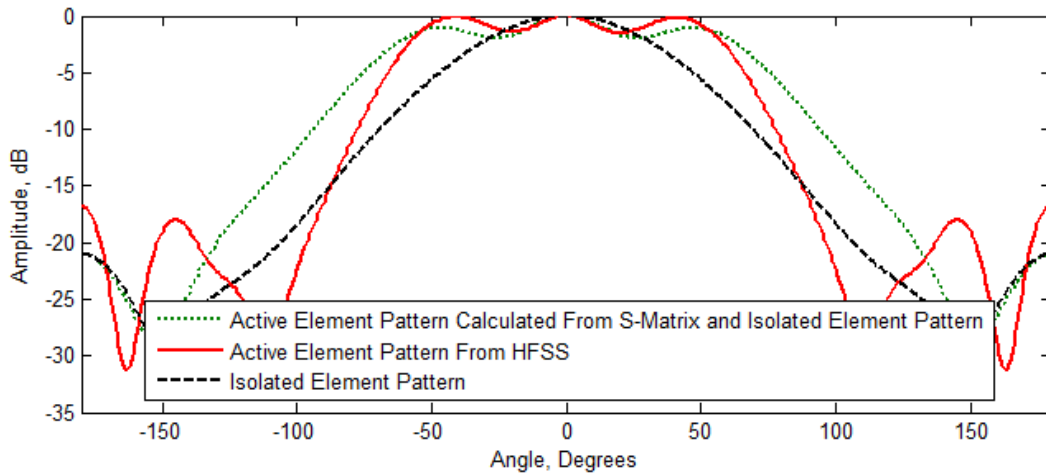


Figure 3-7 H-Plane active element pattern for the center element for 5x1 planar array

In [20] a similar method for compensation of mutual coupling using array S matrix is studied. In this study a matching network is inserted between the feed network and the antenna ports of the antenna array. The matching network parameters are calculated using S matrix of the antenna array. In this way it is possible to eliminate effect of mutual coupling on array radiation pattern.

In this thesis to investigate the effect of mutual coupling, distance between array elements is reduced down to $0.475\lambda_0$ (15mm). Then array element patterns of each element on the array are calculated using (3-4) and these patterns are substituted in (3-3) and array pattern is obtained. In Figure 3-8 radiation patterns for the 5x1 array using S-parameter method, using equation (3-2) with isolated element pattern, using equation (3-2) with active element pattern of the center element and pattern obtained from HFSS are given.

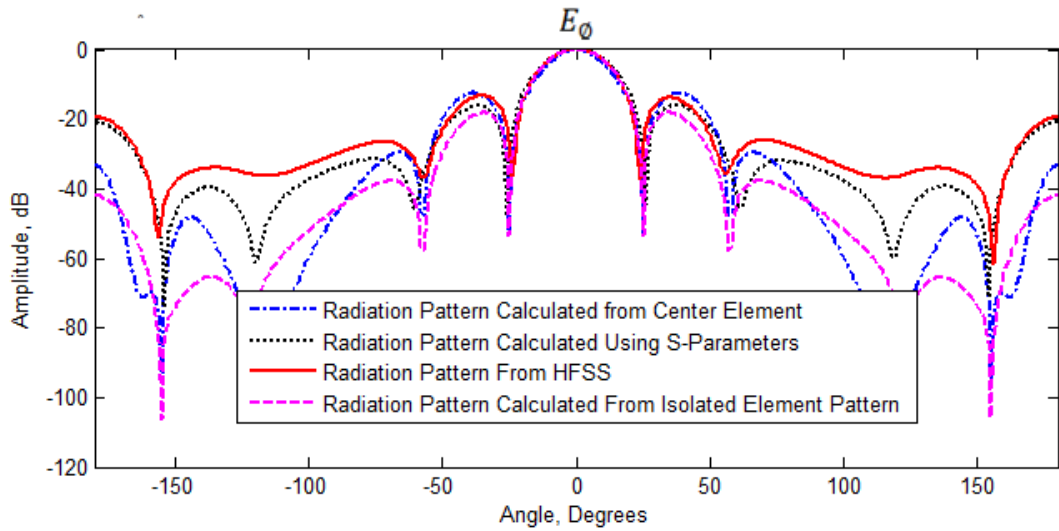


Figure 3-8 H-Plane radiation patterns for 5x1 array with $0.475\lambda_0$ element spacing

From Figure 3-8 it is observed that using S-parameter method a radiation pattern close to HFSS pattern can be obtained. As the spacing between elements decreases mutual coupling increases and pattern obtained using isolated element pattern and center active element pattern become more different than real array pattern.

3.2 Radiation Pattern Calculation of Arrays on Non-Planar Surfaces

In previous part of this chapter array radiation pattern calculation for linear antenna arrays has been introduced. In this part, pattern calculation for non-planar antenna arrays is presented. For non-planar surfaces formulation given in equation (3-2) is not valid, because each element on the antenna array points to a different direction. This makes calculation of array pattern harder. In [21] array pattern calculation for

non-planar geometries has been investigated and formulation given in equation (3-7) is used for pattern calculation.

$$AP = \sum_{n=1}^N e(\phi - \phi_n, \theta - \theta_n) w_n e^{jk(x_n(u-u_s)+y_n(v-v_s)+z_n(\cos\theta-\cos\theta_s))} \quad (3-7)$$

Where,

$$u = \sin\theta \cos\phi$$

$$u_s = \sin\theta_s \cos\phi_s$$

$$v = \sin\theta \sin\phi$$

$$v_s = \sin\theta_s \sin\phi_s$$

$$\theta_s = \text{elevation steering angle}$$

$$\phi_s = \text{azimuth steering angle}$$

$$w_n = \text{complex excitation coefficient for element } n$$

In equation (3-7), $e(\theta, \phi)$ is isolated element pattern. Element pattern in the array factor depends on the position of the element on the antenna array. Formulation given above is used to calculate array pattern for cylindrical, conical and spherical antennas. Keeping amplitude coefficient constant for all the elements on the antenna array, it is possible to synthesize antenna radiation pattern by only modifying the excitation phases of the antenna elements [22]. Unlike planar arrays, conformal antenna array elements are distributed on three dimensional surfaces. Each element has coordinates (x_n, y_n, z_n) . Using distance between elements, number of elements, desired steering angle in ϕ and θ , element coordinates and rotation angles are calculated. Ideally, measuring each element on a non-planar array with a phase center on the element surface and using measured element patterns in (3-3) gives best result in array pattern calculation. However, this is time consuming. Another method is to use full-wave simulation programs. Due to curved geometry number of meshes increase enormously when analyzing conformal antenna arrays on HFSS. For a limited number of antenna elements use of HFSS is efficient. However, as the

number of elements increase, required RAM and computation time for the solution of antenna array increase considerably. Third method is to use active element patterns exported from HFSS. This method is verified in this thesis by exporting active element patterns from HFSS. As defined previously, this data is obtained only exciting one element and terminating other elements in matched loads.

3.2.1 Radiation Pattern Calculation without Phase Correction

It is possible to divide exponential term in equation (3-7) into two parts. First part is progressive phase shift term (3-8) and second part is phase correction term (3-9).

$$\delta_n = -k(x_n \sin \theta_s \cos \phi_s + y_n \sin \theta_s \sin \phi_s + z_n \cos \theta_s) \quad (3-8)$$

$$\psi_n = e^{jk(x_n(u)+y_n(v)+z_n \cos \theta)} \quad (3-9)$$

If the antenna elements on a conformal antenna array are not placed reference to the same phase center, then it is necessary to modify far field phases of the antenna elements reference to the center element. In other words, it is necessary to multiply each antenna element pattern with a phase correction term which is equation (3-9). Additionally, for beam steering purposes it is necessary to excite elements with an additional phase, for this purpose equation (3-8) is used. In Figure 3-9, isotropic element patterns of a cylindrical antenna array are shown. In this case, due to symmetry of cylinder, phase centers of the center element and other four side elements will be the same. So calculating element pattern for the other four elements becomes easier, they are just rotated versions of active element pattern. To steer beam into desired direction, required phase values are calculated using equation (3-8).

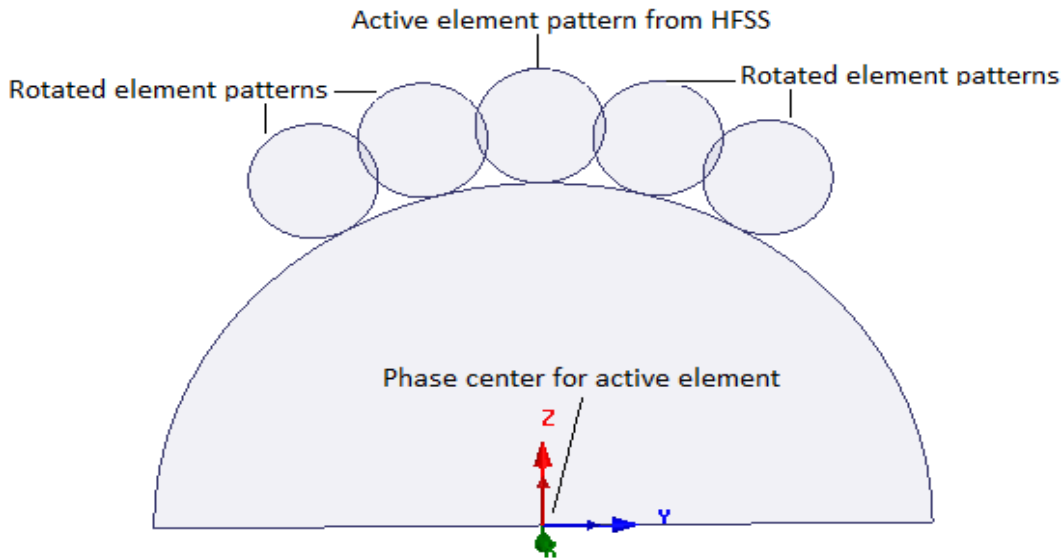


Figure 3-9 A cylindrical antenna array with phase center common for all elements

Similar process is valid for conical surface also. In cylindrical surface active element pattern is rotated on $\phi=90^\circ$ plane to obtain rotated element patterns. Due to geometrical shape of the cone, rotation is carried out on $\theta=\theta_c$ plane where θ_c is cone angle. Cone angle is the angle between bottom surface of the cone and edge of the cone. However, for the spherical antenna array situation is different. In spherical antenna case, elements are rotated both in θ and ϕ planes relative to active element pattern. So even to calculate array pattern in principle planes, 3D radiation pattern is required. Rotating a 3D pattern without loss of information is challenging. This process can be carried out in HFSS easily using relative coordinate system property of the program. Active element pattern can easily be rotated by defining relative coordinate systems. Here relative coordinate system refers to local coordinates of surrounding elements.

3.2.2 Radiation Pattern Calculation with Phase Correction

For the second case, in which phase center of each antenna element is different, phase correction should be applied for array pattern calculation. To obtain all element patterns from active element pattern of the center element, element should be rotated first. Then rotated pattern phase should be corrected using term given in equation (3-9). This case is shown in Figure 3-10.

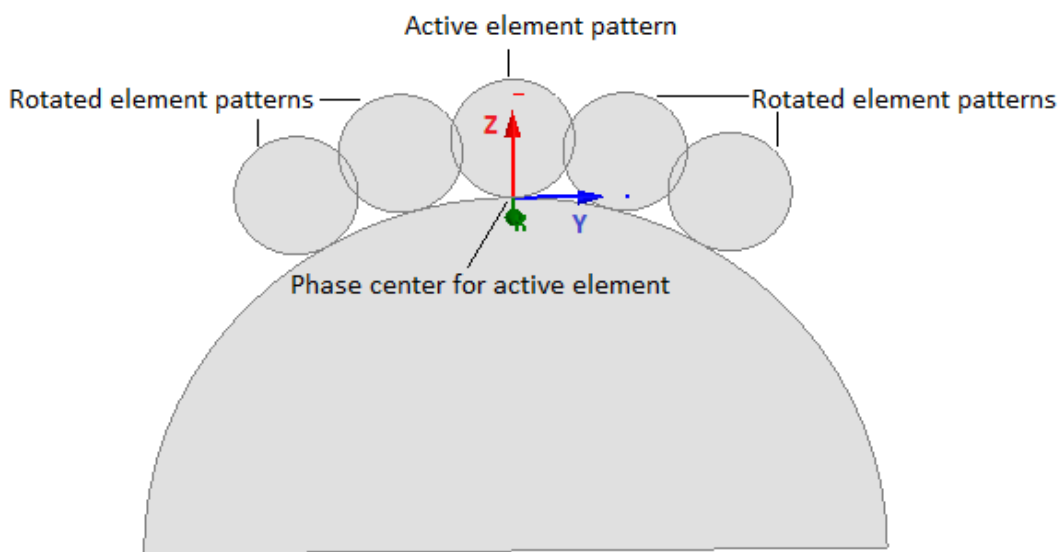


Figure 3-10 A cylindrical antenna array with phase center on the face

In conclusion, for cylindrical, conical and spherical surfaces, far field data for an active element can be exported in two different ways from HFSS. If data is exported relative to a coordinate system which is phase center for other elements also, then no phase correction is required. Only pattern rotation is sufficient. However, if exported complex far field pattern is just specific to one element, then far field phase of the radiation pattern needs to be modified.

In this study global coordinate systems used as reference are given in Figure 3-11. Calculated coordinates and angles in the following chapters are calculated with reference to the given coordinate systems. For the conical antenna array reference point is the center of the bottom face of the cone, for the cylindrical antenna array reference point is the top of the cylinder and similarly for the spherical antenna array reference point is the top of the sphere.

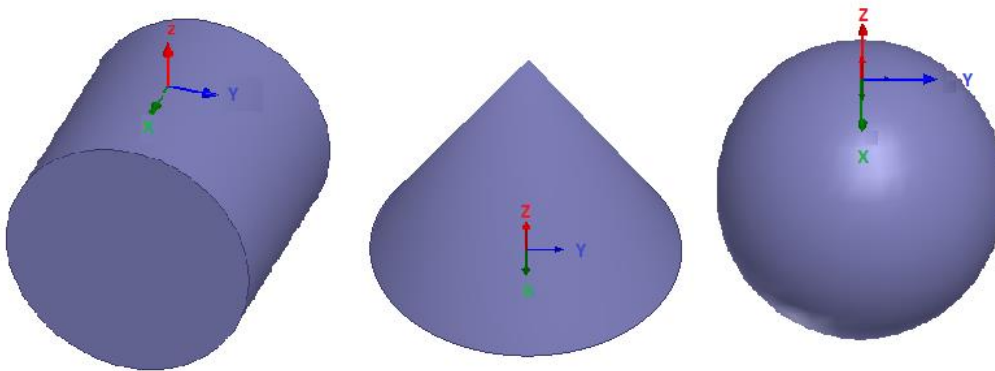


Figure 3-11 Coordinate systems for conical, cylindrical and spherical surfaces

CHAPTER 4

ANTENNA ARRAYS ON CYLINDRICAL SURFACE

The first non-planar antenna structure investigated in the scope of this study is cylindrical antenna array. Cylindrical antenna has the advantage of 360° azimuthal scan coverage due to its geometry. In this chapter, fabrication steps for cylindrical antenna arrays are introduced first. Then measured radiation patterns for fabricated antenna arrays are given, and compared with the ones obtained by simulations.

4.1 Fabrication of Cylindrical Antenna Base

In this study, cylindrical array is designed and fabricated. First, cylinder that microstrip patches are located is produced. The low cost and fast way to produce such base objects is use of a 3D printer. 3D printer uses ABSPlus P430 as dielectric substrate. Produced structure is used for bending the antenna elements in required manner with robust structure. Electrical properties for ABSPlus P430 are given in Table 4-1. As observed from material properties, it can also be used as dielectric substrate for the antennas, but in the present study it is used only as a supporting structure.

Table 4-1 Electrical properties of ABSPlus P430

Electrical Property	Value Range
Dielectric Constant	2.3-2.85
Dissipation Factor	0.0046-0.0053
Dielectric Strength	290V/mil

The produced cylindrical antenna has $5\lambda_0$ diameter. The height of the produced geometry is 50 mm. Where λ_0 is free space wavelength at 9.5 GHz. Fabricated cylindrical geometry is shown in Figure 4-1.

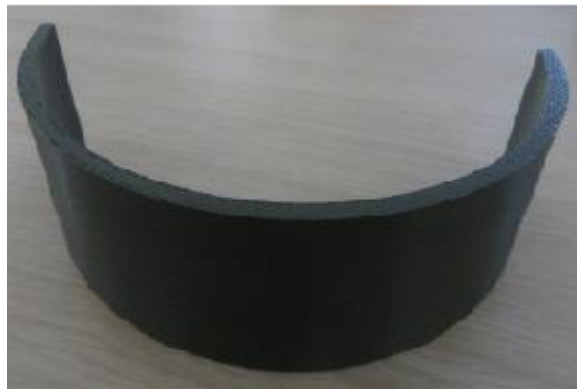


Figure 4-1 Fabricated cylindrical antenna geometry using 3D printer

4.2 Aperture Coupled Patch Antenna Array

In this chapter, fabrication and simulation results for cylindrical aperture coupled patch antenna array are given.

4.2.1 Fabrication of Aperture Coupled Patch Antenna Array

As described in Chapter 2, aperture coupled patch antenna consists of two layers. For proper operation these two layers should be bonded to each other. This process is carried out using 3M double sided, 3 μ m thick tape. Effect of this tape is not taken into account in simulations. In Figure 4-2 photograph of the ground with coupling slots side of the patch antenna is given. Patches are on the other side of the substrate.

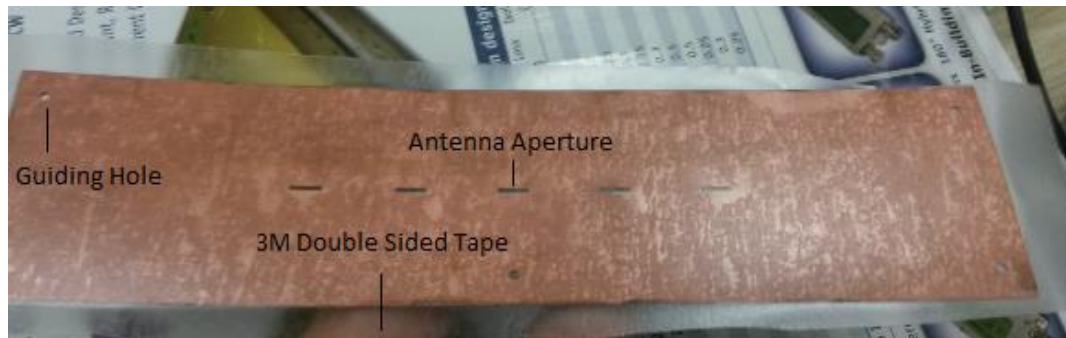


Figure 4-2 Aperture coupled patch antenna ground layer and aperture

Dielectric layer with microstrip line is located on ground plate by the help of guiding holes. This step should be carried out carefully because small misalignments can cause serious performance loss for the antenna. After bonding these two layers, antenna array shown in Figure 4-3 is obtained.



Figure 4-3 Produced aperture coupled patch antenna array

Feed lines of the patches are connected to flexible coaxial lines instead of rigid connectors for the ease of implementation of the array on cylindrical surface. Inner conductor should be weld on the feed line and outer conductor should be weld on the ground plane very close to each other carefully. Although antenna S_{11} value is acceptable in planar case, it becomes unacceptable after bending process. Feed layer of the aperture coupled patch antenna is 0.254mm thick and dielectric layer of the coaxial cable is 0.75 mm thick. Using coaxial cable to feed antenna elements, there is an inevitable air gap between inner conductor and feed line of the antenna. This affects the antenna performance considerably. Antenna active element pattern measurement in 3D spherical near field antenna measurement system (SATIMO) is carried out by connecting excitation probe to the active element and terminating other elements in matched loads. These modifications deform feed lines and consequently antenna radiation pattern. To solve these problems, an antenna array with feed network could have been produced.

4.2.2 Simulation Results for Aperture Coupled Patch Antenna

For cylindrical aperture coupled patch antenna array only HFSS simulations are available due to the problems described in previous section. Aperture coupled patch antenna is actually more convenient for arrays including large number of elements. Because designing feed network is easy and requires no extra space.

Active element region is selected as 5 elements for cylindrical antenna arrays designed in this study. Elements are placed 20mm($0.6329\lambda_0$) apart which makes 15° separation between two elements on a $5\lambda_0$ mm diameter cylinder. Here again λ_0 is free space wavelength at 9.5GHz. Total number of active elements can be changed depending on beam width and directivity requirements. In each scan, a group of five elements will be activated as shown in Figure 4-4. When switching from active

region 1 to active region 2, one element will be turned off and a new element will be excited.

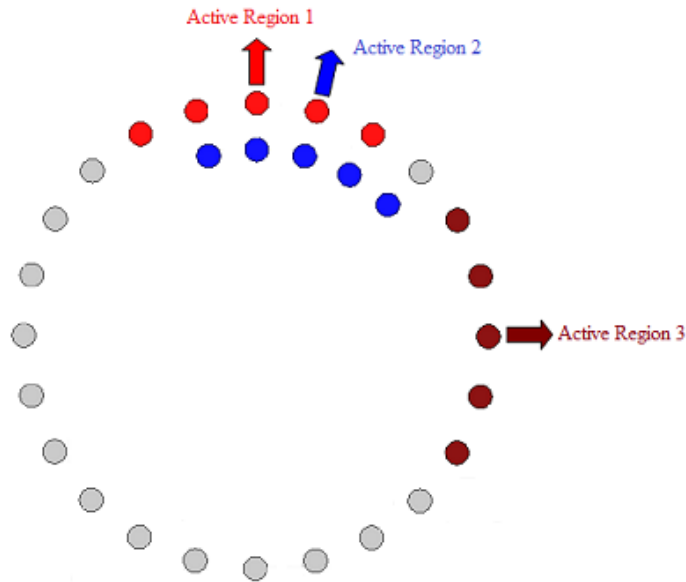


Figure 4-4 Cylindrical antenna array switch schematic

In this way it is possible to scan whole 360° azimuth without loss of any scan point and almost with a fixed beam shape. Similar scan can also be achieved by rotating a five element planar antenna array mechanically around a circular path. However, this method will reduce speed of scan considerably as mechanical movement is slower than electrical switching [23]. Also if there is a problem in mechanical system, whole array becomes defective. However, in electronically scanned arrays, in case of a problem in radiating elements, only broken region will become out of use, other elements can still operate. In this study elements are excited with uniform amplitudes, beam direction and shape are controlled with phase only. It is also

possible to obtain shaped beams, by tapering the amplitudes of the elements, but it is out of scope of this thesis. Due to cylindrical geometry, side lobe level of the synthesized beam increases as the radius of the curvature decreases [24]. Considering advantages of the cylindrical array, this is acceptable.

If only beams directing normal of the center elements are generated, there will be 15° between two beams. To direct beam peak over 360° continuously, each active element block needs to scan $\pm 7.5^\circ$. It is shown that five active elements can scan $\pm 15^\circ$ with acceptable beam deformation. So the produced antenna array is able to steer whole azimuth with a fixed beam. Produced and analyzed antenna is a single row antenna. Antenna arrays with multiple rows can also be designed and produced. In that case beam steering in elevation is also possible.

To show wide angle scan properties of this antenna, a 13 element antenna array has been designed. Patch antenna dimensions were given in Table 2.3. Antenna elements are placed 20mm apart with reference to each other as mentioned before. Using phase calculation formulation given in Chapter 3, 9 different antenna beams have been synthesized. From Figure 4-5 all these beams can be observed. It is obvious that between -55° and $+55^\circ$ scan angles, there is very small difference in beam characteristic. Increasing number of elements and covering the whole cylinder surface with antenna elements, 360° azimuth can be scanned.

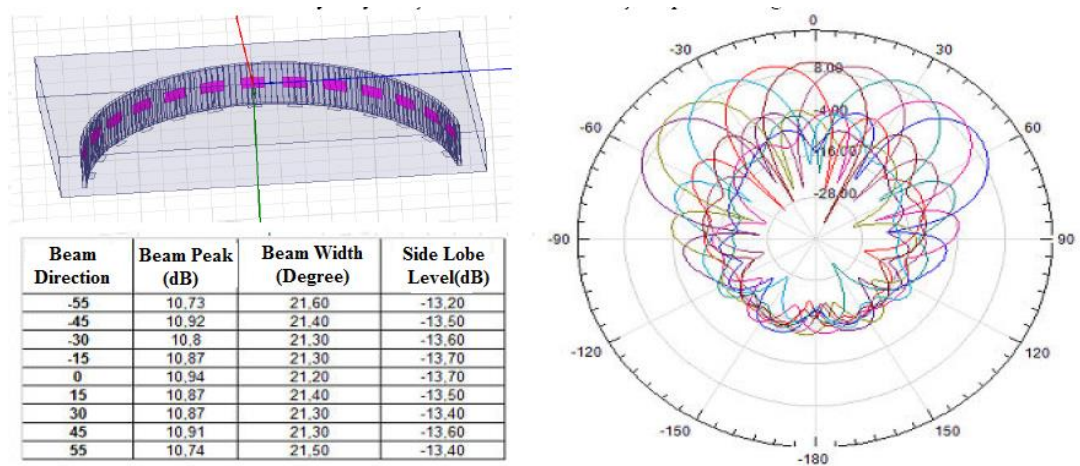


Figure 4-5 13x1 antenna array with different scan angles

4.3 Probe-Fed Patch Antenna Array

Second cylindrical antenna array designed is probe-fed patch antenna array. This antenna array is fabricated and measured. In the following sections steps followed in fabrication, measurement and simulation process are given.

4.3.1 Fabrication of Probe-Fed Patch Antenna Array

For cylindrical antenna array, probe fed patch antenna element is used as an alternative to aperture coupled patch antenna element. Fabrication of this antenna array is easier compared to aperture coupled patch antenna array. To produce the array, a plate of 0.508mm RO5880 substrate is processed. Similar to aperture coupled patch antenna array distance between antenna elements is selected as 20mm. Then coaxial probe is welded to the rectangular patch. Inner conductor of the cable is welded on patch and outer conductor is welded on ground plane. This

step should be carried out carefully, because misalignments affect performance of the antenna. Fabricated coaxial probe fed microstrip patch antenna is given in Figure 4-6.

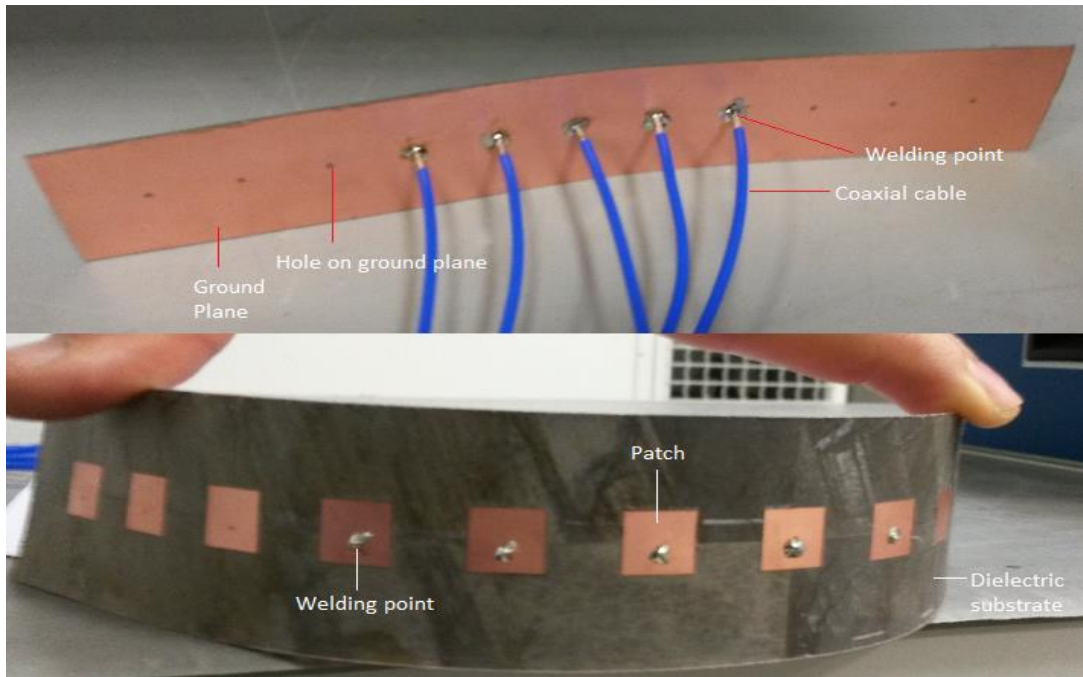


Figure 4-6 Probe fed patch antenna

Before wrapping antenna array on solid base, S parameters of the antennas have been measured. In Figure 4-7 S_{11} for five active elements are plotted on the same graph. While measuring S_{11} of the active element, other antenna ports are terminated in matched loads. Each antenna on the array has over 130 MHz -10dB bandwidth.

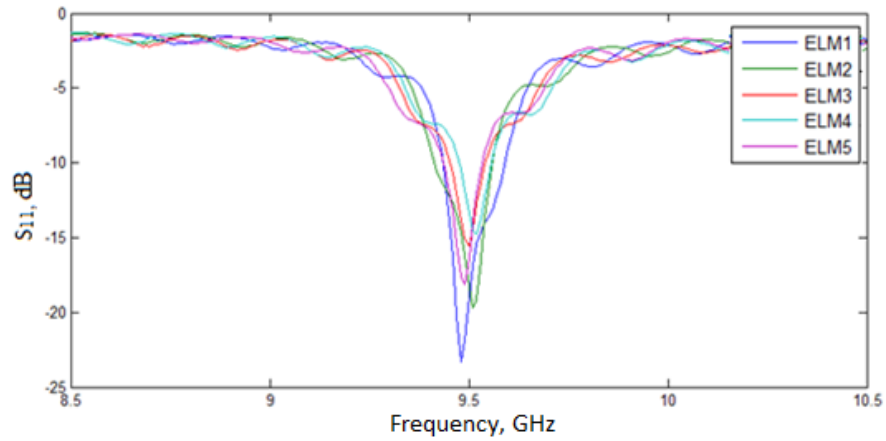


Figure 4-7 Active S_{11} values for 5 elements on cylinder with $5\lambda_0$ curvature

After S_{11} measurement, antenna array is placed on cylindrical surface as seen in Figure 4-8. Antenna is covered on cylinder using 3M double sided tape. After this step, antenna is ready for pattern measurements. In order to minimize reflections from the edge of the cylinder, an RF absorber is placed on the edge of the cylinder.

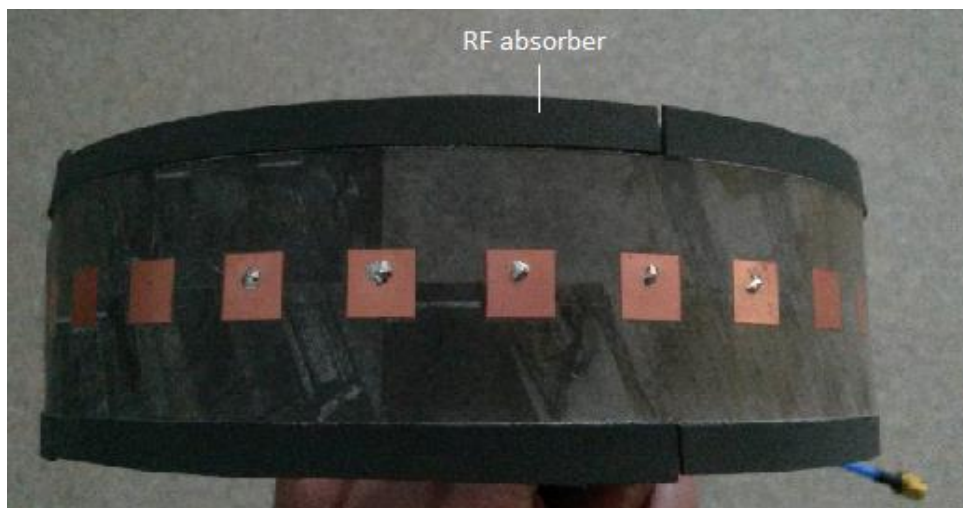


Figure 4-8 Produced cylindrical antenna

4.3.2 Simulation and Measurement Results for Probe-Fed Patch Antenna Array

In this chapter, HFSS simulations and patterns obtained numerically are compared with measurement results for the probe fed patch antenna array. This antenna is first modeled in HFSS on a cylinder of $5\lambda_0$ diameter then it is implemented and measured. HFSS model for the cylindrical array is shown in Figure 4-9.

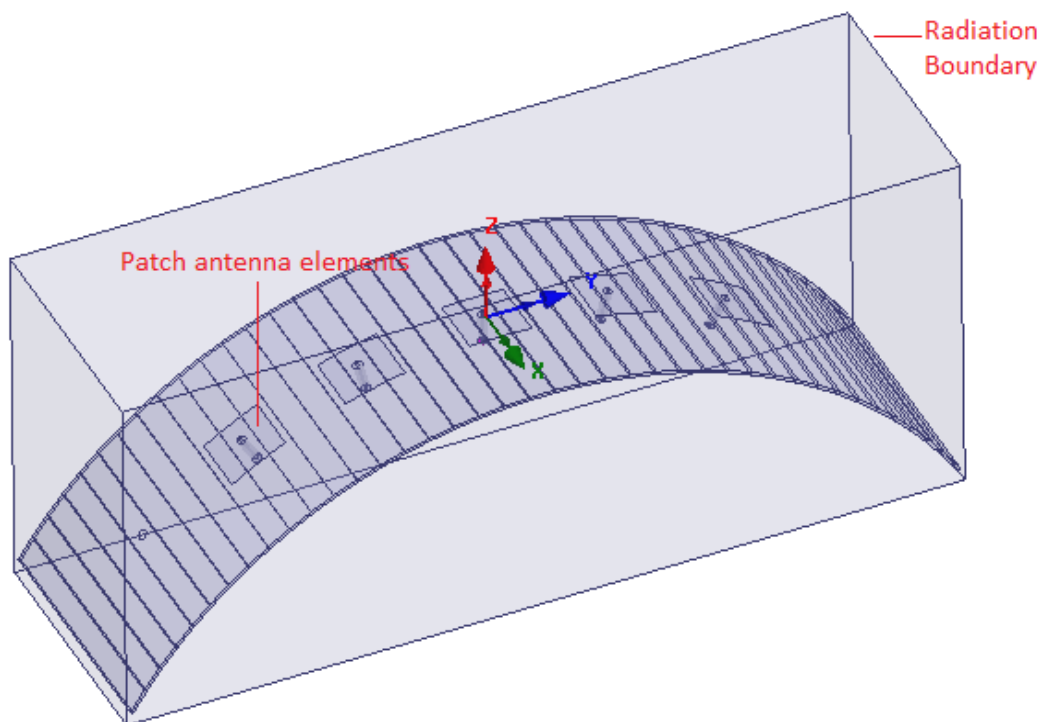


Figure 4-9 HFSS model for 5 element probe fed antenna array

Active element patterns of the produced antenna array are measured in SATIMO near field antenna measurement system. Measurement setup is shown in Figure 4-10.

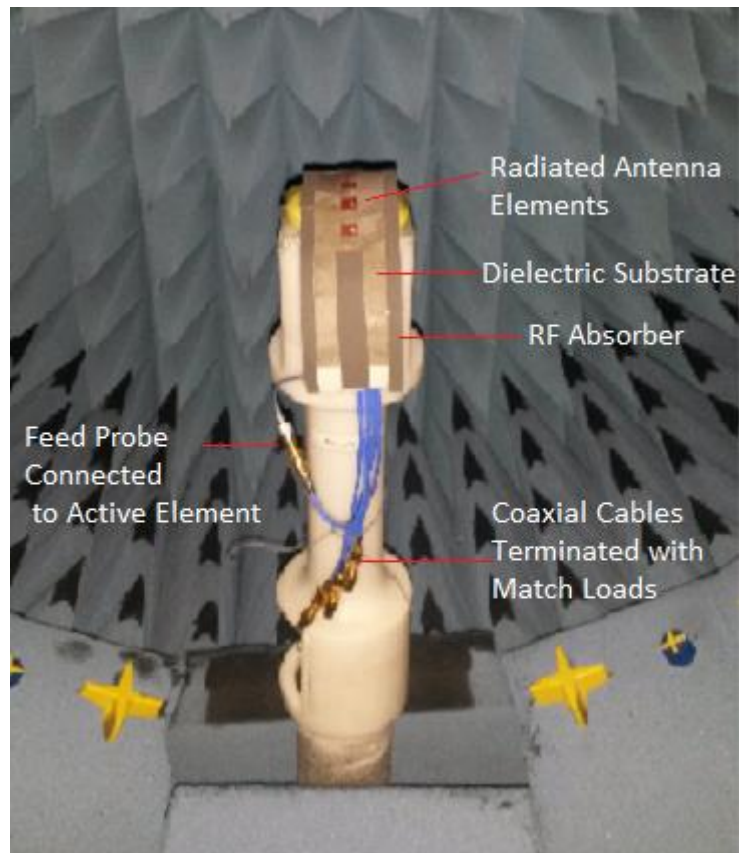


Figure 4-10 Radiation pattern measurement setup for probe-fed cylindrical antenna array

Measurements are carried out with 1° resolution. Using real and imaginary parts of the measured E_θ and E_ϕ polarized fields on $\phi=0^\circ$ and $\phi=90^\circ$ planes, element patterns are plotted in dB scale as shown in Figure 4-11.

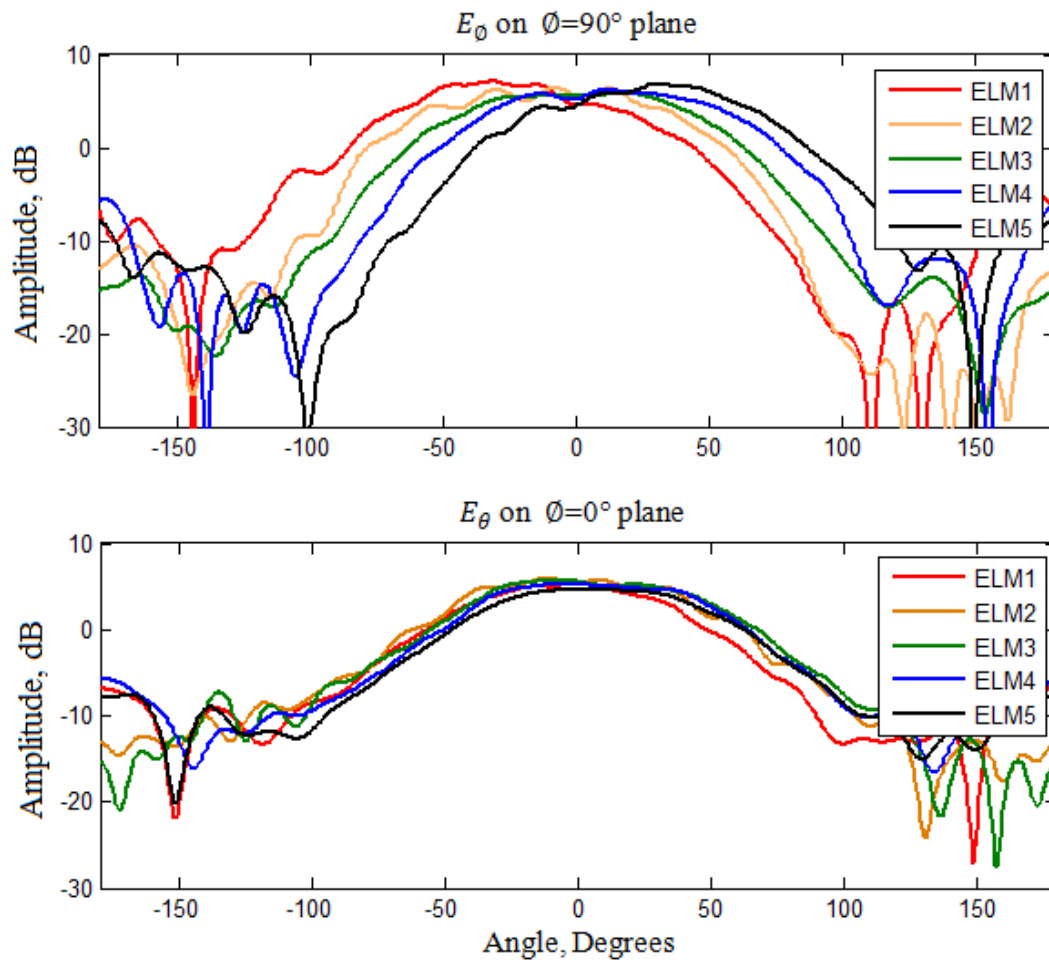


Figure 4-11 Measured ϕ (H-Plane) and θ (E-Plane) polarized active element patterns

From Figure 4-11, it is observed that on $\phi=0^{\circ}$ plane antenna patterns are directed to same angle. On the other hand, on $\phi=90^{\circ}$ plane elements have peaks on different directions which is an expected result due to geometry of antenna. Geometrical coordinates of antenna elements and calculated phase values for beam steering in desired directions are listed in Table 4-2.

Table 4-2 Coordinates, rotation angles and phase values for $5\lambda_0$ cylinder

Element No	1	2	3	4	5
X-Coordinate(mm)	0	0	0	0	0
Y- Coordinate(mm)	-38.3	-19.8	0	19.8	38.3
Z-Coordinate(mm)	-9.9	-2.5	0	-2.5	-9.9
ϕ Rotation Angle(Deg)	0	0	0	0	0
θ Rotation Angle(Deg)	-30	-15	0	15	30
Phase Shift for 0° Scan	113.06	28.72	0	28.72	113.06
Phase Shift for 15° Scan	222.25	86.12	0	-30.63	-3.81
Phase Shift for -15° Scan	-3.81	-30.63	0	86.12	222.25

As observed from Table 4-2, element 3 is the reference element. Phase and coordinates of the other four elements are calculated with reference to the element 3. Using measured element patterns, element coordinates and calculated phase values, array patterns are generated in desired directions using formulations given in Chapter 3. In pattern generation process most important point is the correction of measured phase values. Effect of non-ideal cable length and shape on the far field phase of the array should be compensated. Two different methods can be used for phase compensation. In the first method, S parameter matrix of the antenna array is used. S matrix of the array is obtained using a vector network analyzer. In ideal case, mutual coupling between any two symmetric antenna elements with a reference element must have the same phase and amplitude. Difference is due to production non idealities and should be compensated.

In Figure 4-12 measured phase graphs between center element (Element 3) and two adjacent elements (Element 2 and Element 4) and center element and two edge elements (Element 1 and Element 5) are given.

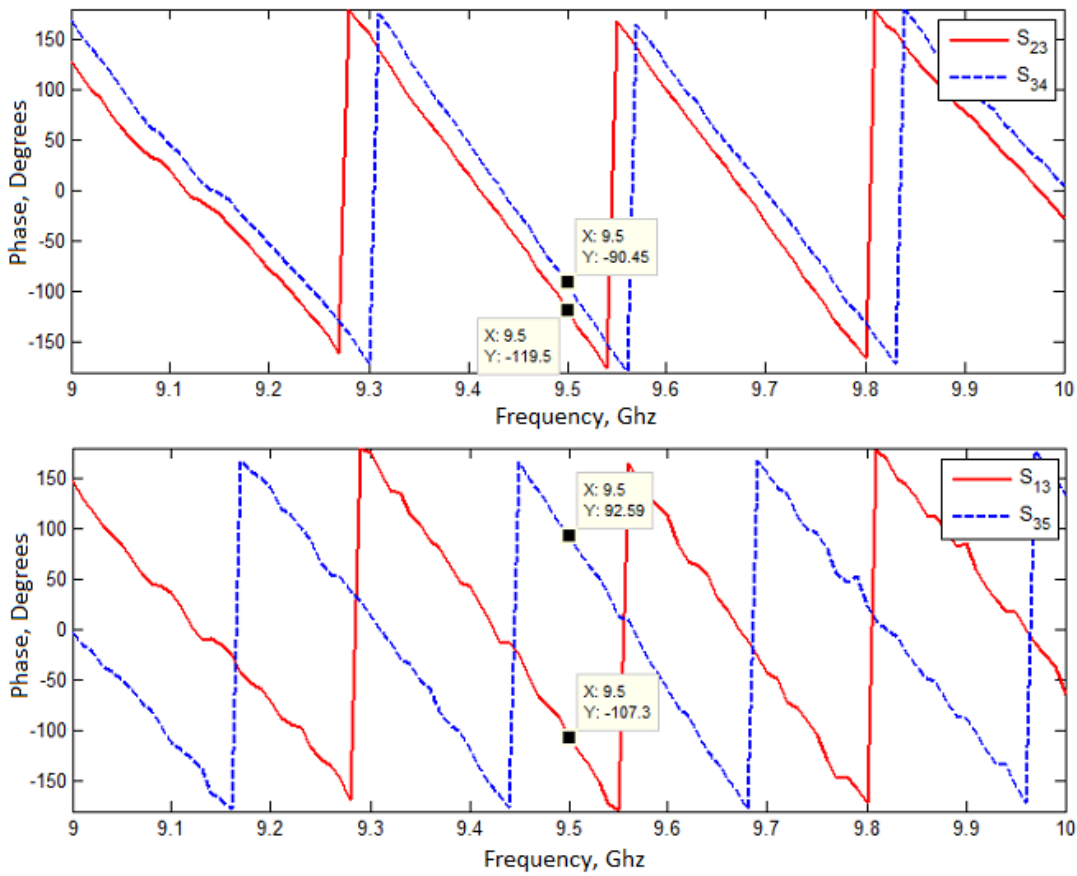


Figure 4-12 Measured S matrix phase values

As observed from Figure 4-12, at center frequency, phase offset between element 2 and element 4 is 29° and phase offset between element 1 and element 5 is 151° . In Figure 4-13 measured amplitude for the mutual coupling between antenna elements are given. Measured amplitudes show only very small variation so it is not necessary to make any modifications on the amplitude coefficients.

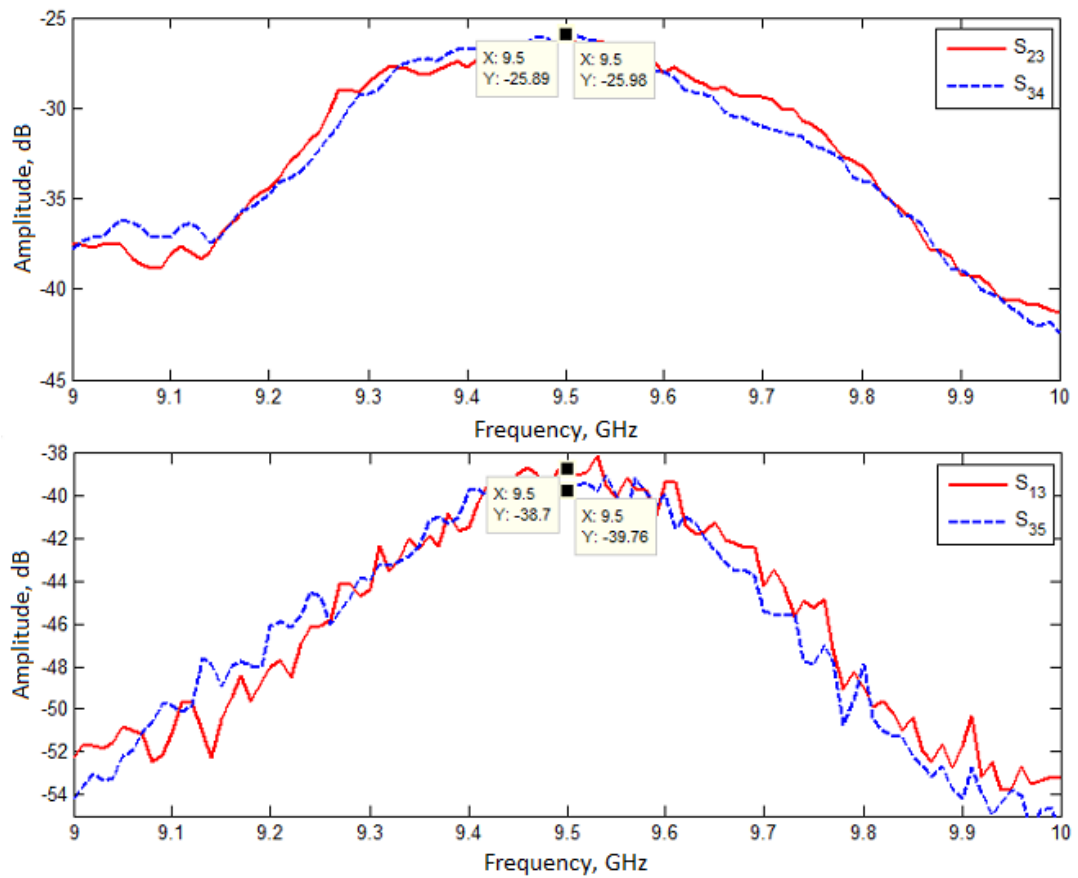


Figure 4-13 Measured S matrix amplitude values

Second method for the phase compensation is using ideal far field phase values obtained from HFSS. Difference between measured and simulated far field phase gives the phase correction required. Values obtained from S parameters are very close to the ones obtained from far field phases. In Table 4-3, simulated and measured phase values are given. Setting element 3 as the reference, phase offset between element 2 and element 4 is 35° and phase offset between element 1 and element 5 is 148° . As a result, two methods yield almost the same result. In the following parts of this study far field phase correction method is used.

Table 4-3 Measured and ideal phase values exported from HFSS

Element No		1	2	3	4	5
Ideal Phase from HFSS	0°	41.7	137	175	137	43
	15°	-66	77	168	-157	160
	-15°	158	-157.8	168.4	78	-64.17
Measured Phase	0°	148	160	141	125	-63
	15°	-147.9	-83.4	-33.2	18.5	-114.8
	-15°	-88	-148.4	127	46.7	166
Phase Correction	0°	-106.3	-23	34	12	106
	15°	81.9	160.4	201.2	-175.5	274.8
	-15°	246	-9.4	41.4	31.3	-230.1

From all these data, it is possible to generate array patterns. In Figure 4-14, Figure 4-15 and Figure 4-16 patterns steered to 0°, 15° and -15° are plotted with measurement, simulation and numerically calculated data. In Table 4-4, Table 4-5 and Table 4-6 pattern properties are given. Measured array radiation pattern is obtained from measured active element patterns numerically. Numerically calculated radiation pattern is obtained from active element pattern of a single element from HFSS. In this case other active element patterns are calculated by the rotation of simulated pattern. Simulated radiation pattern is the array pattern obtained from HFSS.

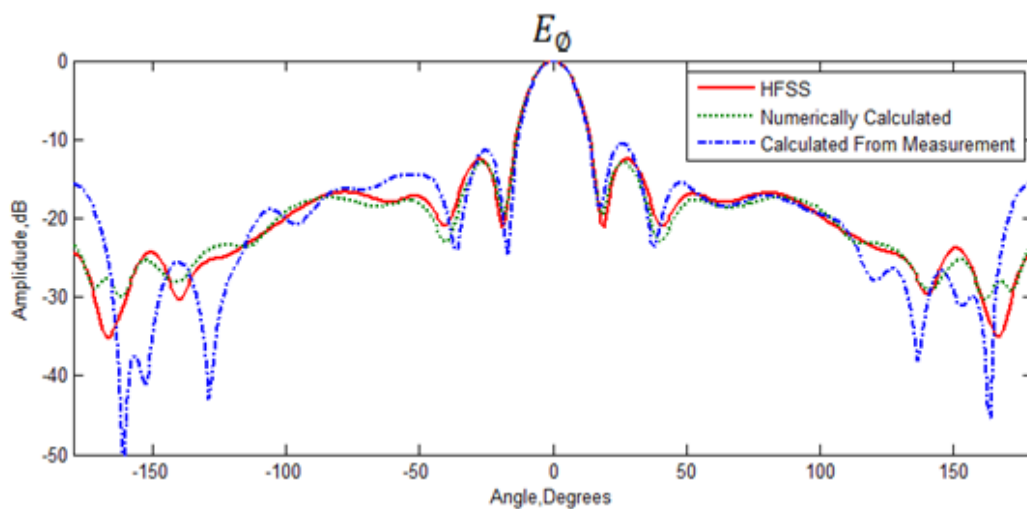


Figure 4-14 H-Plane array radiation pattern directed to 0° on cylinder

Table 4-4 Beam properties on cylinder for 0° scan

Parameter	Measurement		Simulation	
	Angle	Value	Angle	Value
HPBW	-	16 °	-	16 °
Beam Peak	0 °	0 dB	0 °	0 dB
SLL_Left	-25 °	-11.38 dB	-27 °	-12.82 dB
SLL_Right	26 °	-10.54 dB	27 °	-12.9 dB
Null_Left	-17 °	-24.79 dB	-18 °	-19.79 dB
Null_Right	18 °	-18.55 dB	18 °	-19.8 dB

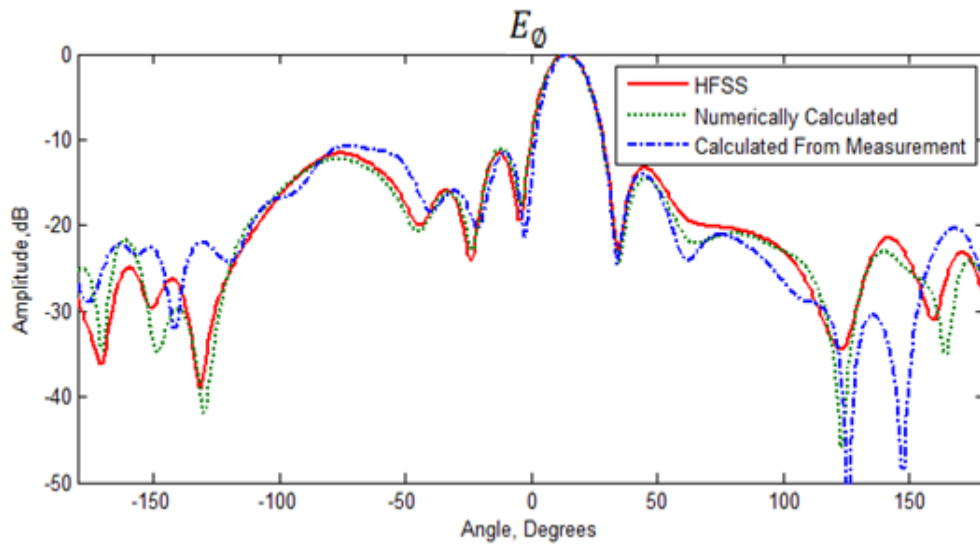


Figure 4-15 H-Plane array radiation pattern directed to 15° on cylinder

Table 4-5 Beam properties on cylinder for 15° scan

Parameter	Measurement		Simulation	
	Angle	Value	Angle	Value
HPBW	-	16 °	-	16.5 °
Beam Peak	14 °	0 dB	14 °	0 dB
SLL_Left	-10 °	-11.48 dB	-12 °	-11.05 dB
SLL_Right	44 °	-13.96 dB	45 °	-14.65 dB
Null_Left	-3 °	-21.29 dB	-4 °	-18.04 dB
Null_Right	34 °	-24.43 dB	34 °	-23.5 dB
Grating Lobe	-72 °	-10.73 dB	-78 °	-12.23 dB

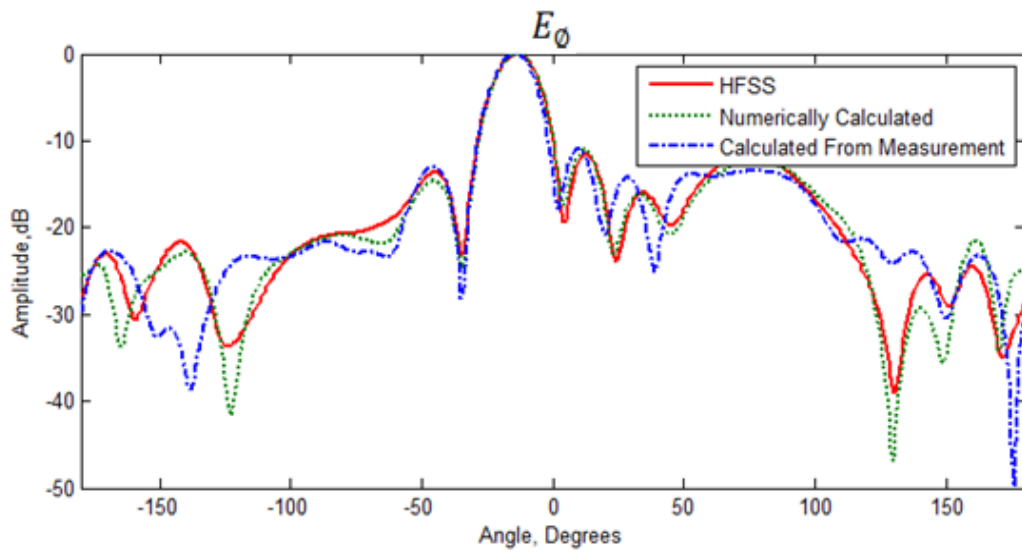


Figure 4-16 H-Plane array radiation pattern directed to -15° on cylinder

Table 4-6 Beam properties on cylinder for -15° scan

Parameter	Measurement		Simulation	
	Angle	Value	Angle	Value
HPBW	-	16.2°	-	16.6°
Beam Peak	-14°	0 dB	-14°	0 dB
SLL_Left	-46°	-13 dB	-45°	-14.38 dB
SLL_Right	10°	-10.93 dB	12°	-11.22 dB
Null_Left	-35°	-28.2 dB	-34°	-23.32 dB
Null_Right	2°	-17.76 dB	4°	-18.06 dB
Grating Lobe	79°	-13.49 dB	78°	-12.09 dB

From simulation and measurement results it is obvious that antenna can scan effectively between $+15^\circ$ and -15° . For such antenna geometry, by switching antenna elements proportionally, it is possible to scan whole azimuth without loss of scan [25]. Half power beam width and side lobe level show little variation during steering operation. Also array pattern calculated numerically using complex active element pattern of Element 3(Center element) has very consistent values with HFSS simulation and array pattern calculated from measured active element pattern. Small difference between pattern calculated from measurements and simulation is expected to be due to non-ideal measurement setup and production tolerances. Difference between HFSS and numerically calculated pattern is expected to be due to side element effects.

On Figure 4-17 simulation and pattern calculated from measured active element patterns are plotted on $\phi=0^\circ$ plane for the same array, when the beam is steered to 0° . Simulation and measurement results agree each other. In this case HPBW is 89° for both simulation and measurement case. Difference in two patterns is in the back lobe of the antenna pattern and it does not have considerable effect on antenna performance.

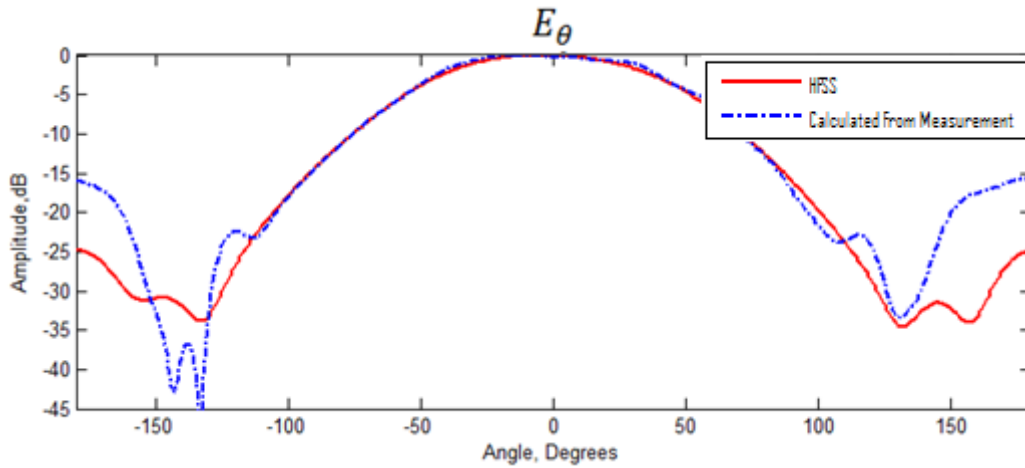


Figure 4-17 E-Plane radiation pattern of cylindrical array on $\phi=0^\circ$

If mutual coupling level between antenna elements is strong then the difference between numerically calculated array pattern and actual array pattern increases. For this purpose element separation of cylindrical antenna array is reduced from 15° to 12° . The S matrix method described in Chapter 3 is applied to this cylindrical antenna array. In Figure 4-18, numerically calculated pattern using active element pattern of the center element, array radiation pattern obtained from HFSS, array pattern calculated using active element patterns of all five elements and pattern obtained using S matrix of the array with isolated element pattern are plotted on same graph.

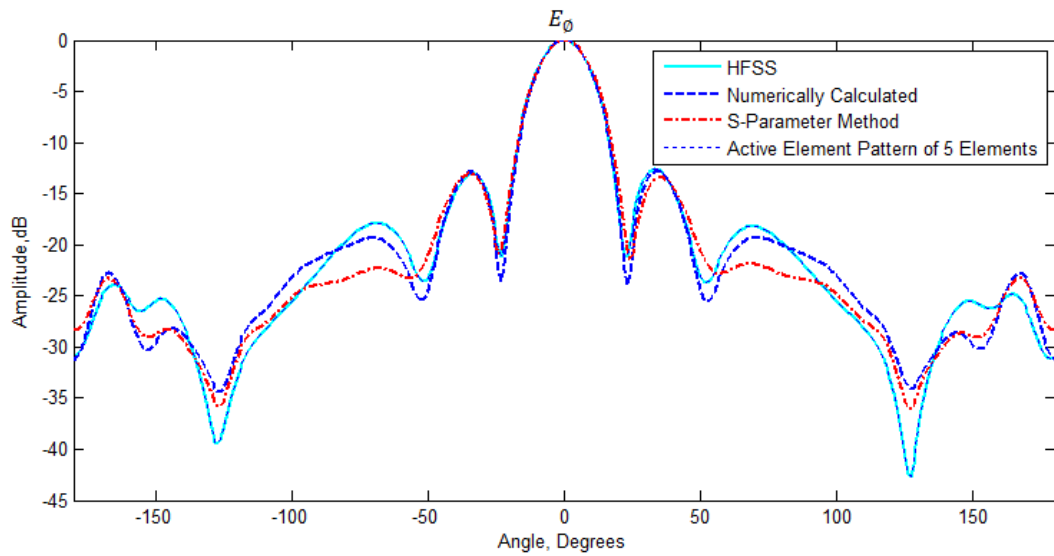


Figure 4-18 H-Plane radiation patterns for 5x1 antenna array with 12° separation

As observed from Figure 4-18 all these methods almost yield similar patterns and one can use any of the methods described to obtain radiation pattern of the array.

CHAPTER 5

ANTENNA ARRAYS ON CONICAL SURFACE

Second non-planar antenna structure investigated in the scope of this study is the conical antenna array. Like cylindrical surface, conical surface is also singly curved. This property makes it attractive for conformal antenna applications. Similar to cylindrical array, it has the advantage of 360° azimuthal scan coverage [26]. In this chapter fabrication steps for conical antenna array are introduced first. Then simulation and measurement results for the fabricated antenna are given.

5.1 Fabrication of Conical Antenna Array

Fabrication steps for conical antenna array are similar to cylindrical antenna array. 3D printer is used for the fabrication of antenna support structure. Surface of the conical structure is covered with aluminum tape to simulate a PEC structure on the cone. 7 planar antennas with dimensions given in Table 2-2 are produced and glued on conical surface as shown in Figure 5-1. In this antenna array, active element patterns of only five elements located at the center of the array are measured. Two side elements are placed to reduce side element effect on active element pattern.

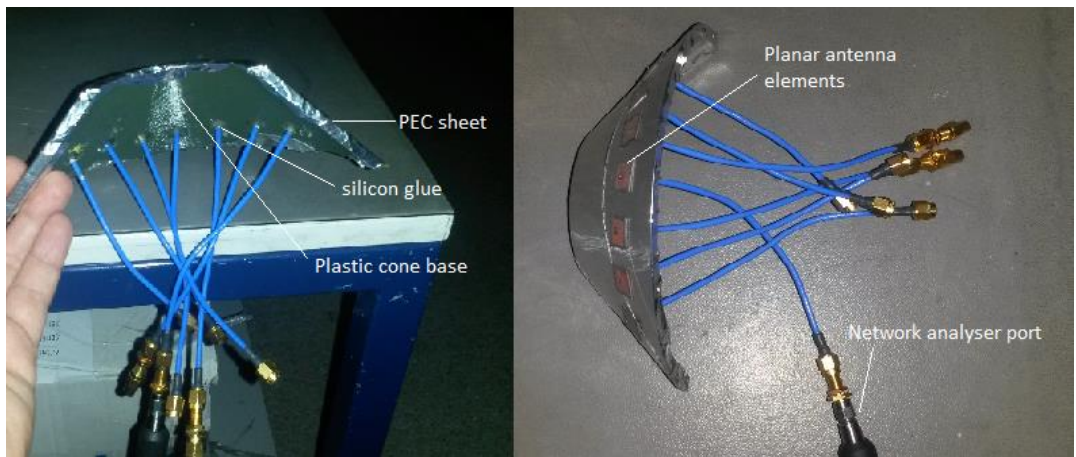


Figure 5-1 Produced conical antenna

The cone has $5\lambda_0$ mm base diameter and $3\lambda_0$ mm height, where λ_0 is the free space wavelength at 9.5GHz. From these dimensions cone angle is calculated to be 50° . Antenna elements are placed with a separation angle of 18° , which corresponds to 19.75mm circumferential distance. After production of conical antenna, S_{11} of the antenna elements have been measured. Active S_{11} values of each antenna element in the array are plotted in Figure 5-2. Each antenna element on conical array has over 130 MHz -10dB bandwidth.

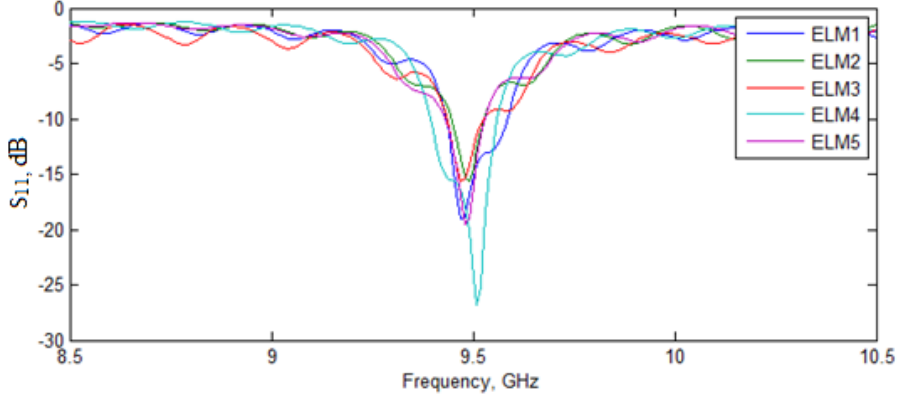


Figure 5-2 S_{11} for conical array

5.2 Simulation and Measurement Results

To investigate array pattern synthesis on conical surface, an active element region of five elements is selected as shown in Figure 5-3. By switching the active element region properly, antenna beam can steer 360° in azimuth.

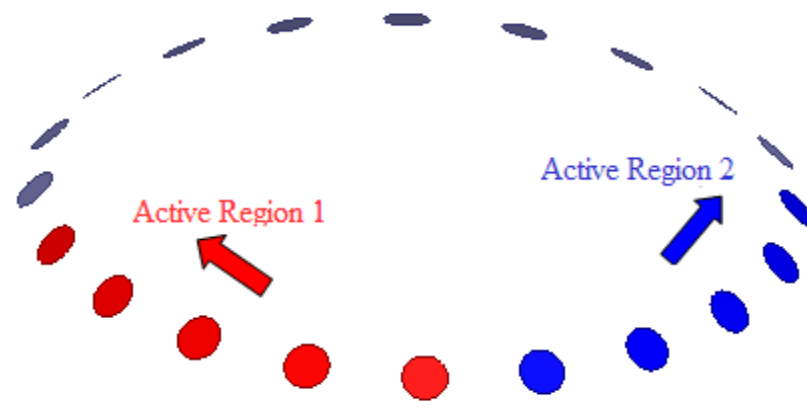


Figure 5-3 Conical antenna array switching schematic

Antenna array is first modelled in HFSS. HFSS model for the designed antenna is given in Figure 5-4.

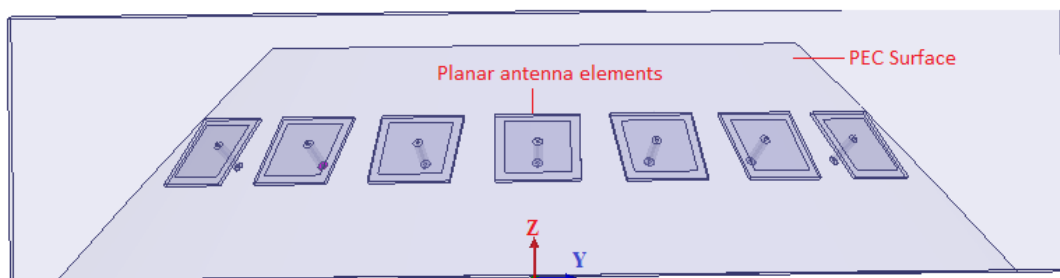


Figure 5-4 HFSS model for faceted conical array

Antenna pattern measurement is carried out in SATIMO spherical near field antenna measurement system. Measurement setup is shown in Figure 5-5.

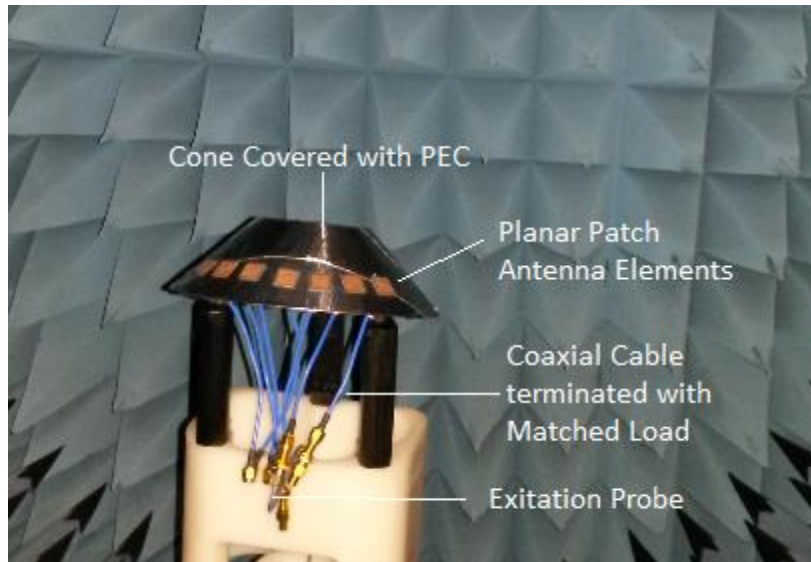


Figure 5-5 Conical antenna array measurement setup

Conical antenna elements are placed 18° apart on conical substrate. This separation angle is higher than the angle used in cylindrical antenna array. As the radius of element placement plane is 16mm less than radius of cone base, 18° separation corresponds 19.75mm circumferential distance between two elements. Element coordinates and phase offsets of each element are calculated numerically using method described in Chapter 3. Calculated coordinates and phase values are given in Table 5-1.

Table 5-1 Coordinates, rotation angles and phase values for conical array

Element No	1	2	3	4	5
X-Coordinate(mm)	53.5	62.9	66.1	62.9	53.5
Y- Coordinate(mm)	-38.9	-20.4	0	20.4	38.9
Z-Coordinate(mm)	15.4	15.4	15.4	15.4	15.4
ϕ Rotation Angle(Deg)	-36	-18	0	18	36
θ Rotation Angle(Deg)	50.2	50.2	50.2	50.2	50.2
Phase Shift for 0° Scan	52	-36	-66	-36	52
Phase Shift for 15° Scan	255	121	51	31	63
Phase Shift for -15° Scan	63	31	51	121	255

Like cylindrical antenna case, active element region has five elements. Each block needs to scan $\pm 9^\circ$ in order to cover whole azimuth. Measured active element patterns are plotted in Figure 5-6.

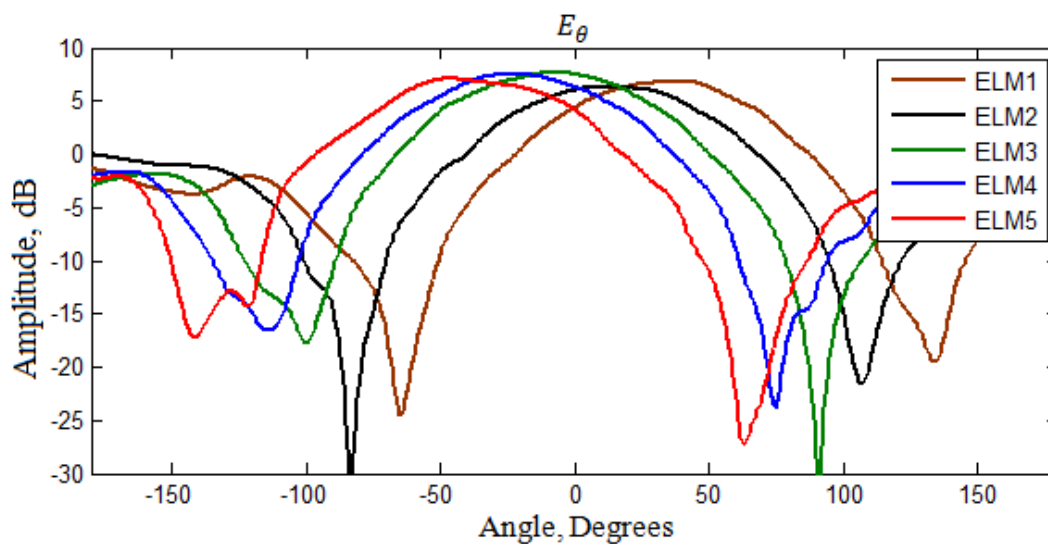


Figure 5-6 Measured active element radiation patterns on cone

Cables connected to antenna elements on conical surface are not identical. This non ideal feed structure can be corrected using ideal far field phase values from HFSS. In Table 5-2 measured and ideal far field phase values are given for conical array. Also required phase correction for antenna array is calculated and given on the same table.

Table 5-2 Measured and ideal phase values exported from HFSS

Element No		1	2	3	4	5
Ideal Phase from HFSS	0°	-145.5	-69.74	-37.78	-70.18	-144.9
	15°	116	-134	-62	-40	-77
	-15°	-78	-39	-62	-134	117
Measured Phase	0°	-166	-100	-97	-147	-128
	15°	-111	-78	-125	138	126
	-15°	88	-173	-113	-107	-43
Phase Correction	0°	20.43	30.26	59.22	76.82	-16.9
	15°	227	-56	63	-178	-203
	-15°	-166	134	51	27	160

Array patterns are generated on broadside and $\pm 15^\circ$ scan angles using same method used for cylindrical antenna array. Obtained patterns are shown in Figure 5-7, Figure 5-8 and Figure 5-9. Also beam properties are provided in Table 5-3, Table 5-4 and Table 5-5.

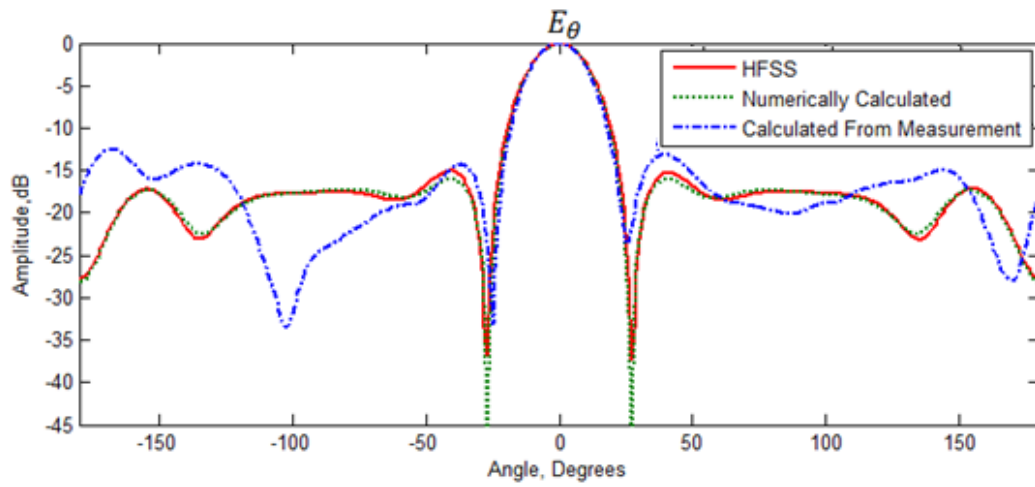


Figure 5-7 E-Plane array radiation pattern directed to 0° on cone on $\theta=50^\circ$ plane

Table 5-3 Beam properties on cone for 0° scan on $\theta=50^\circ$ plane

Parameter	Measurement		Simulation	
	Angle	Value	Angle	Value
HPBW	-	21.5°	-	22°
Beam Peak	1°	0 dB	0°	0 dB
SLL_Left	-36°	-14.33 dB	-40°	-15.06 dB
SLL_Right	40°	-13.09 dB	40°	-15.03 dB
Null_Left	-24°	-33.16 dB	-27°	-36.81 dB
Null_Right	26°	-23.51 dB	27°	-37.29 dB

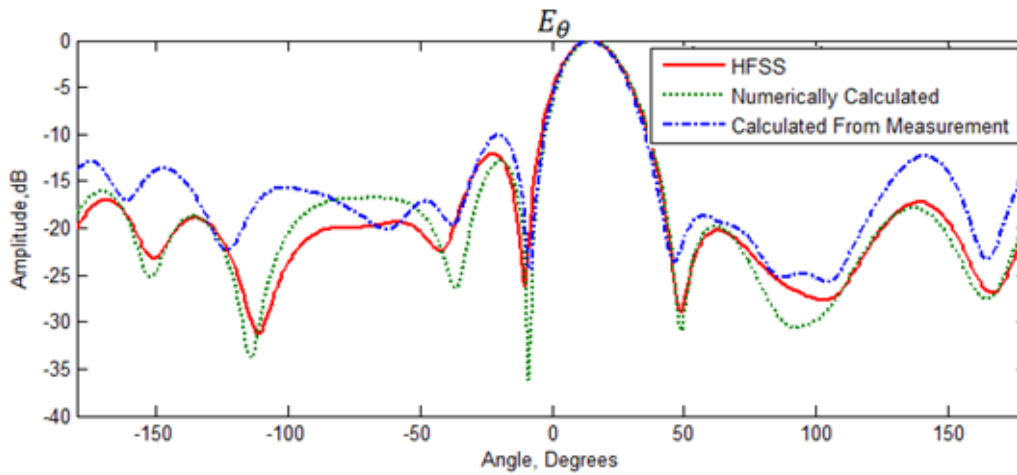


Figure 5-8 E-Plane array radiation pattern directed to 15° on cone on $\theta=50^\circ$ plane

Table 5-4 Beam properties on cone for 15° scan on $\theta=50^\circ$ plane

Parameter	Measurement		Simulation	
	Angle	Value	Angle	Value
HPBW	-	22.2 °	-	23 °
Beam Peak	14 °	0 dB	14 °	0 dB
SLL_Left	-20 °	-10.06 dB	-22 °	-12.08 dB
SLL_Right	57 °	-18.71 dB	63 °	-20.22 dB
Null_Left	-8 °	-24.42 dB	-10 °	-26.27 dB
Null_Right	46 °	-23.67 dB	49 °	-28.98 dB

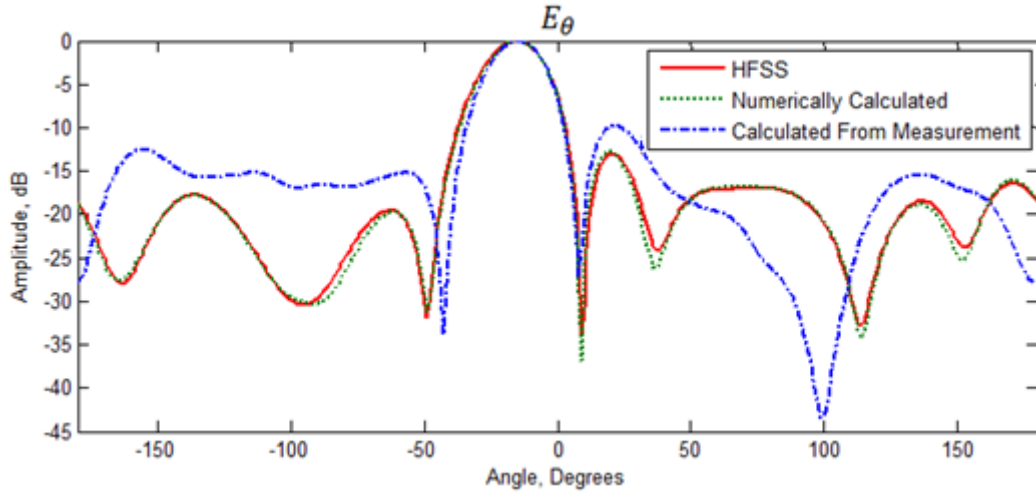


Figure 5-9 E-Plane array radiation pattern directed to -15° on cone on $\theta=50^\circ$ plane

Table 5-5 Beam properties on cone for -15° scan on $\theta=50^\circ$ plane

Parameter	Measurement		Simulation	
	Angle	Value	Angle	Value
HPBW	-	22°	-	23.5°
Beam Peak	-15°	0 dB	-15°	0 dB
SLL_Left	-57°	-15.22 dB	-63°	-19.54 dB
SLL_Right	21°	-9.69 dB	21°	-13.06 dB
Null_Left	-43°	-33.95 dB	-49°	-31.94 dB
Null_Right	8°	-27.15 dB	9°	-33.89 dB

A good agreement between simulation and measurement results is observed on the main beam of the radiation pattern. At the side lobes there is slight difference between measurement and simulation. Actually, this difference is expected because of production non idealities. Elements are placed on the cone surface by hand and alignment of the elements is not so accurate. This is the most important reason for the difference. The misalignment can be observed from mutual coupling between antenna elements. In Figure 5-10, mutual coupling between center element and two adjacent elements and between center element and two edge elements are given.

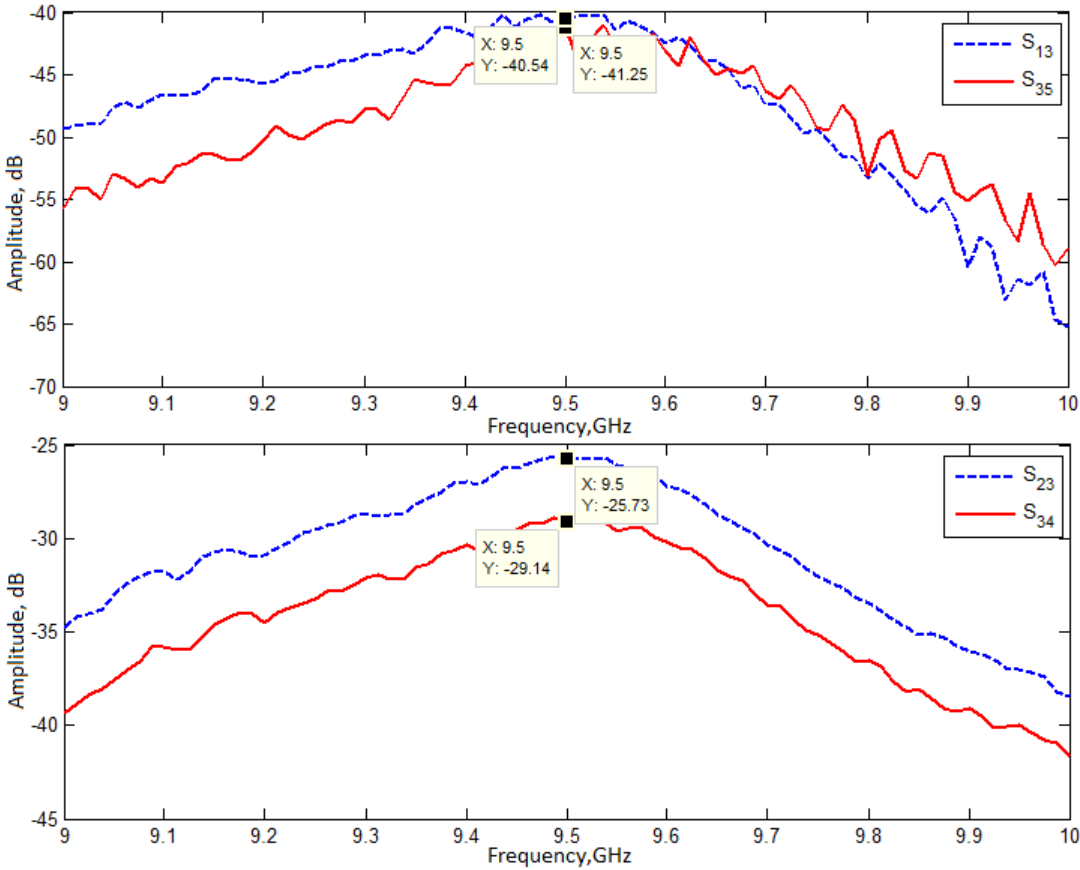


Figure 5-10 Mutual coupling between antenna elements on cone

From mutual coupling levels it can be observed that the coupling level between element 3 and element 1 is higher than the coupling level between element 3 and element 5. Similarly, the coupling level between element 3 and element 2 is higher than the coupling level between element 3 and element 4. Measurements of a more precisely fabricated antenna should have better match with simulations. On the other hand, HFSS simulation and numerically calculated patterns are very close to each other. This is also an expected result because active element patterns are obtained using 7 elements but array pattern is synthesized using 5 center elements. In this way effect of edge elements is minimized.

CHAPTER 6

ANTENNA ARRAYS ON SPHERICAL SURFACE

Last antenna of interest in this study is spherical antenna. Cylindrical and conical antenna geometries have the advantage of 360° azimuth coverage. On the other hand, due to its geometry spherical antenna array has the advantage in spherical scan coverage [27]. In this chapter, first, production steps for spherical antenna array is given then simulation and measurement results for this array are presented.

6.1 Fabrication of Spherical Antenna Array

Fabrication steps for the spherical antenna array are similar to fabrication steps for the conical antenna. Hemispherical support structure is fabricated using 3D printer. Then array elements are located on this structure. The beam scanning property for spherical array is again based on switching active element region. To show the radiation characteristics, a 7 element sector is selected for active region on the antenna surface. As seen in Figure 6-1, elements are placed in same direction in order to reduce cross polarization.

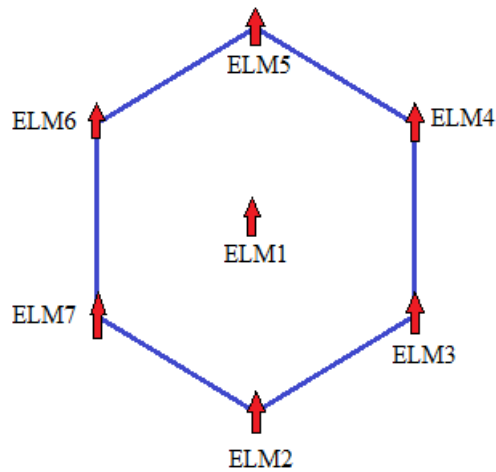


Figure 6-1 Element placement for spherical array block

ELM1 is placed on $\theta=0^\circ$ and $\phi=0^\circ$ point. To obtain the coordinates of ELM2, ELM1 is shifted by 15° in increasing theta direction on $\phi=0^\circ$ plane. Coordinates of ELM3-ELM7 are obtained by shifting ELM2 by 60° on $\theta=15^\circ$ plane in increasing ϕ direction. Produced antenna elements are placed on spherical surface as shown in Figure 6-2.



Figure 6-2 Produced spherical antenna array

After fabrication of the antenna array, active S_{11} values of each antenna element in the array are measured. Measurement results are shown in Figure 6-3.

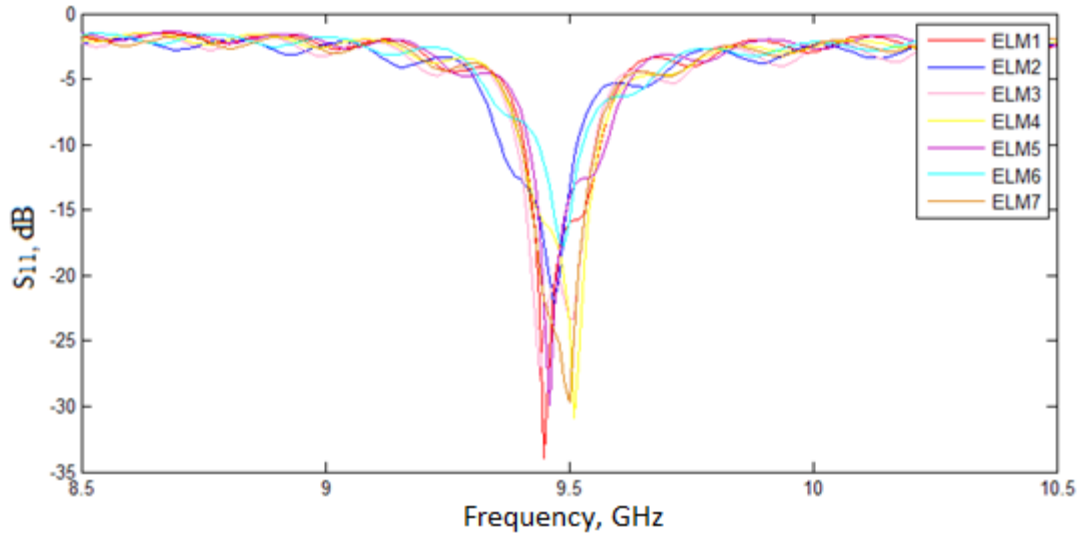


Figure 6-3 Active S_{11} values for spherical antenna elements

6.2 Simulation and Measurement Results

Similar to cylindrical and conical geometry, elements are excited with uniform amplitude. Phase offsets, element coordinates required for desired radiation direction are calculated numerically. Calculated values are shown in Table 6-1. To cover whole hemisphere without loss of points, each sub block needs to scan $\pm 15^\circ$ in both ϕ and θ planes.

Table 6-1 Coordinates, rotation angles and calculated phase values for spherical array

Element No	1	2	3	4	5	6	7
X-Coordinate(mm)	0	19.8	9.9	-9.9	-19.8	-9.9	9.9
Y- Coordinate(mm)	0	0	17.1	17.1	0	-17.1	-17.1
Z-Coordinate(mm)	0	-2.5	-2.5	-2.5	-2.5	-2.5	-2.5
ϕ Rotation Angle(Deg)	0	0	60	120	180	240	300
θ Rotation Angle(Deg)	15	15	15	15	15	15	15
Phase Shift for $\phi=0^\circ, \theta=0^\circ$ Scan	0	28.72	28.72	28.72	28.72	28.72	28.72
Phase Shift for $\phi=90^\circ, \theta=15^\circ$ Scan	0	27	-37	-37	-27	93	93
Phase Shift for $\phi=0^\circ, \theta=15^\circ$ Scan	0	-45	-9	64	101	64	-9

Spherical antenna is first modelled in HFSS. Then it is measured in SATIMO spherical near field antenna measurement system. HFSS model for the antenna and the measurement setup is shown in Figure 6-4.

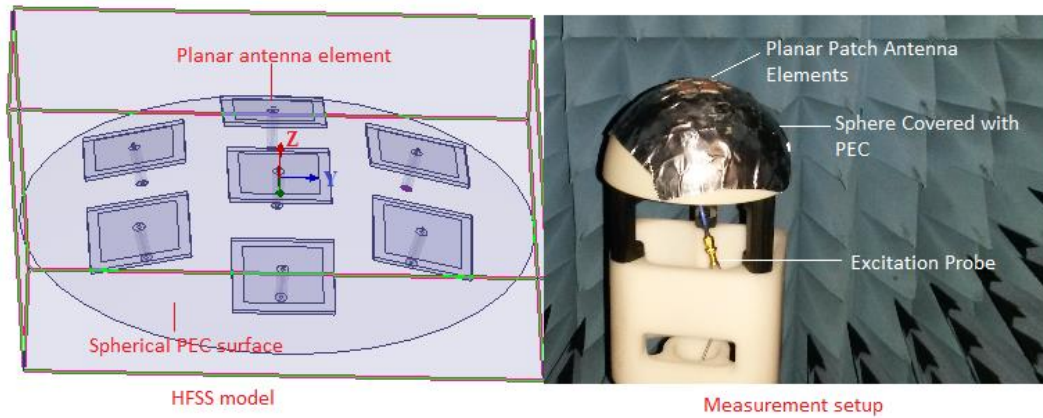


Figure 6-4 HFSS model and measurement setup for spherical antenna

Measured active element patterns for the antenna elements on spherical surface are given in Figure 6-5.

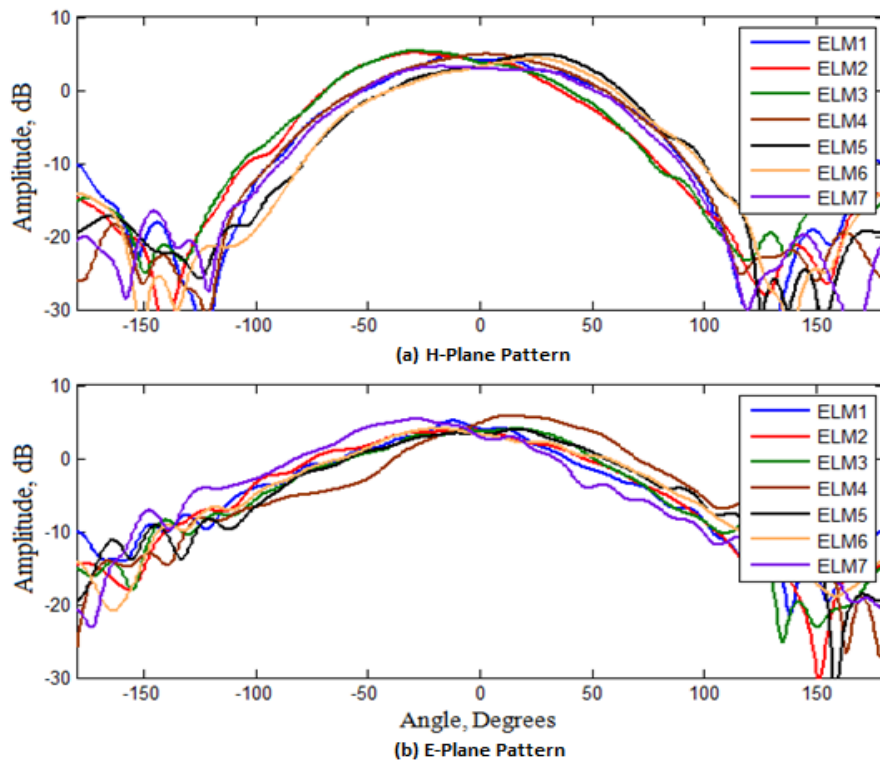


Figure 6-5 Measured active element patterns on $\theta=90^\circ$ (a) and $\theta=0^\circ$ (b) plane

Measured phases for the active element patterns are corrected using ideal far field phase values exported from HFSS like in cylindrical and conical arrays as described in previous chapters. These values are given in Table 6-2. Using element coordinates, progressive phase values and phase correction values in equation (3-7), array beam is steered to $\pm 15^\circ$ in both $\phi=0^\circ$ and $\phi=90^\circ$ planes. Also array radiation pattern steered to $\phi=0^\circ$ and $\theta=0^\circ$ in E and H plane are given. In Figure 6-6, Figure 6-7, Figure 6-8, Figure 6-9 E and H plane radiation patterns for the antenna array are given. In these graphs radiation pattern from measurement is obtained by first measuring all active element patterns of the antenna elements then using these patterns, total array radiation pattern is calculated. Numerically calculated array pattern is obtained by using active element pattern of the center element of 7 element array. This pattern is exported from HFSS and rotated on both ϕ and θ planes to obtain other six active element patterns. HFSS pattern is directly obtained from HFSS. Port excitation phases of each element are given in Table 6-1. Beam parameters for these radiation patterns are given in Table 6-3, Table 6-4, Table 6-5 and Table 6-6.

Table 6-2 Measured and ideal phase values exported from HFSS for spherical array

Element No		1	2	3	4	5	6	7
Ideal Phase from HFSS	E_{θ} on 0°	170	141	138	137	139	136	139
	E_{θ} on 0°	-9	-38	-41	-42	-41	-43	-40
	$\phi=90^{\circ}$ $\theta=15^{\circ}$	-13	21	-16	-67	-107	-70	-14
	$\phi=0^{\circ}$ $\theta=15^{\circ}$	168	141	-164	-166	138	79	83
Measured Phase	E_{θ} on 0°	-91	-34	-112	-102	-60	0	22
	E_{θ} on 0°	88	145	67	77	119	-179	-157
	$\phi=90^{\circ}$ $\theta=15^{\circ}$	-94	-58	-72	-42	-32	-34	-41
	$\phi=0^{\circ}$ $\theta=15^{\circ}$	69	72	0	68	165	-141	177
Phase Correction	E_{θ} on 0°	261	175	250	239	199	136	117
	E_{θ} on 0°	-97	-183	-108	-119	-160	136	117
	$\phi=90^{\circ}$ $\theta=15^{\circ}$	81	79	56	-25	-75	-36	27
	$\phi=0^{\circ}$ $\theta=15^{\circ}$ degree	99	69	-164	-234	-27	220	-94

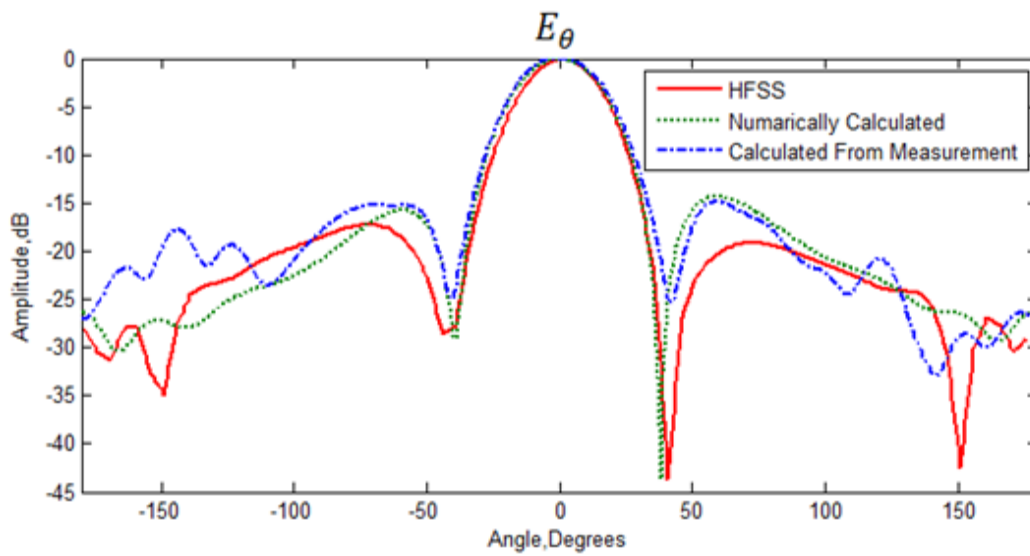


Figure 6-6 E-Plane array radiation pattern directed to 0° on sphere $\phi=0^\circ$ plane

Table 6-3 Beam properties on sphere for 0° scan on $\phi=0^\circ$ plane

Parameter	Measurement		Simulation	
	Angle	Value	Angle	Value
HPBW	-	32.5 °	-	29 °
Beam Peak	-1°	0 dB	1 °	0 dB
SLL_Left	-69 °	-15.25 dB	-72 °	-17.27 dB
SLL_Right	59 °	-14.84 dB	71 °	-19.12 dB
Null_Left	-41 °	-25.05 dB	-43 °	-28.38 dB
Null_Right	42 °	-25.05 dB	41 °	-43.75 dB

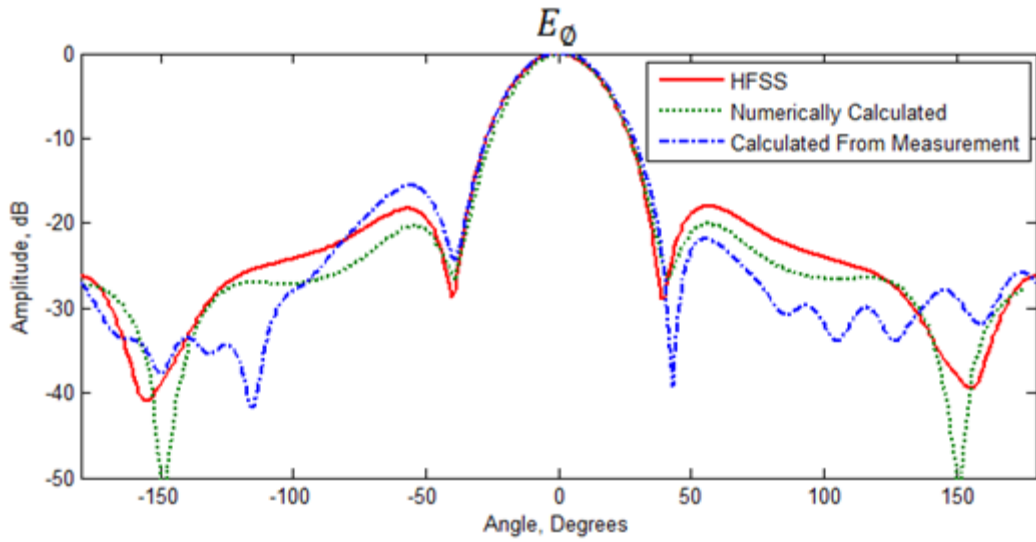


Figure 6-7 H-Plane array radiation pattern directed to 0° on sphere $\phi=90^\circ$ plane

Table 6-4 Beam properties on sphere for 0° scan on $\phi=90^\circ$ plane

Parameter	Measurement		Simulation	
	Angle	Value	Angle	Value
HPBW	-	31.5 °	-	31 °
Beam Peak	0°	0 dB	0 °	0 dB
SLL_Left	-56 °	-15.57 dB	-56 °	-18.29 dB
SLL_Right	55 °	-21.78 dB	56 °	-17.97 dB
Null_Left	-38 °	-23.86 dB	-40 °	-28.64 dB
Null_Right	43 °	-39.28 dB	39 °	-28.97 dB

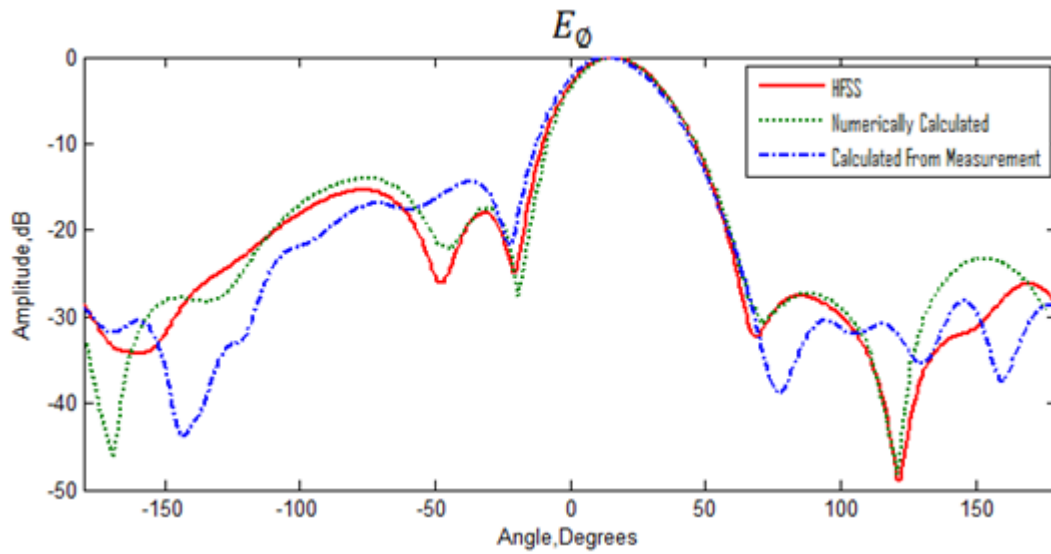


Figure 6-8 H-Plane array radiation pattern directed to 15° on sphere $\phi=90^\circ$ plane

Table 6-5 Beam properties on sphere for 15° scan on $\phi=90^\circ$ plane

Parameter	Measurement		Simulation	
	Angle	Value	Angle	Value
HPBW	-	31.5 °	-	32 °
Beam Peak	13°	0 dB	16 °	0 dB
SLL_Left	-37 °	-14.34 dB	-32 °	-17.95 dB
SLL_Right	94 °	-30.46 dB	86 °	-27.61 dB
Null_Left	-22 °	-21.66 dB	-21 °	-24.83 dB
Null_Right	77 °	-38.76 dB	69 °	-32.39 dB

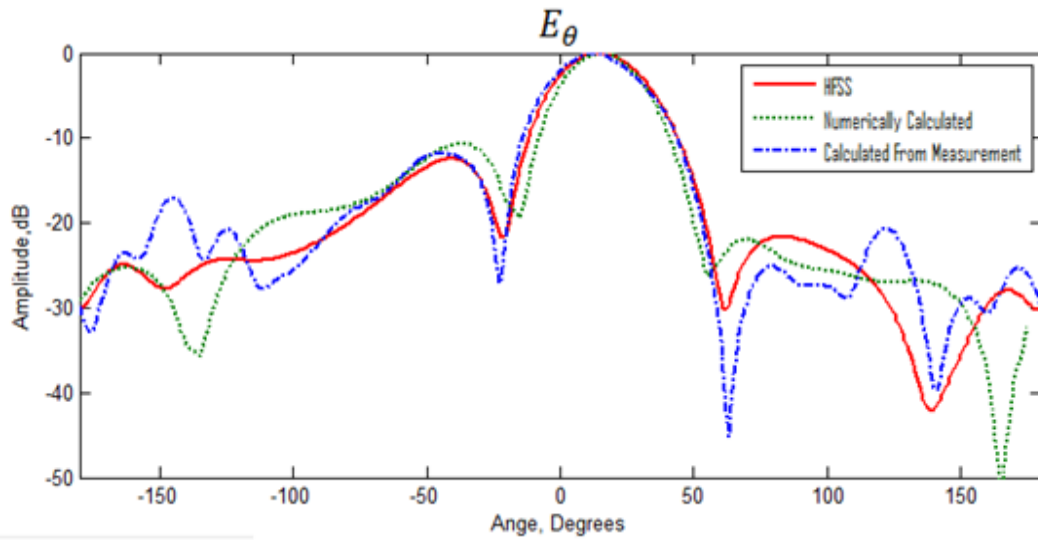


Figure 6-9 E-Plane array radiation pattern directed to 15° on $\phi=0^\circ$ plane

Table 6-6 Beam properties on sphere for 15° scan on $\phi=0^\circ$ plane

Parameter	Measurement		Simulation	
	Angle	Value	Angle	Value
HPBW	-	32 °	-	32 °
Beam Peak	14°	0 dB	14 °	0 dB
SLL_Left	-45 °	-11.81 dB	-40 °	-13.4 dB
SLL_Right	79 °	-25.13 dB	83 °	-21.63 dB
Null_Left	-23 °	-27.22 dB	-21 °	-21.75 dB
Null_Right	63 °	-45.11 dB	62 °	-30.25 dB

Simulation, measurement and numerically calculated array pattern results show acceptable differences. Main difference between measurement and simulation results originates from misalignments of the antenna elements.

Finally, using numerically proposed array pattern generation method, array pattern for a large spherical array is calculated on $\theta=0^\circ$ and $\theta=90^\circ$ planes. Antenna array has 3 rings structure and total elements on the active region is 19. First two rings are the same as rings shown in Figure 6-1 . Third ring has 12 elements, in which elements are separated 30° apart on $\theta=30^\circ$ plane. Antenna geometry with only active elements is shown in Figure 6-10.

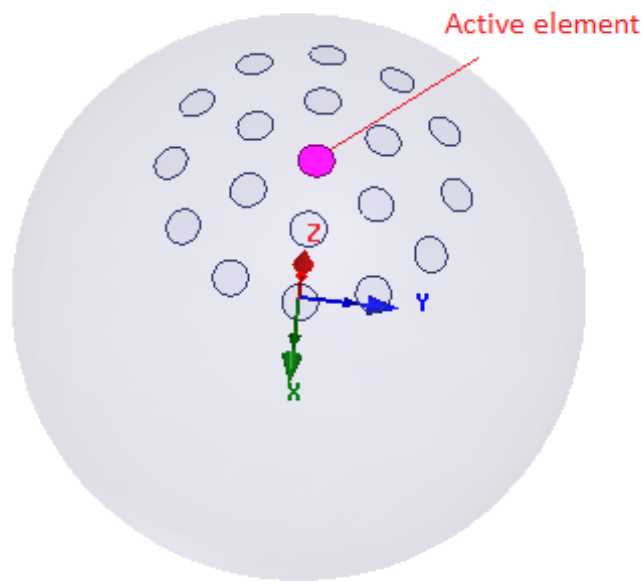


Figure 6-10 19 elements spherical array

Obtained array patterns are shown in Figure 6-11 and Figure 6-12. On these graphs phase compensated and phase uncompensated patterns are shown. In phase uncompensated case all elements are excited with same phase. In phase compensated case center element is excited with 0° , 6 element ring is excited with 28.72° and 12 element ring is excited with 113° to direct beam to 0° . These phase values are again calculated using formulation given in Chapter 3. It is observed that, phase compensation has significant effect of beam shape and directivity.

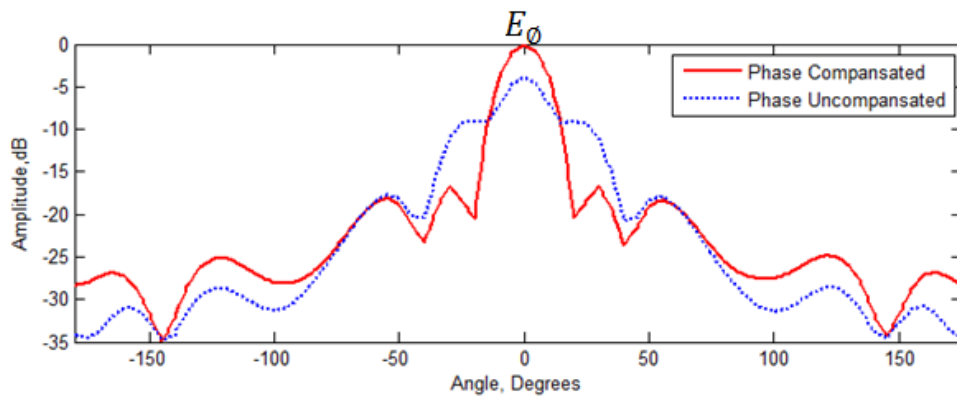


Figure 6-11 H-Plane radiation pattern for 19 element array conformed on sphere

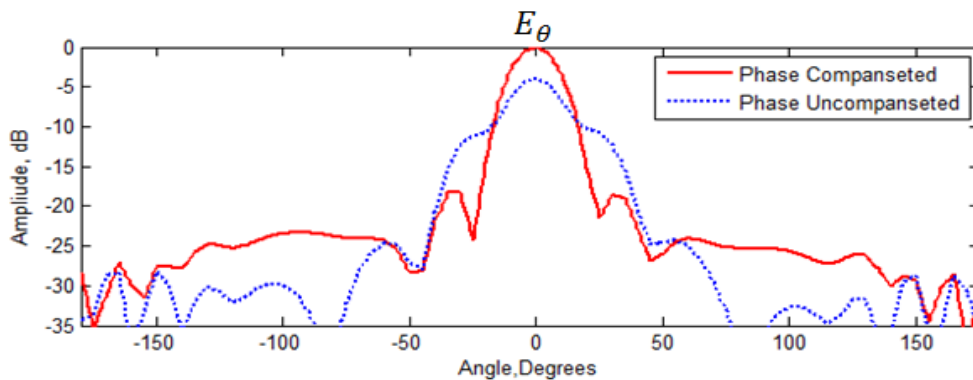


Figure 6-12 E-Plane radiation pattern for 19 element array conformed on sphere

Normally, obtaining radiation pattern for such an array by full wave simulation tools requires long simulation time. However, using method described in Chapter-3 these two patterns are obtained in almost a minute. In [28], phase compensation for antenna arrays on spherical surfaces is studied. It has been observed that phase compensation on antenna arrays with similar geometry have radiation patterns very close to the ones obtained in this study.

CHAPTER 7

CONCLUSIONS

In this study, beam scanning properties of cylindrical, conical and spherical antenna arrays are investigated. Antenna arrays with limited number of elements placed on these surfaces are produced and measured. From measurements and simulations, beam scanning is successfully observed.

In Chapter 2, basic antenna elements used on the arrays are introduced. Information about their structure is given. Parametric studies on slot length and stub length are given for the aperture coupled patch antenna. Moreover, dimensions and radiation patterns of aperture coupled and coaxial fed patch antenna are given.

In Chapter 3, array factor calculation for planar surfaces is introduced first. Then array pattern calculation for non-planar surfaces is given. The concept of active element pattern is introduced. Array pattern calculation using active element pattern and pattern generation using isolated element pattern with the S matrix of the antenna array are developed and used to analyze nonplanar arrays. Concept of phase center for antenna arrays is introduced.

In Chapter 4, 5 and 6 fabrication steps for cylindrical, conical and spherical antenna arrays are explained. Simulation and measurement results are given for all three types of antenna arrays. Beside HFSS simulation and measurement results, array pattern calculated using active element pattern is compared with these two results.

This study is focused on investigating array patterns on non-planar surfaces. It is shown that antenna arrays on cylindrical, conical and spherical surfaces are suitable for wide angle beam scanning.

For cylindrical and conical array case only single line array is studied. It is possible to use two dimensional antenna arrays on these surfaces. In that case, it is possible to steer antenna beam in elevation too. Also for spherical array, antenna array containing seven elements is studied. For this antenna it is possible to increase number of elements in each block to have a narrower and more directive beam. Similar argument is valid for cylindrical and conical antenna arrays.

Throughout this study, amplitudes of excitation coefficients are taken as unity. By an appropriate tapering of element coefficients, patterns with low side lobe levels can be obtained. Polarization of the antenna arrays are not studied in detail. It is possible to investigate polarization properties of the antennas on non-planar surfaces in future studies. In this study, beams in different scan angles are synthesized numerically using active element pattern. It is necessary to design a feed network for these antenna structures. Designed feed network must be able to control each element phase and amplitude separately. Design of the feed network for such an antenna array is also a challenging task for future studies.

REFERENCES

- [1] Nurul H. Noordin, Nakul Haridas, Ahmed O. El-Rayis, Ahmet T. Erdoğan, Tuğrul Arslan "Antenna Array with Wide Angle Scanning Properties", 6th European Conference on Antennas and Propagation, 2011.
- [2] Inas Khalifa and Rodney G. Vaughan, "Geometric Design and Comparison of Multifaceted Antenna Arrays for Hemispherical Antenna Arrays", IEEE Transactions on Antennas and Propagation, Vol. 57, No.9, September 2009
- [3] Inas Khalifa and Rodney G. Vaughan, "Geometrical Design of Pyramidal Antenna Arrays for Hemispherical Scan Coverage", IEEE Transactions on Antennas and Propagation, Vol. 55, No.2, September 2007
- [4] Thomas E. Morton, Krishna M. Pasala, "Performance Analysis of Conformal Conical Antenna Arrays for Airborne Vehicles", IEEE Transactions on Aerospace and Electronic Systems, vol.46 no.3, July 2006
- [5] Peter Knott, "Faceted vs. Smoothly Curved Antenna Front-End for a Conformal Array Radar Demonstrator", Research Institute for High Frequency Physics and Radar, Germany, 2008
- [6] Daniel B. Ferreira, J.C.da S. Lacava, "Microstrip Antennas Conformed onto Spherical Surfaces", Brazil, April 2011

- [7] Alfredo Catalani et all. “Ku-Band Hemispherical Fully Electronic Antenna for Aircraft in Flight Entertainment”,International Journal of Antenna and Propagation,Article ID 230650-2009
- [8] Lars Joseffsson, Patric Persson., “Conformal Array Antenna Theory and Design”, The IEEE Press Series on Electromagnetic Wave Theory, USA 2006.
- [9] www.mathworks.com (Last Accessed on 10.04.2015)
- [10] www.ansoft.com (Last Accessed on 12.04.2015)
- [11] Kunal Parikh, “Simulation of Rectangular, Single Layer, Coax-Fed Patch Antennas Using Agilent High Frequency Structure Simulator(HFSS)”, Virginia Polytechnic University, December 2003
- [12] Kin-Lu Wong, ”Design of Nonplanar Microstrip Antennas and Transmission Lines”, Wiley, 1999
- [13] Ali Özgür Taşoğlu, “Analysis and Design of Cylindrically Conformal Microstrip Antennas”, METU Master Thesis, July 2011
- [14] Jeong Phill Kim, “Optimum Design of an Aperture Coupled Microstrip Patch Antenna”, Microwave and Optical Technology Letters, Vol.30 No.1, 5 March 2003
- [15] Peter L. Sullivan,Daniel H. Schaubert, “Analysis of an Aparture Coupled Microstrip Antenna”, IEEE Transactions on Antennas and Propagation, vol.ap-34, No.8, August 1986
- [16] www.satimo.com (Last Accessed on 15.04.2015)

- [17] David M. Pozar, "A Review of Aperture Coupled Microstrip Antennas", University of Massachusetts at Amherst, 1996
- [18] David M. Pozar, "The Active Element Pattern", IEEE Transactions on Antennas and Propagation, vol.34, No.8, August 1994
- [19] Hans Steyskal, Jeffrey S. Herd, "Mutual Coupling Compensation in Small Antenna Arrays", IEEE Transactions on Antennas and Propagation, vol.38, No.12, December 1990
- [20] J.L. Masa Campos, J.M. Fernandez, M. Sierra-Castaner, M. Sierra Perez, "Coupling Characterization and Compensation Model for Antenna Arrays", Journal of Microwave and Optoelectronics, Vol. 4, No. 2, December 2005
- [21] Randy L. Haupt, "Antenna Arrays A Computational Approach", Wiley-IEEE Press, April 12, 2010
- [22] Pramod Kumar, A.K. Singh, "Phase Only Pattern Synthesis for Antenna Array Using Genetic Algorithm for Radar Applications", Indian Journal of Radio&Space Physics, Vol 46, pp259-264, August '013
- [23] Wulf-Dieter Wirth, "Radar Techniques Using Array Antennas", The Institution of Electrical Engineers, 2001
- [24] Kin-Lu Wong, "Design of Nonplanar Microstrip Antennas and Transmission Lines", Wiley, 1999
- [25] Egemen Yıdırım, Erdinç Erçil, Doğanay Doğan, "L Band Silindirik Anten Çalışmaları", 6. URSI Konferansı, İstanbul, 2012

[26] Ahmed K. Aboul-Seoud, Alaa El-Din S. Hafez, Ahmed M. Hamed, Mohamed Abd-El-Latif, "A Conformal Conical Phased Array Antenna for Modern Radars", IEEE, 2014

[27] Adnan Affandi, Mubashshir Husain, Navin Kasim, "Optimization for Spherical Phased Array Antenna", International Refereed Journal of Engineering and Science, Volume 2, Issue 2, February 2013

[28] Benjamin D. Braaten, Sayan Roy, Irfan Irfanullah, Sanjay Mariyal, Dimitris E. Anagnostou, "Phase-Compensated Conformal Antennas for Changing Spherical Surfaces", IEEE Transactions on Antennas and Propagation, Vol. 62, No. 4, April 2014

APPENDIX A

MODELLING CONFORMAL ANTENNA ARRAYS USING HFSS

HFSS is one of the most popular commercial tool for simulating 3-D full-wave electromagnetic fields. This appendix is prepared as a guide for modeling conformal antenna structures in HFSS. Assigning multiple ports to antenna arrays and simulating array excitation coefficients is explained. Also exporting far field simulation data with reference to a phase center is explained. In Figure A-1 a general view of Ansoft HFSS is given.

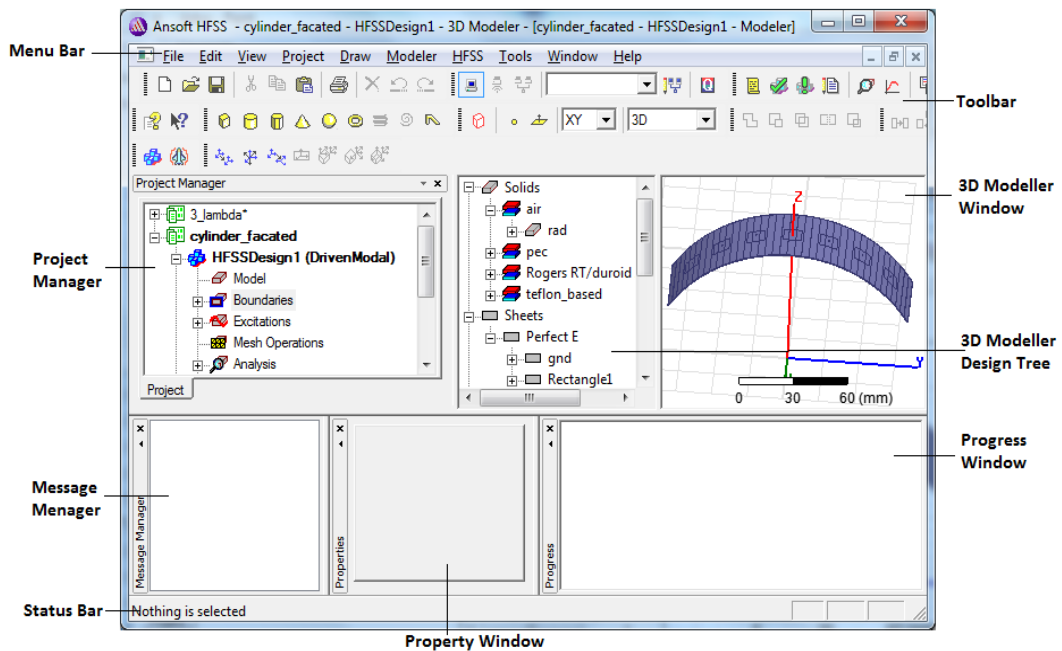


Figure A-1 Main view of HFSS software

In Project Manager and 3D Modeler Tree structure of the designed project can be observed. Message Manager allows user to view any errors or warnings occur before the simulation process. Property Window allows users to change parameters of the model. Progress Window shows simulation process. Finally 3D Modeler Window contains modelled structure.

In this document modeling steps for a 5 element cylindrical antenna array is explained step by step. Dielectric material used in the array is 0.508mm thick RO5880. First step is modeling a 0.508mm thick plate. First draw two cylinders with r mm and $r+0.508$ mm radius. Then subtracting these two bodies gives a cylindrical structure with 0.508mm thickness.

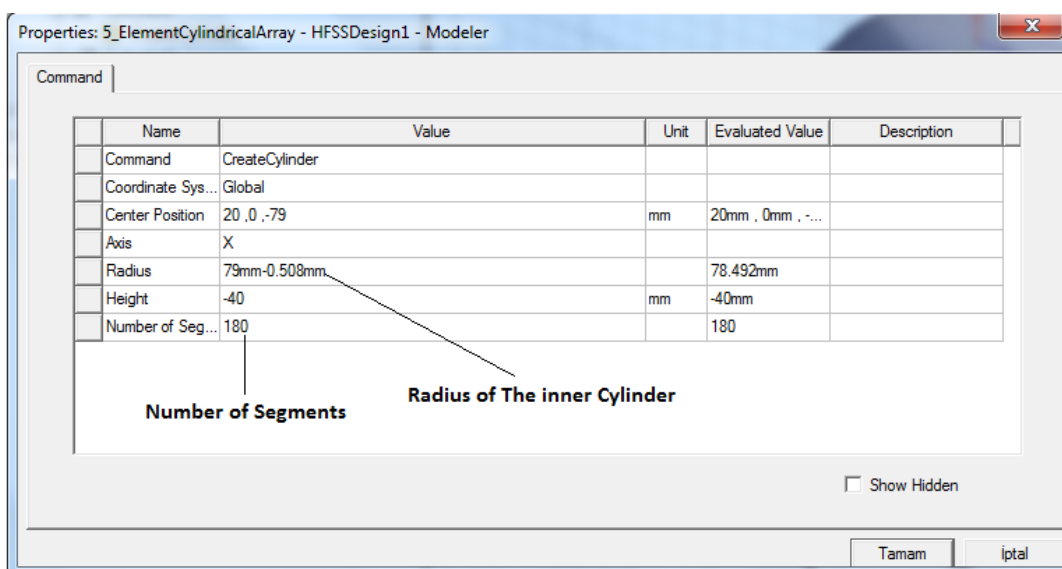


Figure A-2 Property window for cylinder

In Figure A-2 property window for the inner cylinder is given. This cylinder is modelled 0.508 mm smaller in radius than the outer cylinder. Number of segments for this cylinder is selected as 180. This means a single segment corresponds to 2° . Number of segments can be selected smaller. After creating two cylinders small

cylinder is subtracted from the large cylinder. Using the subtract tool shown in Figure A-3 this operation can be done.

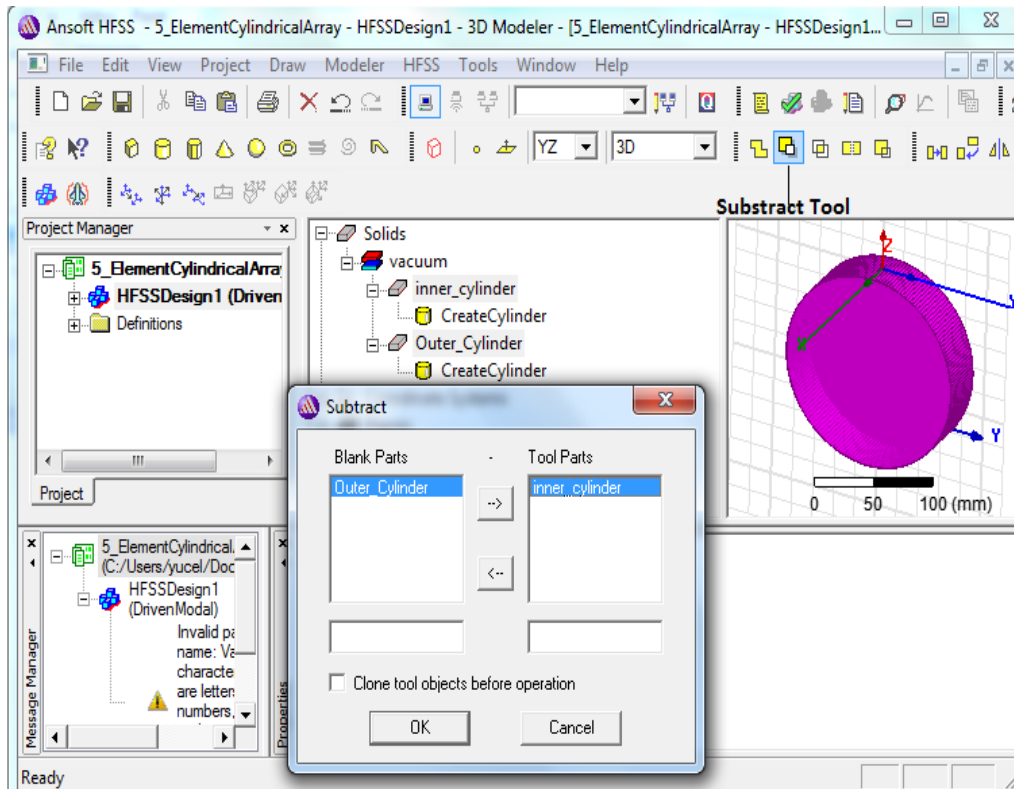


Figure A-3 Subtract option

Subtracting two cylinders leaves us a ring as shown in Figure A-4. Then a material can be assigned to the created ring by right clicking on the object name in 3D modeler design tree.

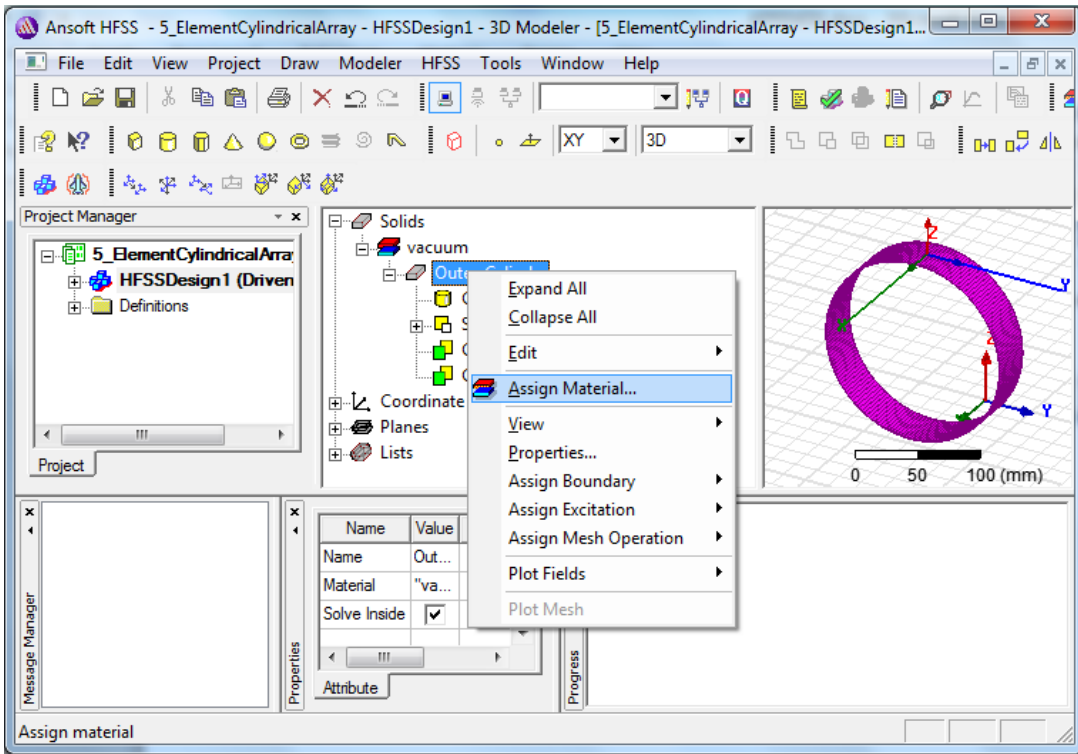


Figure A-4 Material assign option

In Figure A-5 HFSS material library is shown. In this library RO 5880 is available as default .It is also possible to add a new material to HFSS material library by using ‘Add Material’ button.

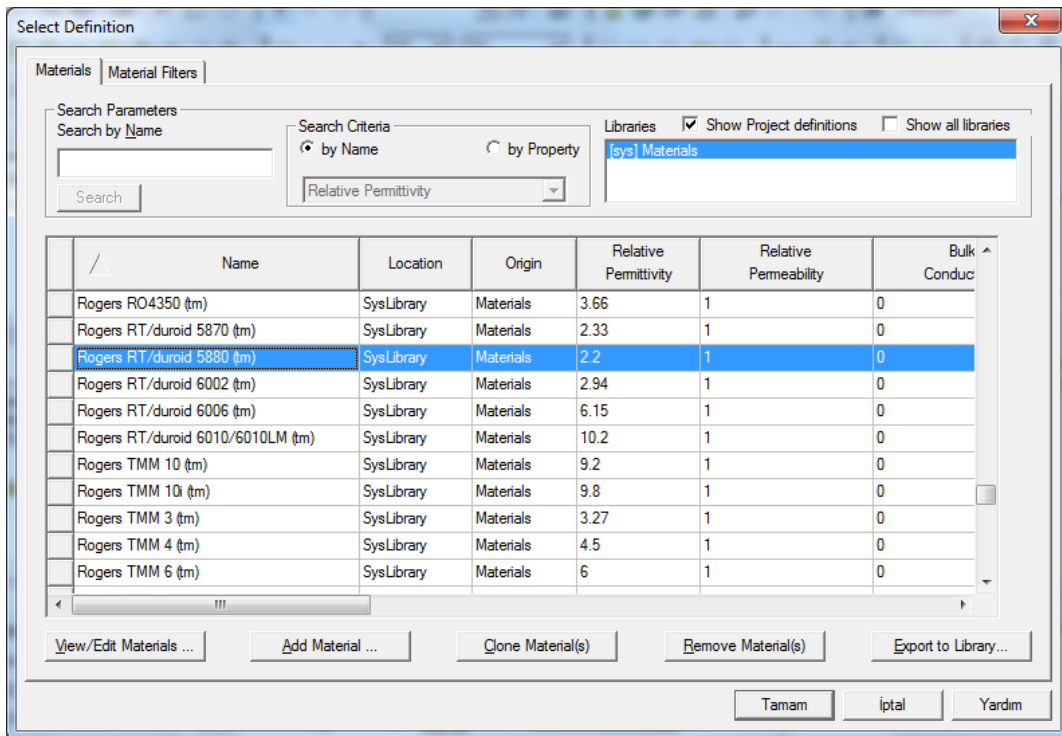


Figure A-5 HFSS material library

This ring can also be modelled by using only a single cylinder. In that case an object need to be created from the outer surface of the cylinder and then it should be thickened 0.508mm. Creating an object from surface of another object and thickening a plate is explained in the following parts of this documents.

Since the created cylinder is faceted, probe that feed the antenna should be on the planar side of the faceted structure. It is possible to rotate the whole cylinder. On that case modeled patch antenna will be on the planar side. Modeling probe on the planar part is much more easier than modeling it on the edge of the two faceted parts. To do this a reference coordinate system, which is the center of the cylinder, is required. It can be done using 'Modeller' option of the HFSS as shown in Figure A-6. The new coordinate system is -79mm away from the global coordinate system.

This offset value is entered using the coordinate entry segments at the bottom of the HFSS window.

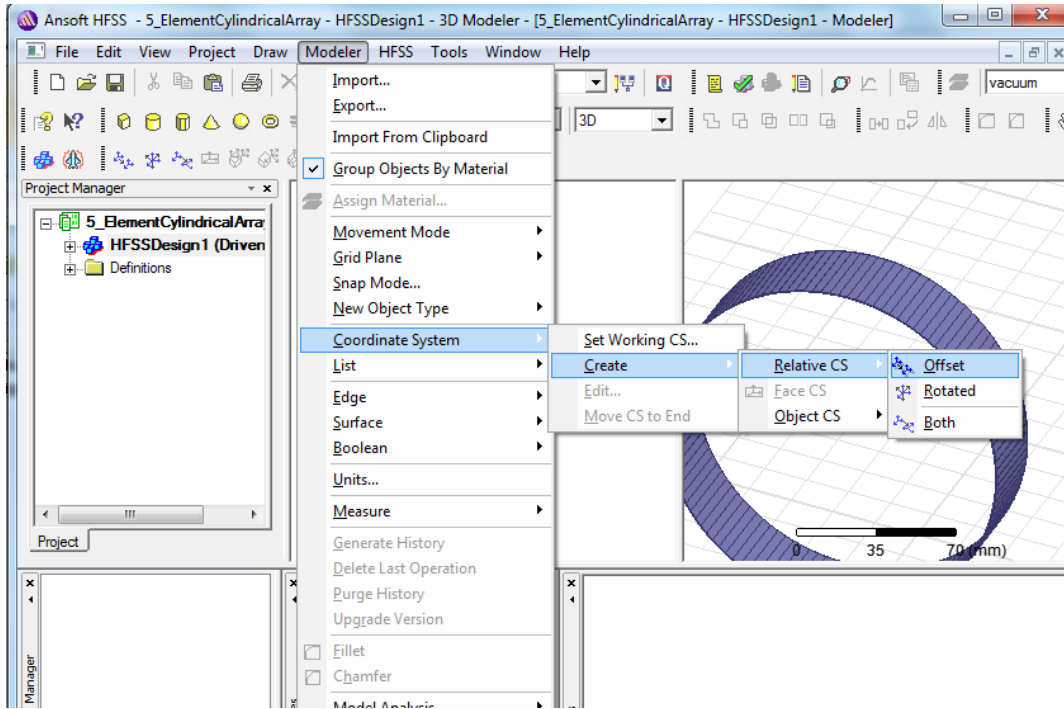


Figure A-6 Create relative coordinate system menu

After creating a relative coordinate system, the created coordinate system should be set as the active coordinate system. This can be done by following the steps in Figure A-7 and Figure A-8.

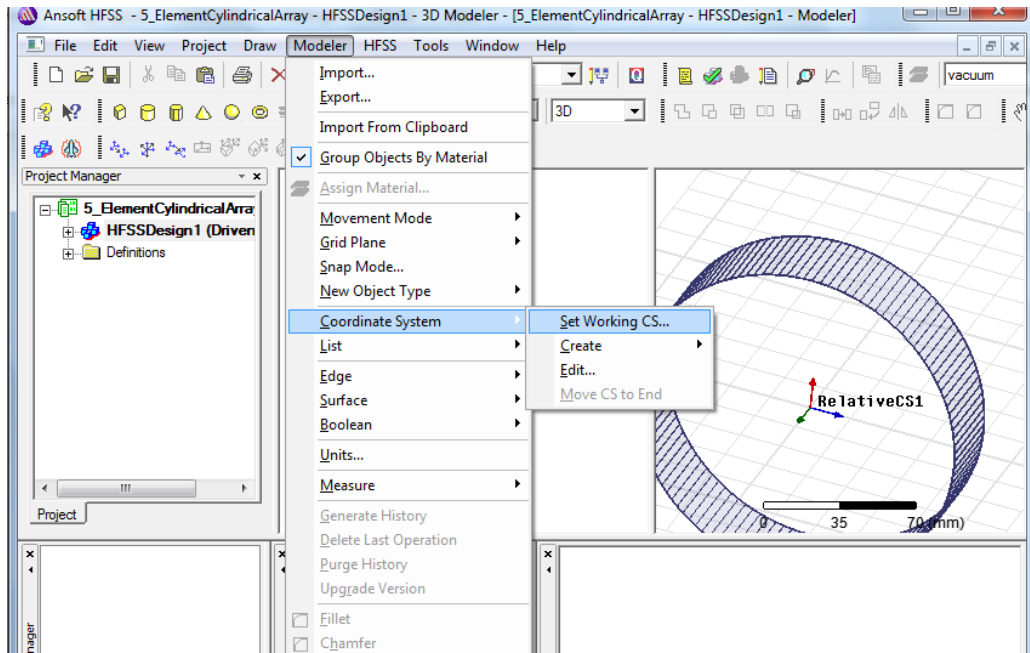


Figure A-7 Set relative coordinate as the reference coordinate Step 1

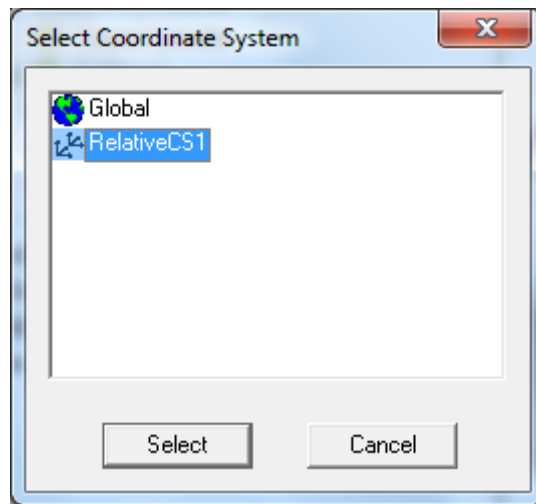


Figure A-8 Set relative coordinate as the reference coordinate Step 2

Using 'Rotate' option shown in Figure A-9, the whole cylinder can be rotated.

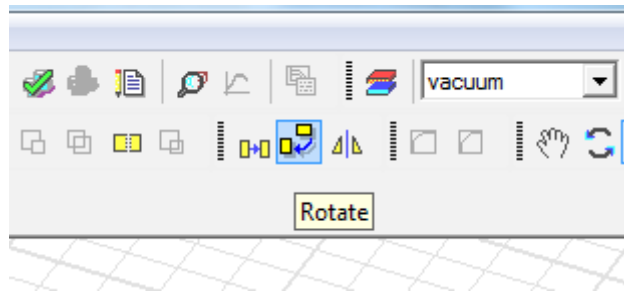


Figure A-9 Rotate option

Entering desired rotation angle in Angle segment and selecting rotation axis as 'X' axis, as shown in Figure A-10 rotation operation is completed.



Figure A-10 Rotate menu

After rotating cylinder reference coordinate system should be selected as 'Global' again as shown in Figure A-11.

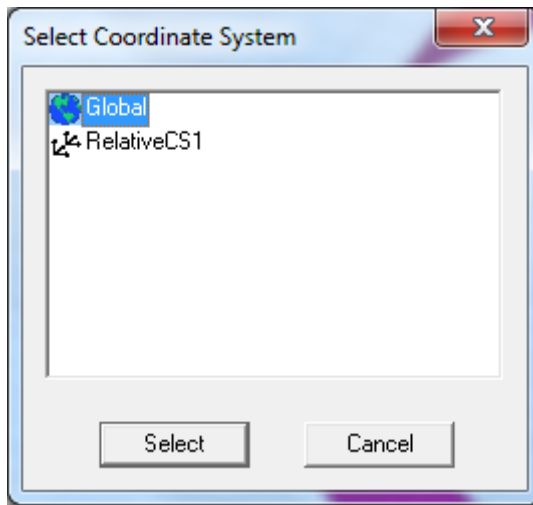


Figure A-11 Set reference coordinate system

To create patch antenna on the planar face on the cylinder, a face coordinate system should be assigned on the planar face. First face selection mode should be activated. It can be selected as shown in Figure A-12.

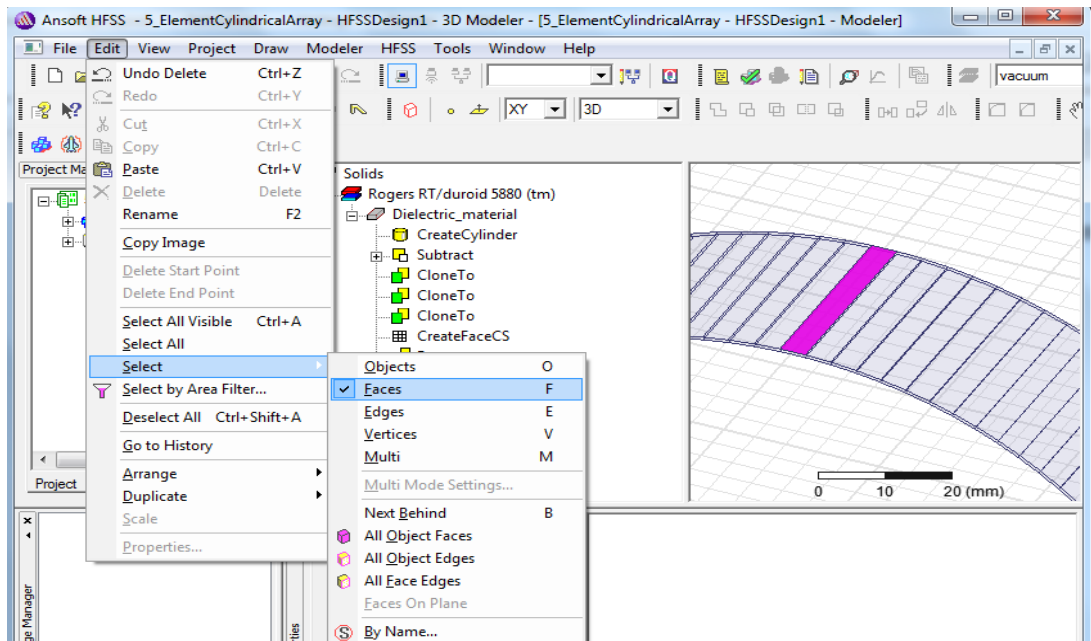


Figure A-12 Face Coordinate system selection

By activating face selection mode in HFSS now it is possible to select a planar face and assign a coordinate system to it. First planar surface should be selected by left clicking on the surface. It will be highlighted as shown in Figure A-13.

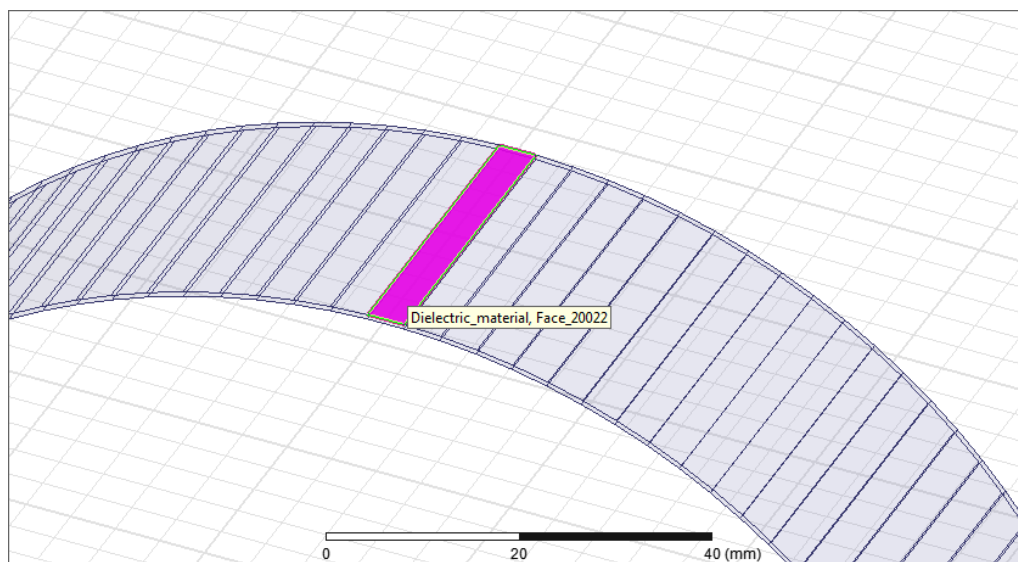


Figure A-13 Selected planar face

In 'Modeller' option 'Create Face CS' can be selected as shown in Figure A-14.

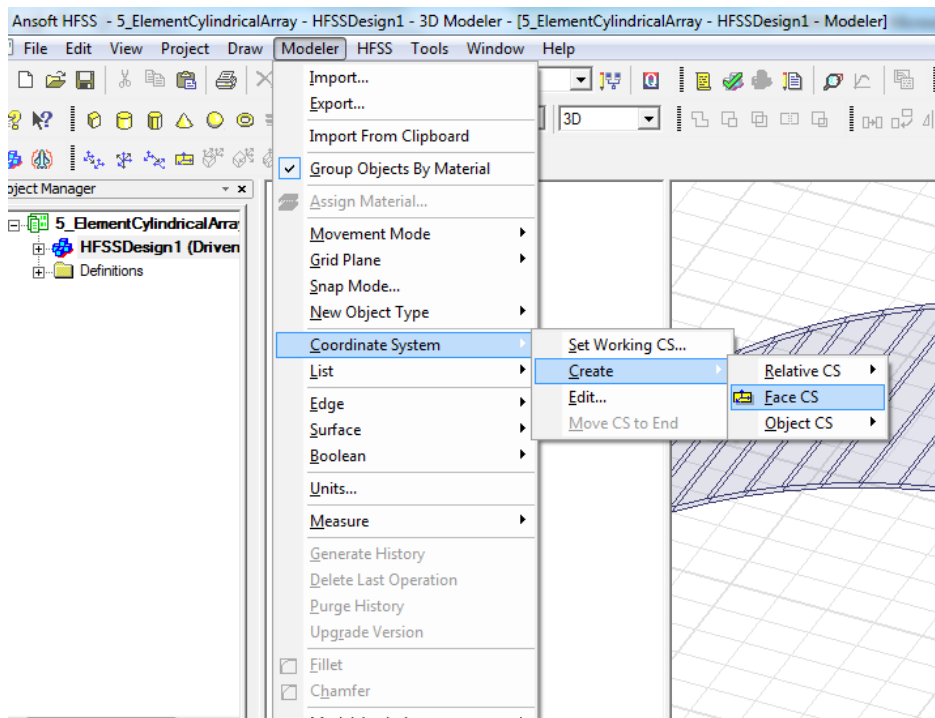


Figure A-14 Face coordinate system creation

Then right clicking on the center of the face and on the middle of the one edge, a face coordinate system is created as shown in Figure A-15.

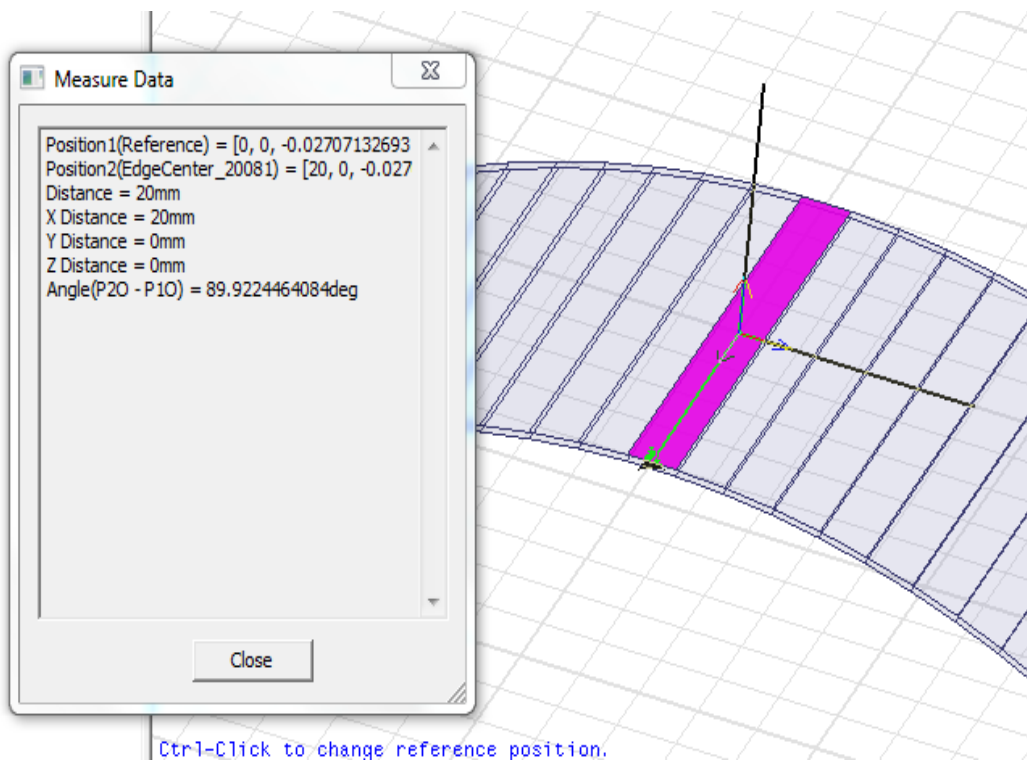


Figure A-15 Face coordinate center selection

Created coordinate system should set as reference coordinate as shown in Figure A-16.

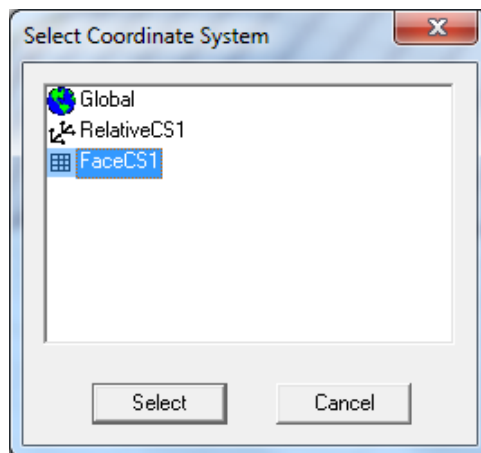


Figure A-16 Set Face coordinate as reference coordinate system

In this step patch antenna can be created on the cylindrical surface with reference to Face Coordinate system. In Figure A-17 first patch antenna created is given.

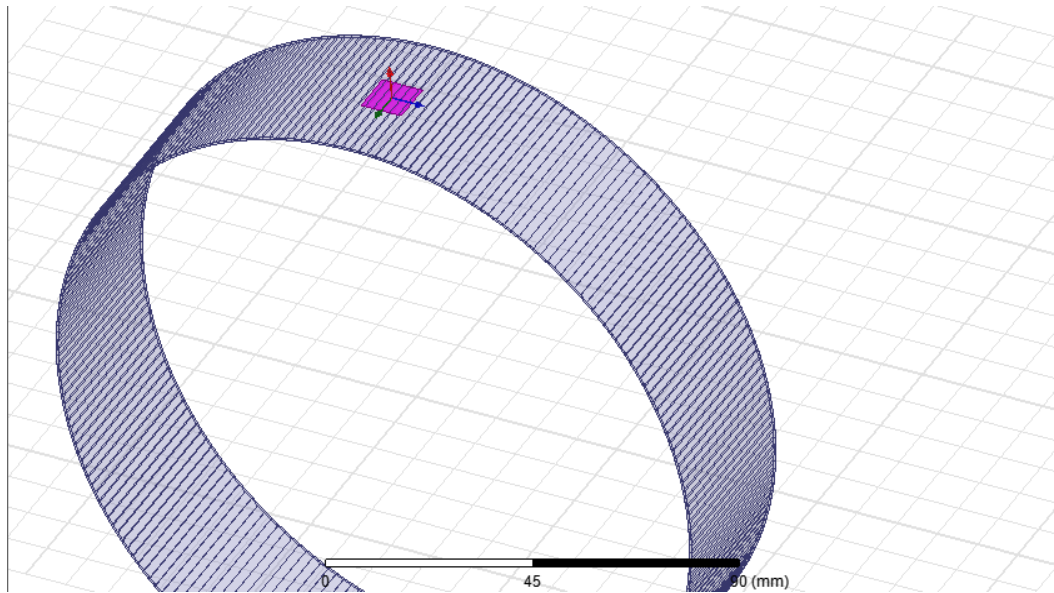


Figure A-17 Modelled patch antenna

This antenna has a face contact with the cylinder. By selecting both objects in the Modeller tree as shown in Figure A-18, patch antenna can be wrapped on cylinder.

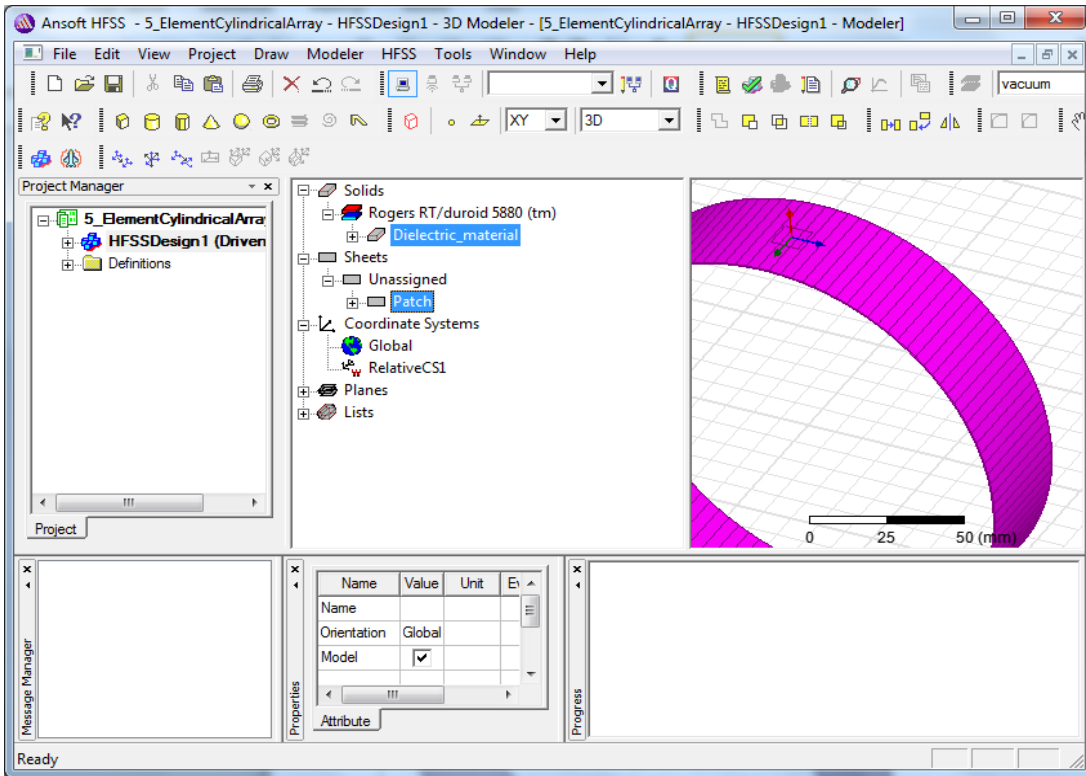


Figure A-18 Patch and cylinder on modeler tree

After selecting both objects, using ‘Wrap Sheet’ option of the HFSS, patch antenna can be wrapped on the cylinder as shown in Figure A-19.

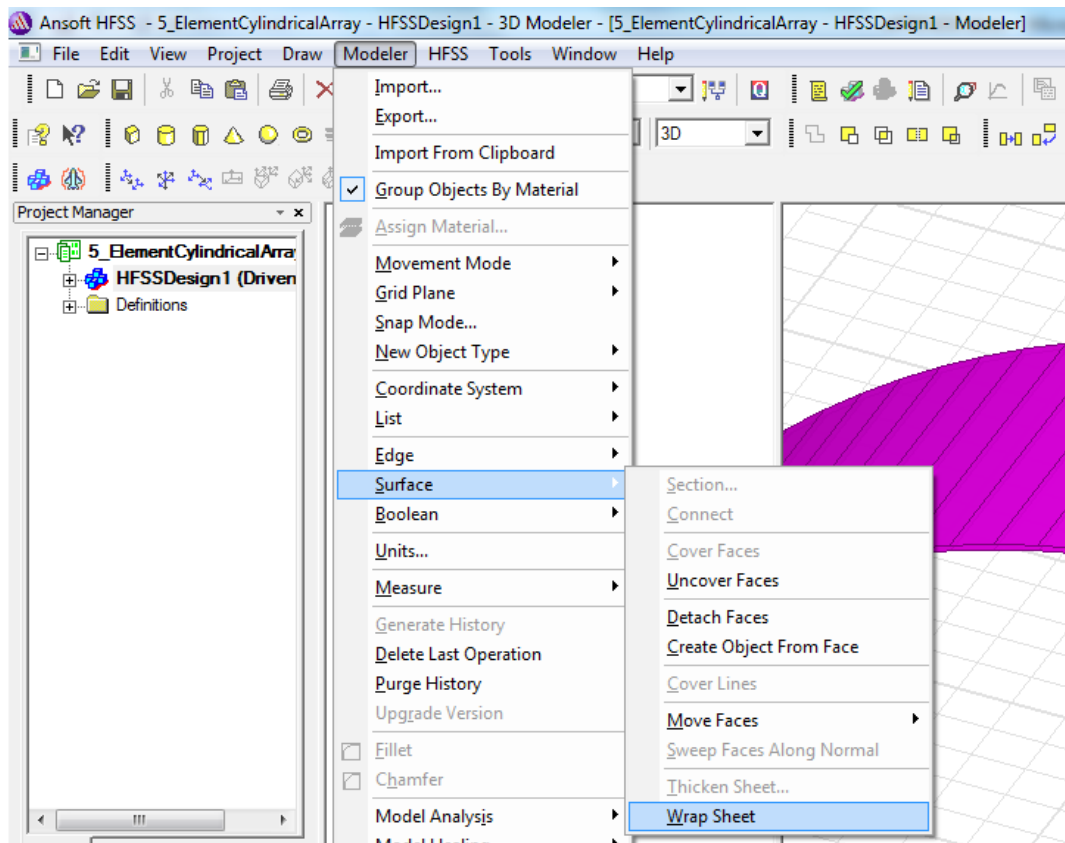


Figure A-19 Wrap Sheet option

After this operation, in material history 'WrapSheet' section appears as shown in Figure A-20. Deleting this section under the wrap operation.

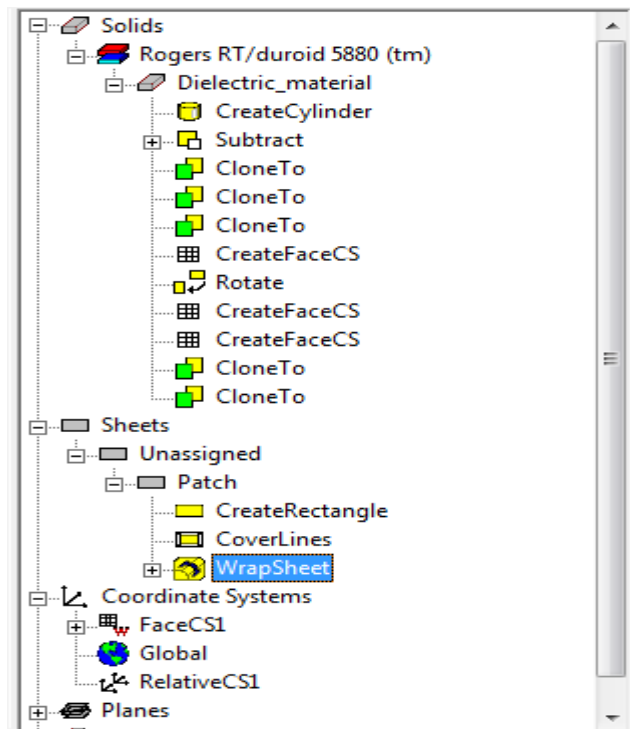


Figure A-20 WrapShhet in modeler tree

To reduce the simulation time modelled ring should be splitted in two parts, and unused part should be removed. As in this work only 5 elements are placed on the cylindrical structure, it is not necessary to use the whole cylinder. To do this a reference coordinate system should be set to Reletive Coordinate System1 which is the center of the cylinder created before. Then select split option in the toolbar as shown in Figure A-21.

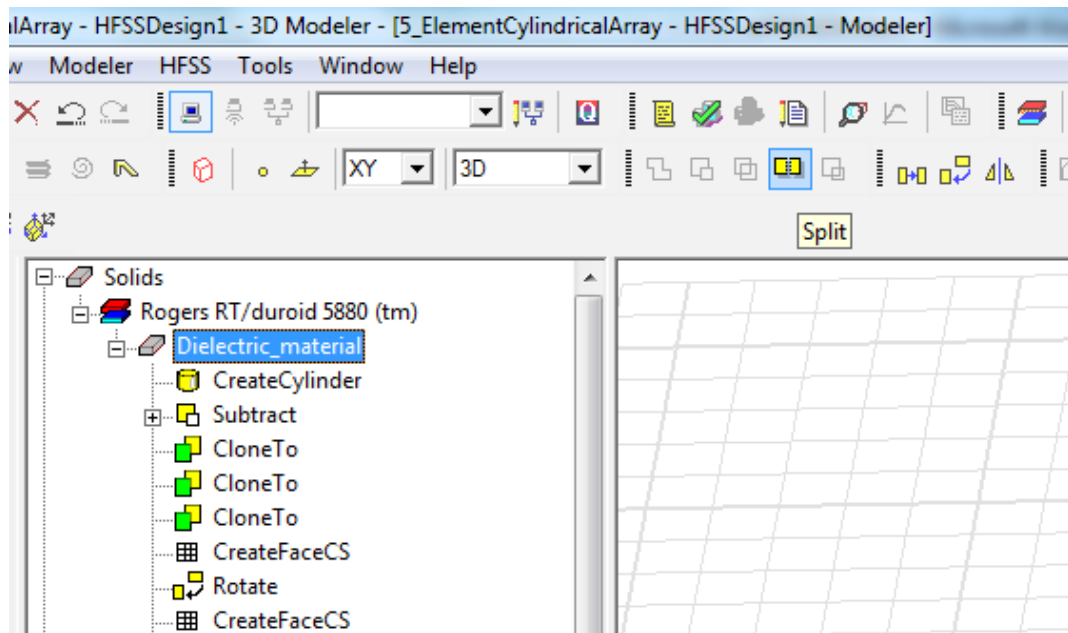


Figure A-21 Split Option in HFSS toolbar

In the split menu, Split plane, Keep fragments and Split objects options should be selected properly as given in Figure A-22.

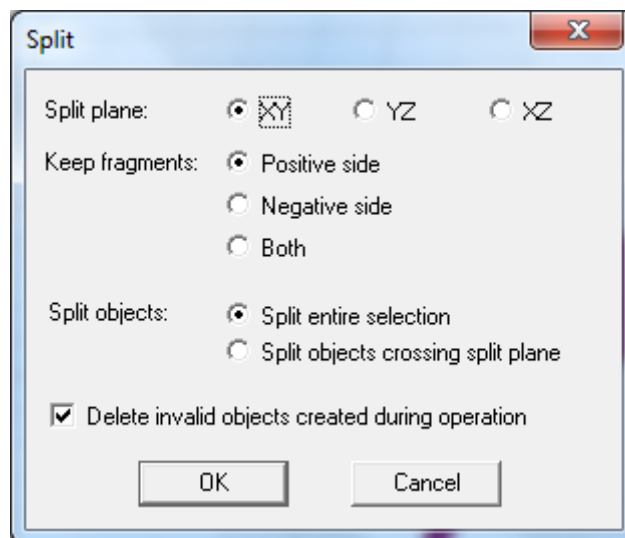


Figure A-22 Split menu

The splitted cylinder is given in Figure A-23.

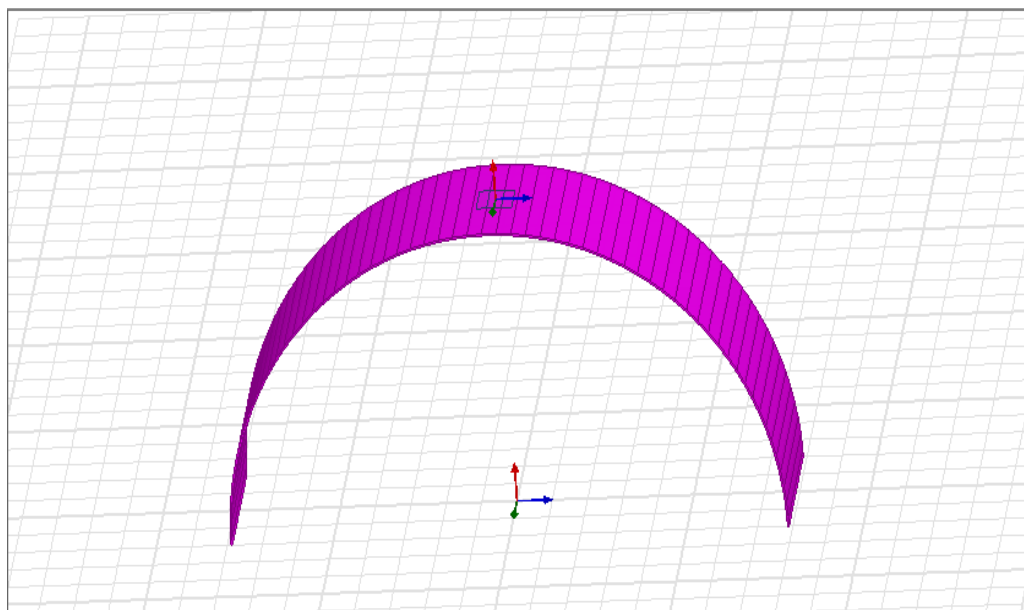


Figure A-23 Splitted cylinder

In HFSS it is possible to create objects from surface of another object. For a coaxial probe fed patch antenna bottom side of the cylinder is ground plane. Surfaces of all the bottom side of the cylinder should be selected first, then using create object option shown in Figure A-24 faceted ground plane is created. This plane initially consists of several planar plates. Using Unite option shown in Figure A-25 a single plane is obtained.

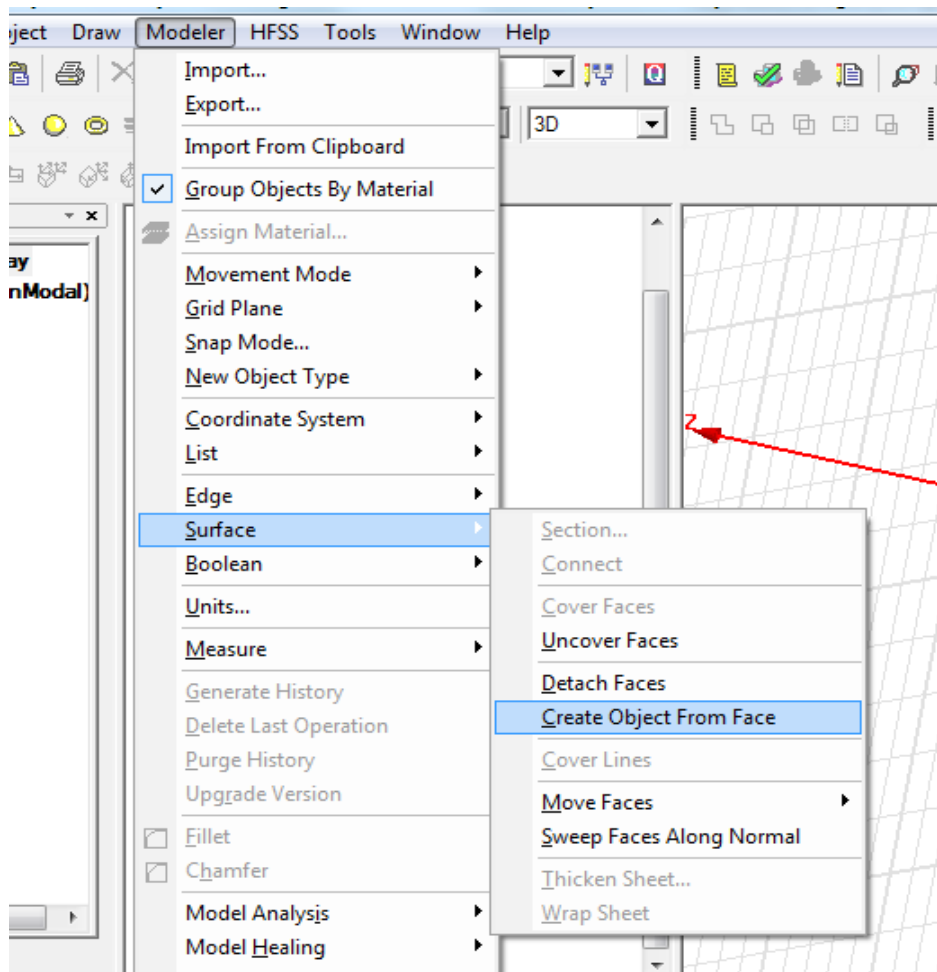


Figure A-24 Create object from face option

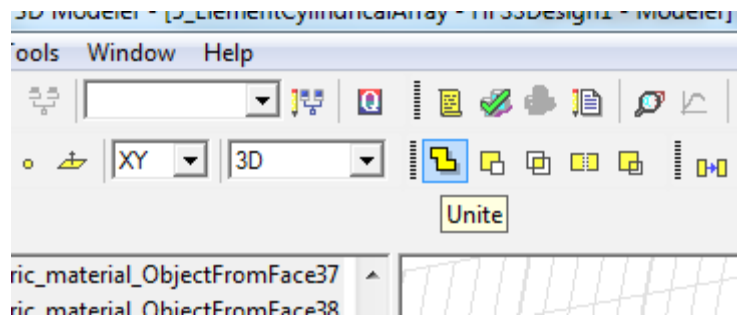


Figure A-25 Unite option in HFSS

For the probe-fed patch antenna a probe, a feed and a coaxial probe is required. All three structures are cylindrical. Property window for the probe is given in Figure A-26. Similarly feed and coaxial part of the probe can be modelled.

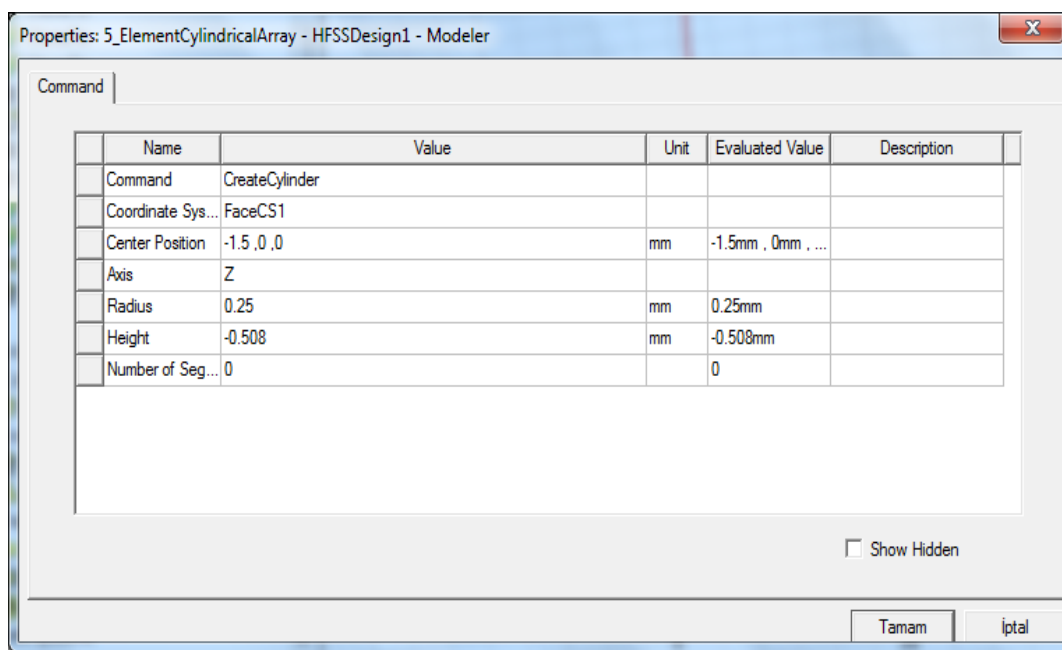


Figure A-26 Property window for the probe

On the ground plane a hole is required to allow incoming wave to couple the antenna. It can be done following Figure A-27, A-28, A-29 and A-30.

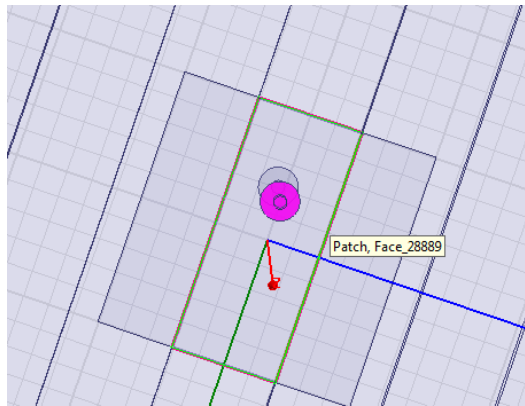


Figure A-27 Select face of the coaxial probe

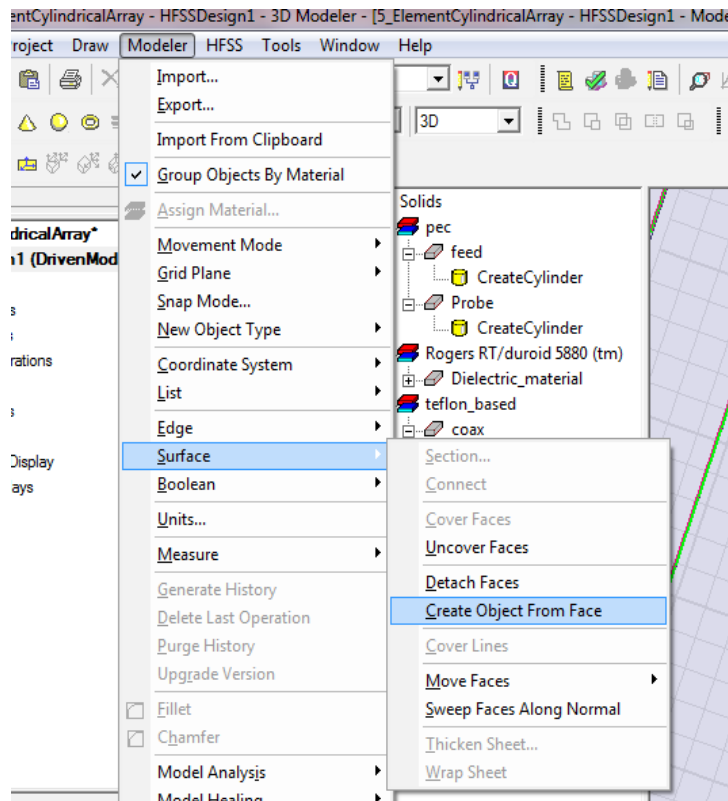


Figure A-28 Create object from selected coaxial face

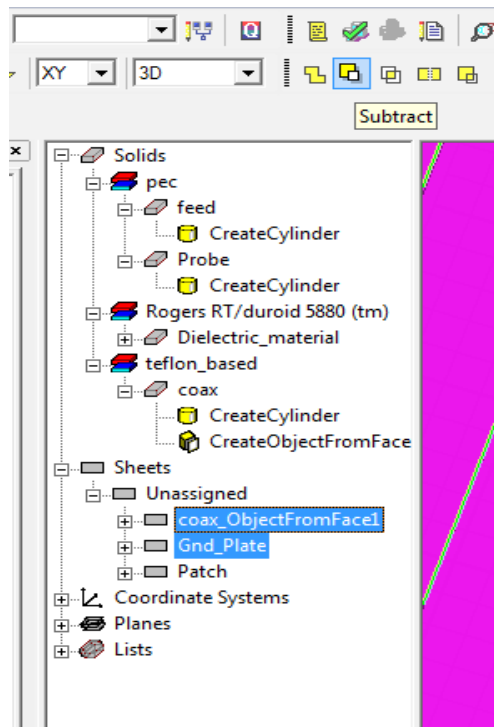


Figure A-29 Select both Ground and coax face object

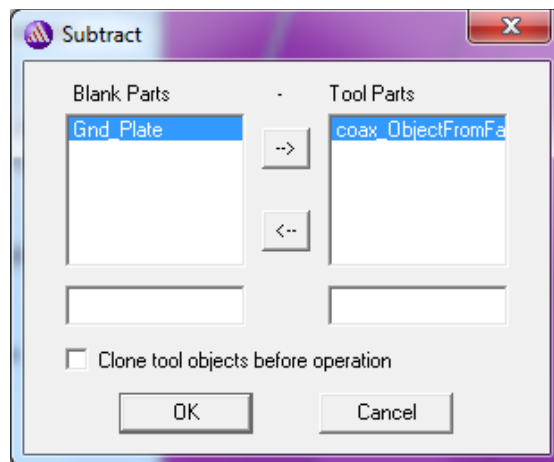


Figure A-30 Subtract two objects

After these operations ground plane will have a hole as shown in Figure A-31.

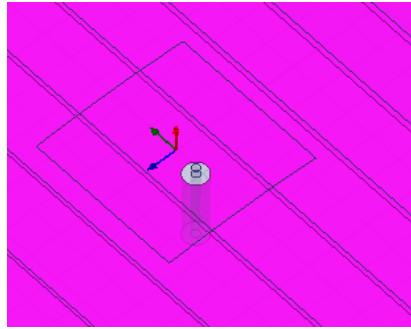


Figure A-31 Ground plane with hole

Feed and probe part of the coaxial probe are modelled as ‘PEC’ in HFSS material library. The dielectric part is modelled as ‘Teflon Based’ in HFSS material library. Due to the curved geometry coaxial probe will be located in the radiation boundary. So the surface of the coaxial probe should be modelled as Perfect E on HFSS following Figure A-32.

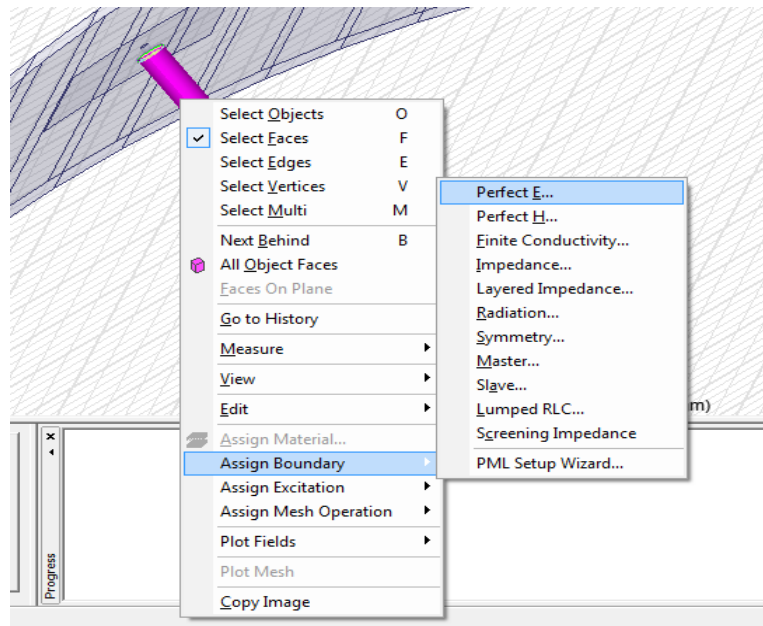


Figure A-32 Assigning Perfect E boundary to coaxial probe

Also excitation port of the coaxial probe will remain in the radiation boundary. So it is necessary to place a PEC plate at the end of the coaxial probe following the steps defined in Figure A-33, A-34, A-35 and A-36.

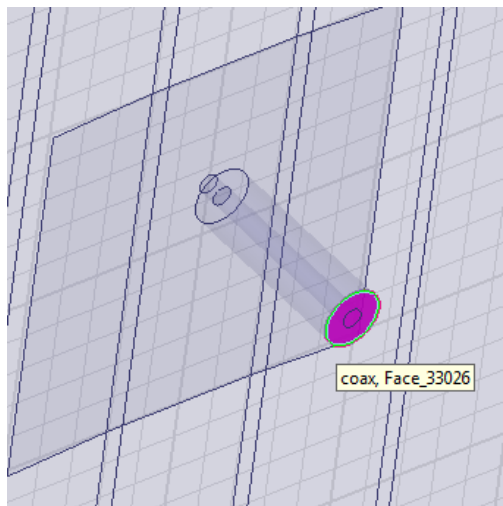


Figure A-33 Selection of the coaxial face and creating an object

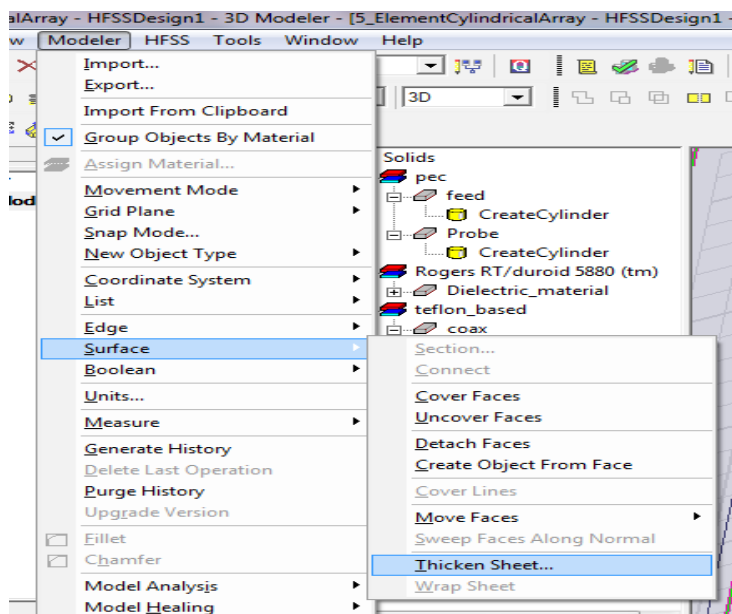


Figure A-34 Thickening the created sheet

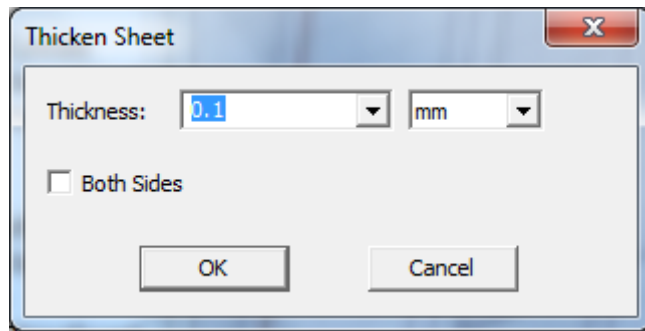


Figure A-35 Thicken Sheet menu

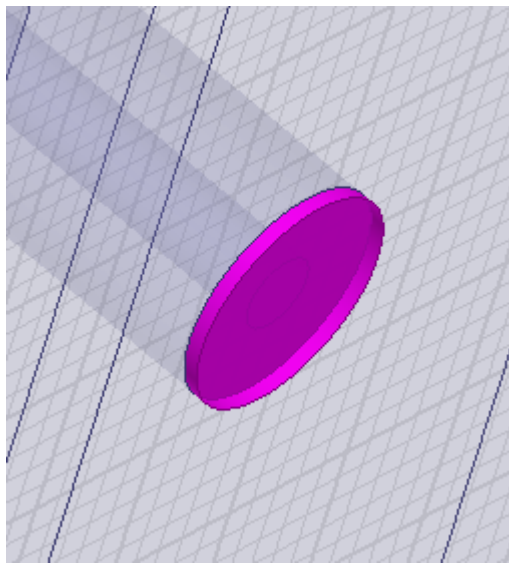


Figure A-36 Created PEC plate for excitation port

In the next step it is necessary to define an excitation for the antenna. This process is shown in detail in Figure A-37, A-38, A-39, A-40, A-41 and A-42.

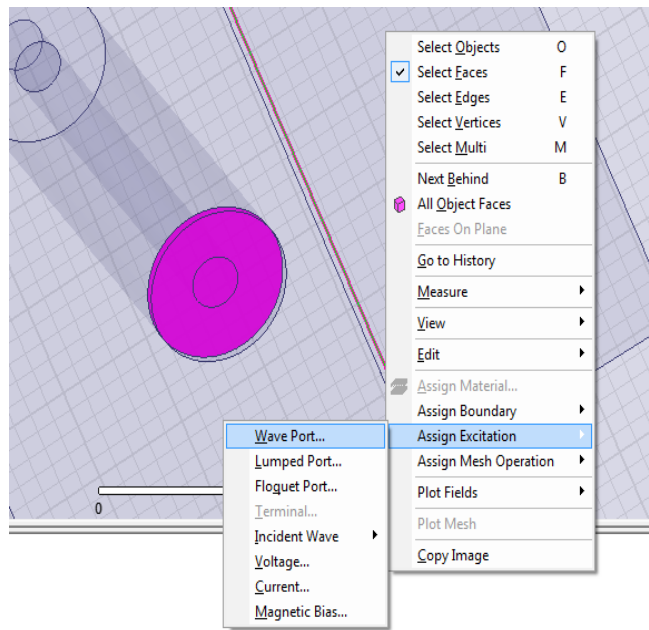


Figure A-37 Assign excitation for the selected port

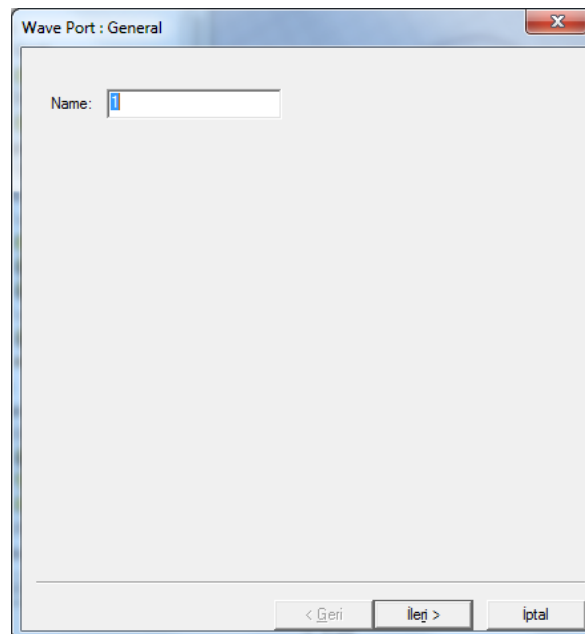


Figure A-38 Wave port menu-Port Name

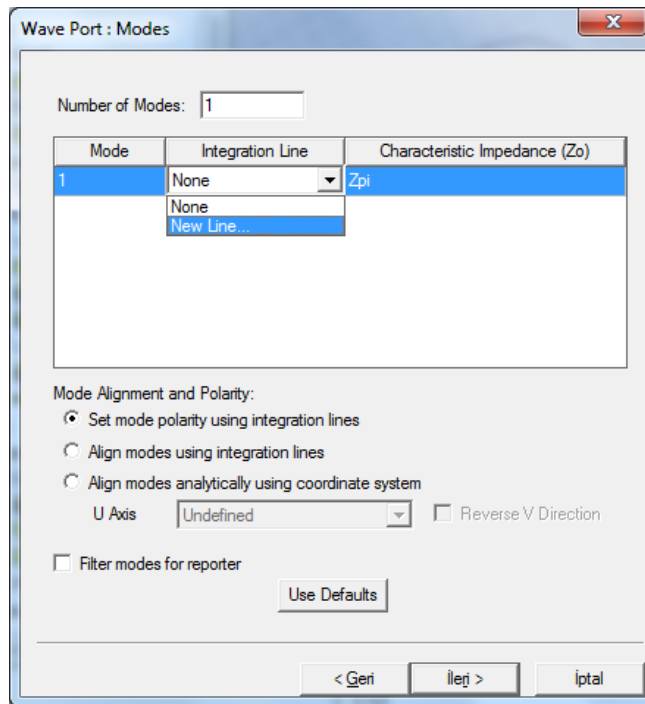


Figure A-39 Wave Port Menu-Selecting new integration line

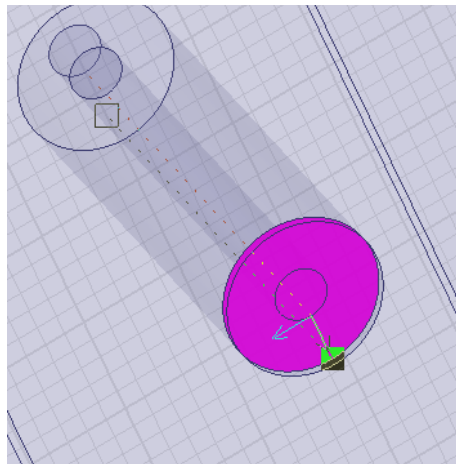


Figure A-40 Selecting integration line start and end points

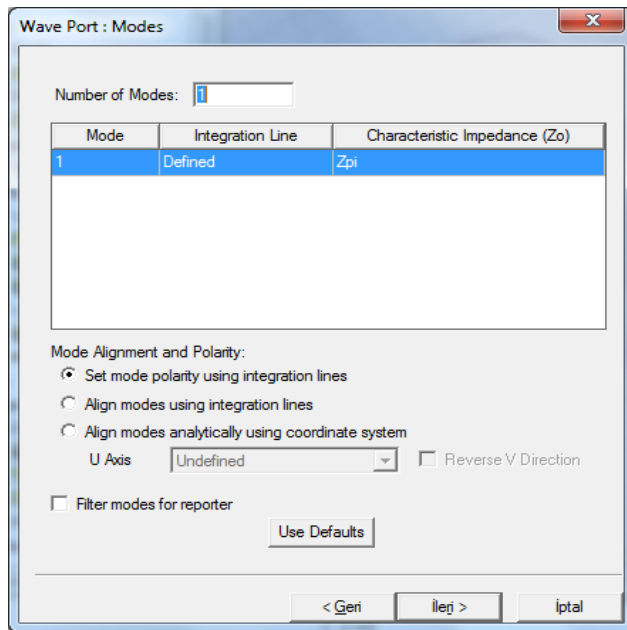


Figure A-41 Wave Port Menu-New integration line is defined

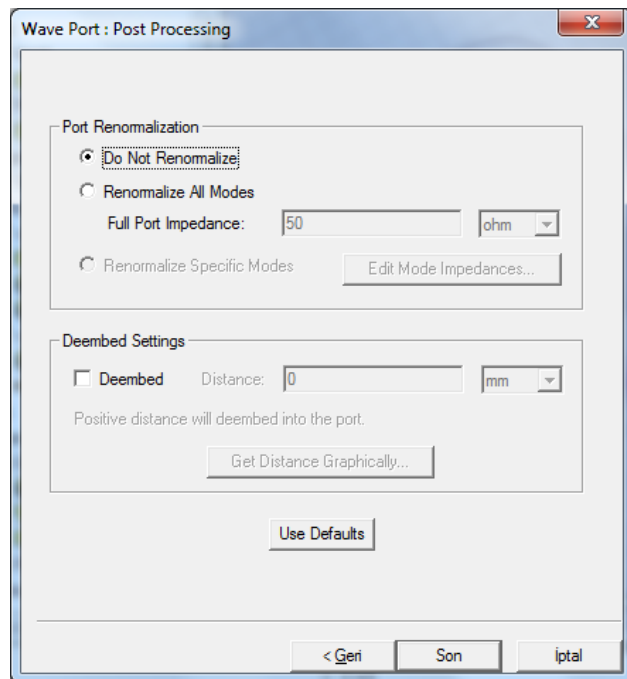


Figure A-42 Wave Port Menu-finishing the operation

An excitation port should be specified by adding a solution setup. In these steps solution frequency, sweep and convergence details of the simulation are defined. Details of these steps are given in Figure A-43, A-44, A-45 and A-46.

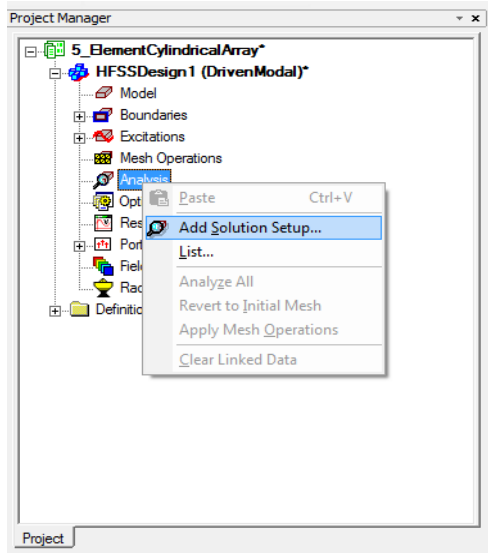


Figure A-43 Add solution setup

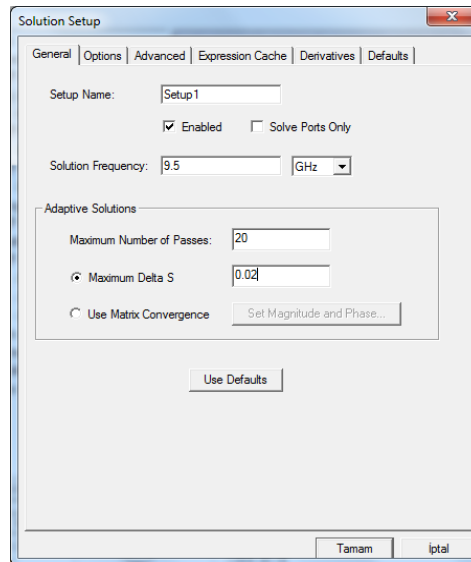


Figure A-44 Define solution frequency, number of passes and convergence limit

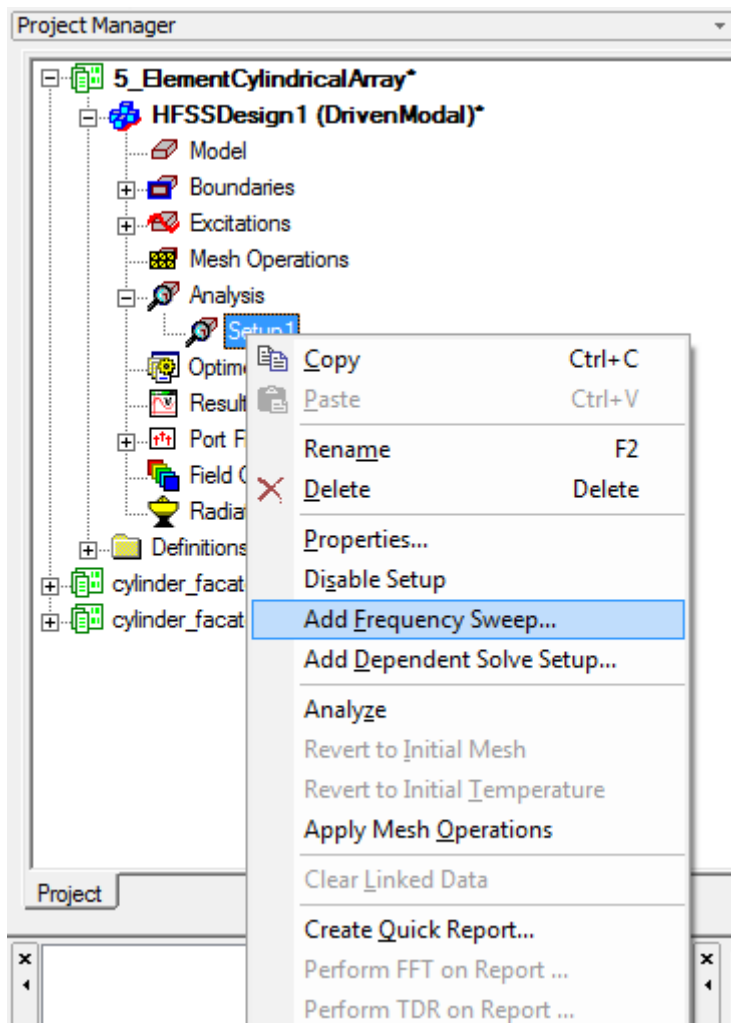


Figure A-45 Add Frequency Sweep

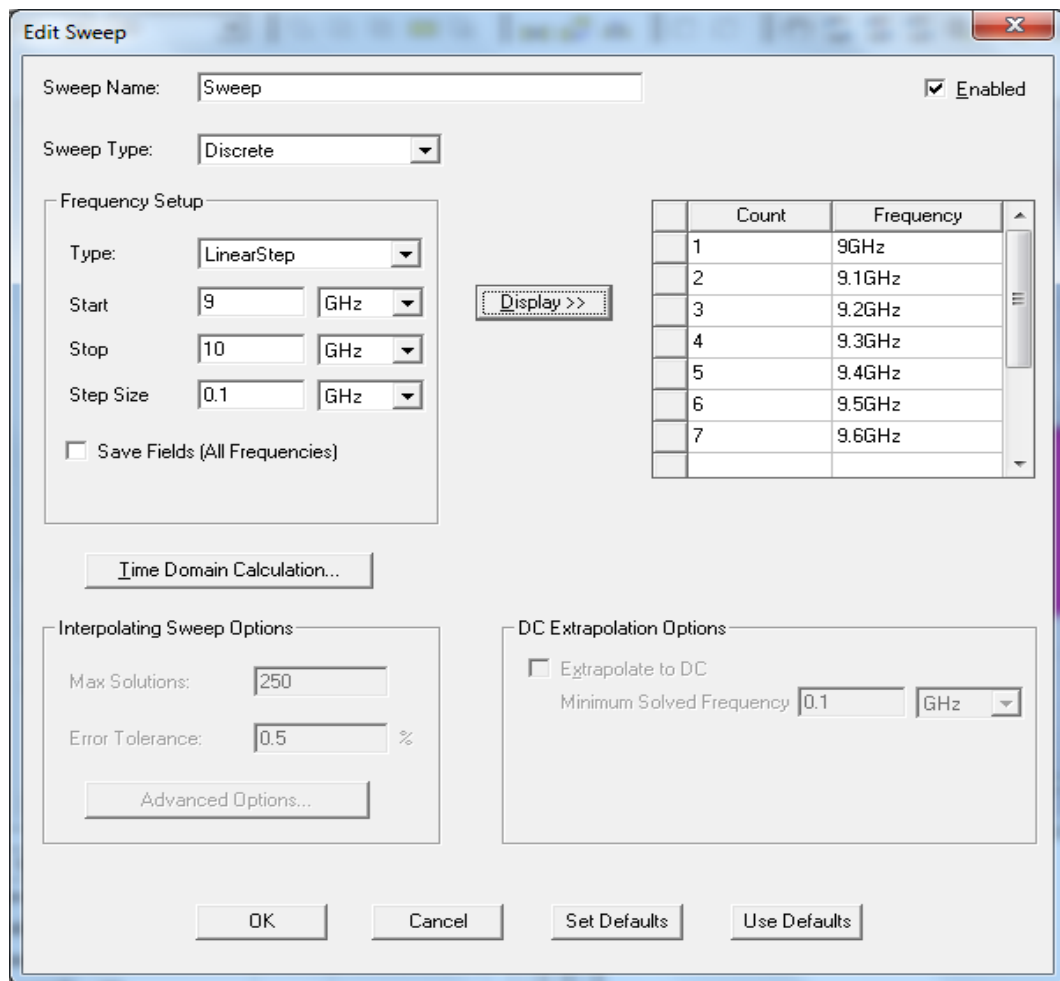


Figure A-46 Define sweep type and start-stop frequencies

Ground plane and patch antenna surfaces are modelled as Perfect E as shown in Figure A-47 and A-48.

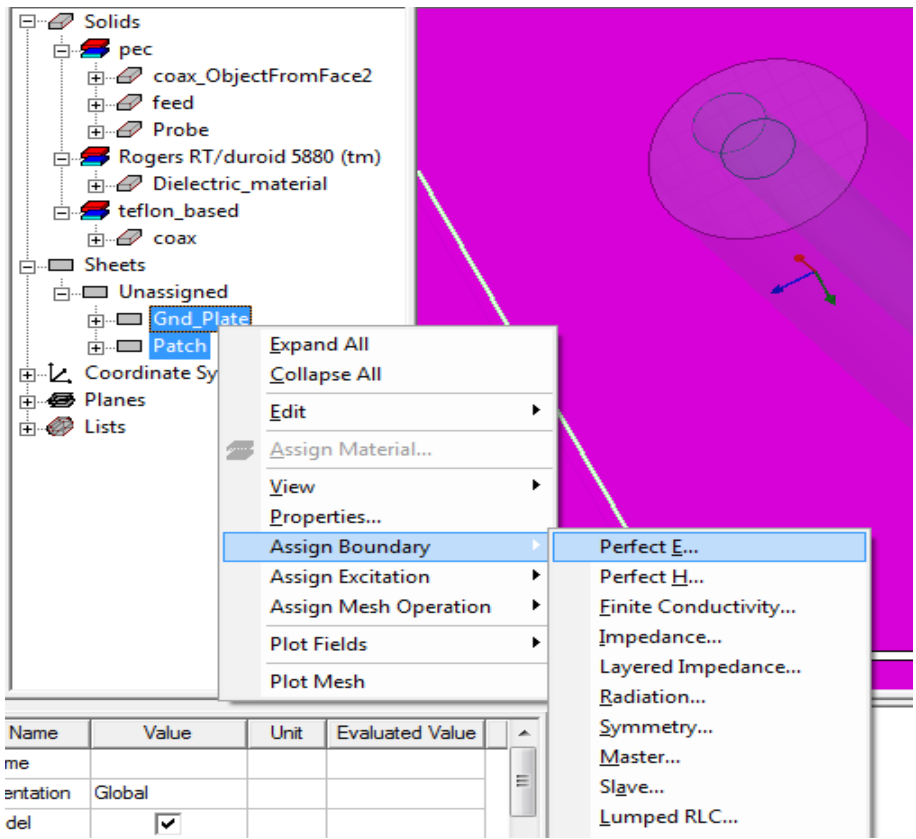


Figure A-47 Assign Perfect E boundary

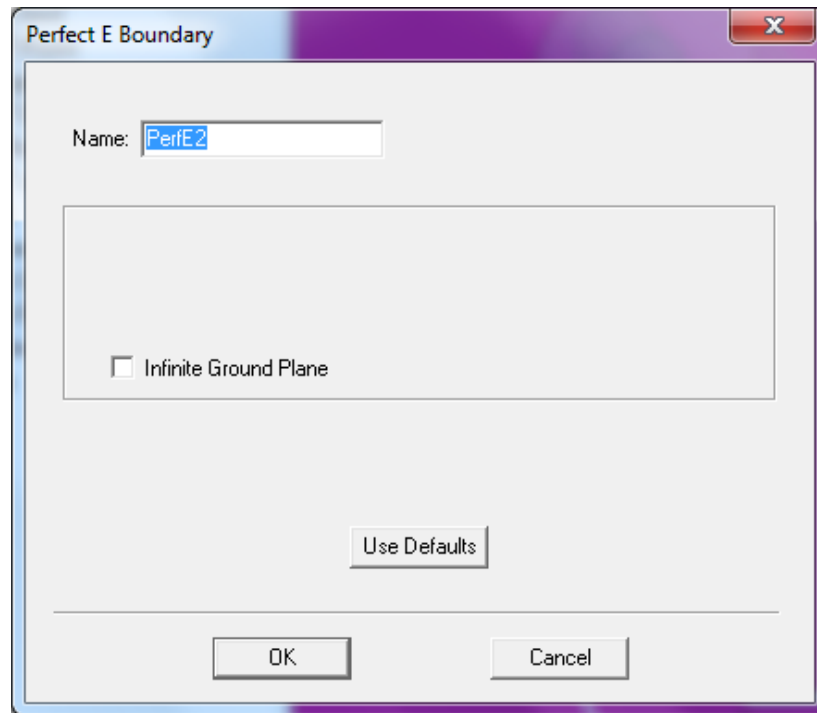


Figure A-48 Define name for Perfect E boundary

Following similar steps described up to now, it is possible to model the whole cylindrical array. The modeled antenna array is shown in Figure A-49.

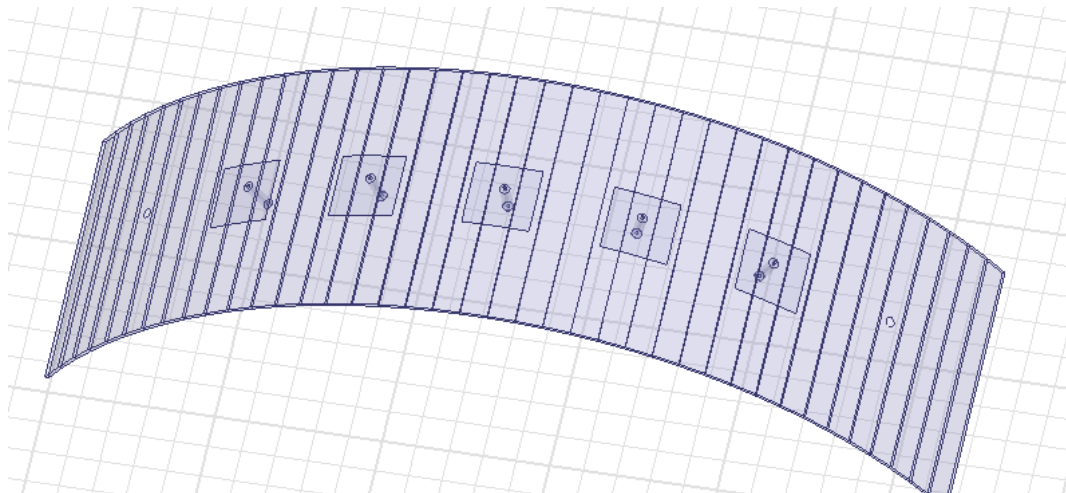


Figure A-49 Modeled 5x1 antenna array

After this step it is necessary to insert a radiation boundary. Radiation boundary should be at least $\lambda_0/4$ away from the radiating elements. It is a rectangular box covering whole antenna. The box should be modeled as air. Then following steps described in Figure A-50 and A-51 radiation boundary for the designed antenna is implemented.

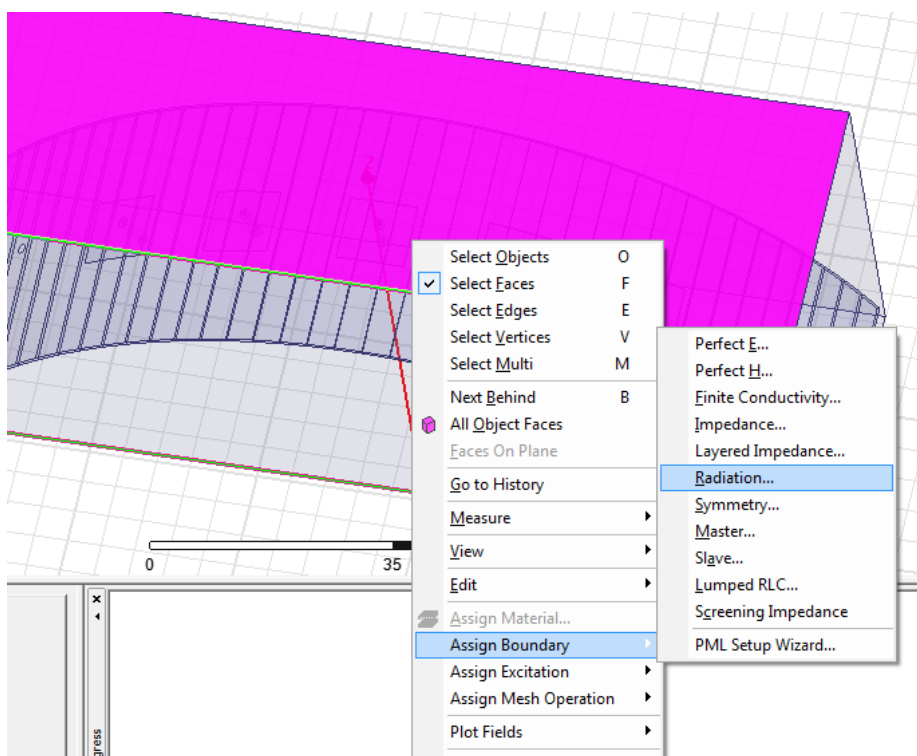


Figure A-50 Assign radiation boundary

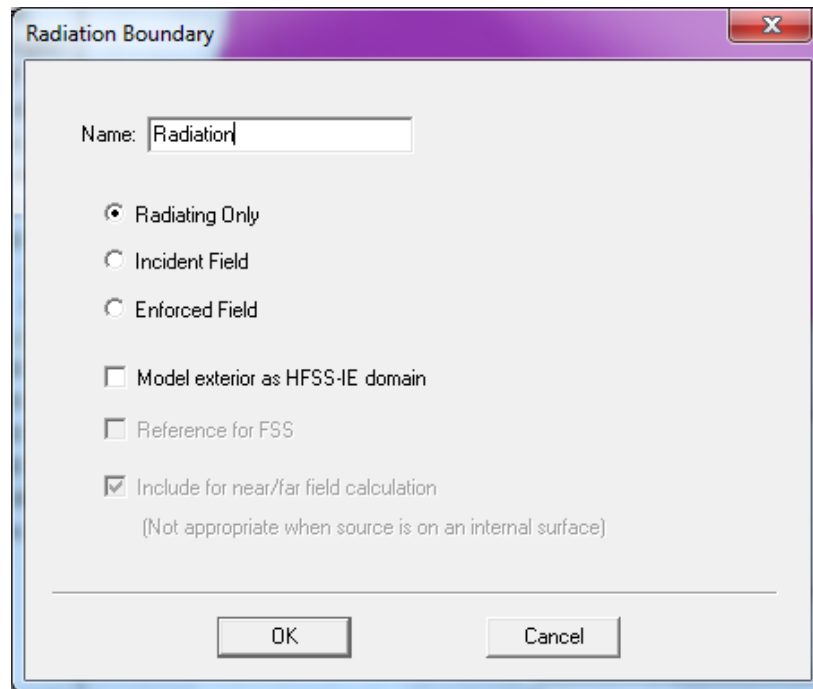


Figure A-51 Define radiation boundary name

To obtain radiation pattern of the antenna array it is necessary to insert Far Field Radiation boundary. As shown in Figure A-52 an infinite sphere can be attached to the predefined radiation boundary.

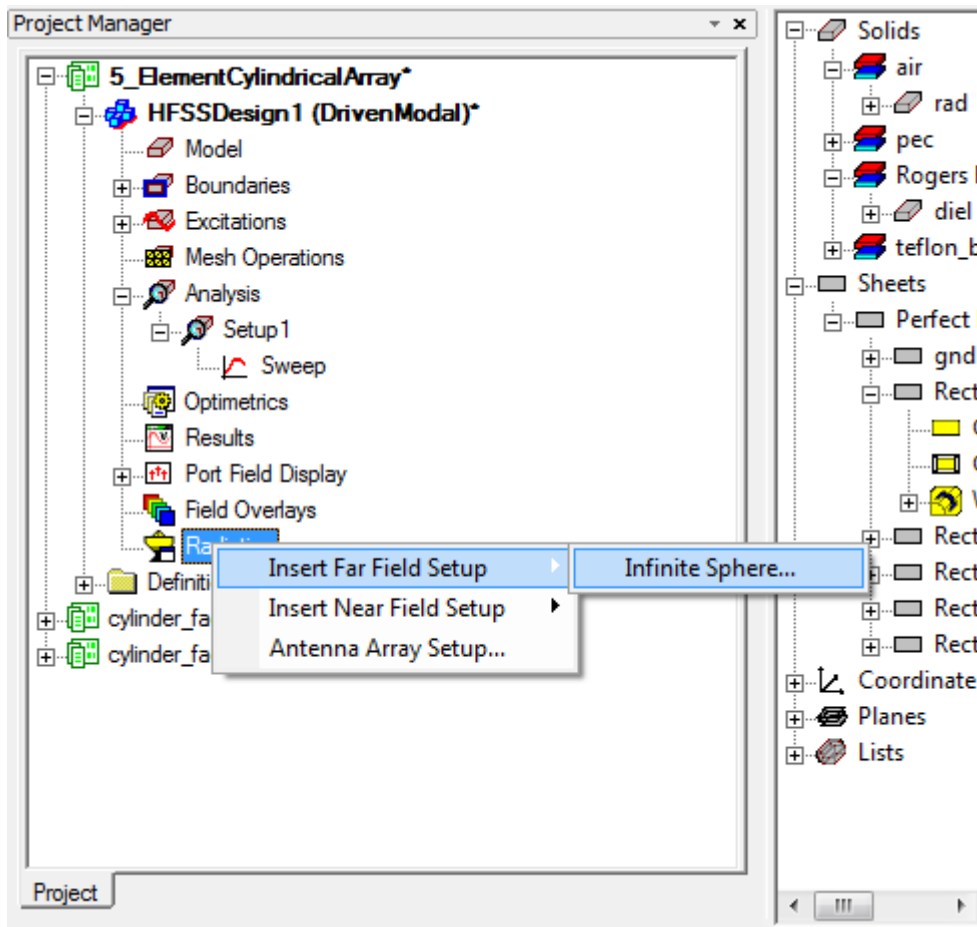


Figure A-52 Insert infinite far field sphere

Using Figure A-53 Phi and Theta values of the infinite sphere can be defined. These two parameters are very important in post HFSS data processing.

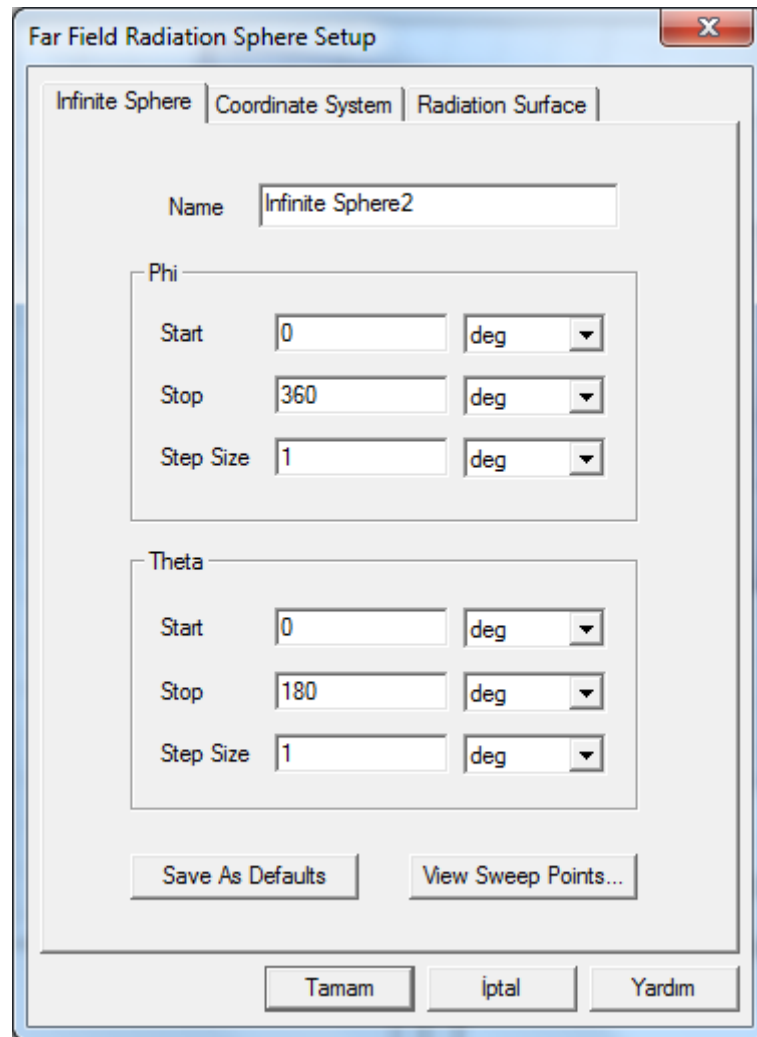


Figure A-53 Define Phi and Theta angles

Figure A-54 is the default state for the Coordinate system of the infinite sphere. In this case the far field data uses Global Coordinate as the phase center.

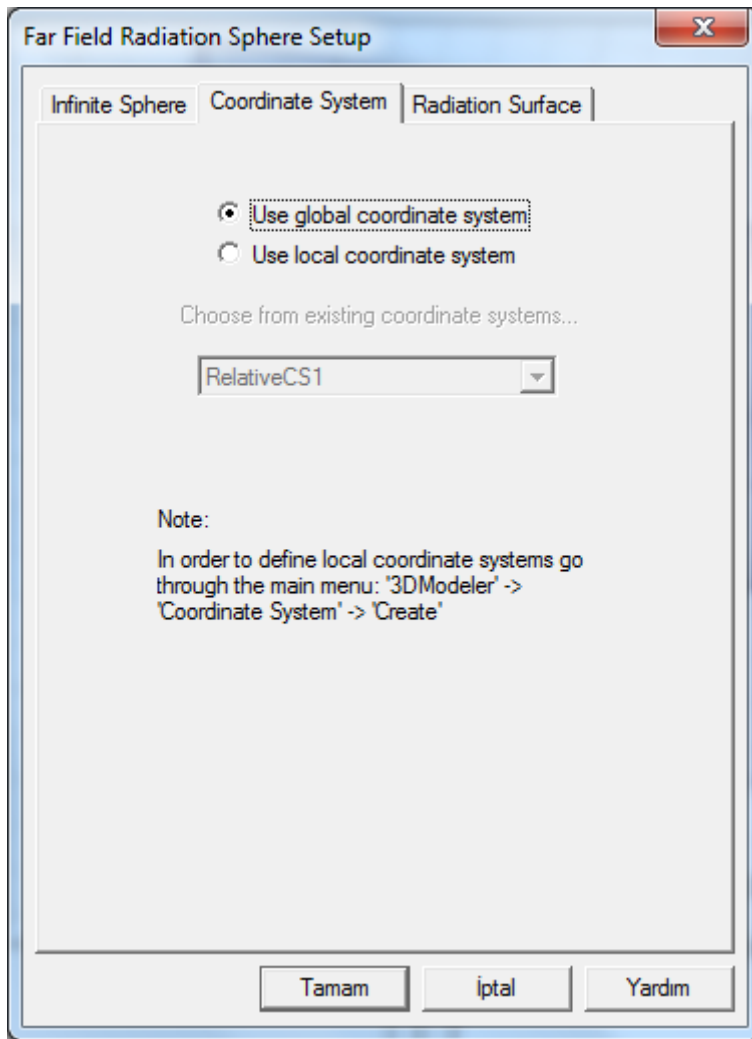


Figure A-54 Define Phi and Theta angles

As shown in Figure A-55 phase center for the infinite sphere can be selected on a different coordinate system. Selecting a symmetric point for the desired antenna element as phase center, it is possible to use the pattern with some manipulations instead of other elements.

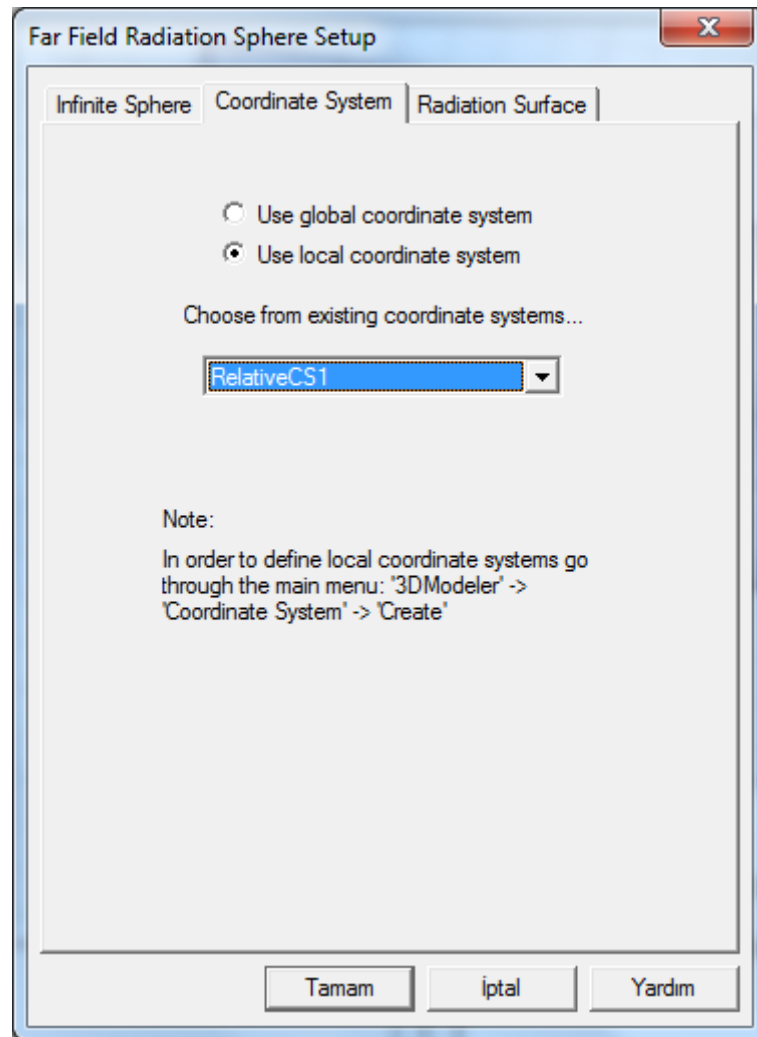


Figure A-55 Select a different Phase center

When the simulation process is completed for the designed antenna array, it is possible to define different excitation coefficient for each antenna element. In this way it is possible to observe beam steering properties of the antenna array without a feed network. This process can be done following steps defined in Figure A-56.

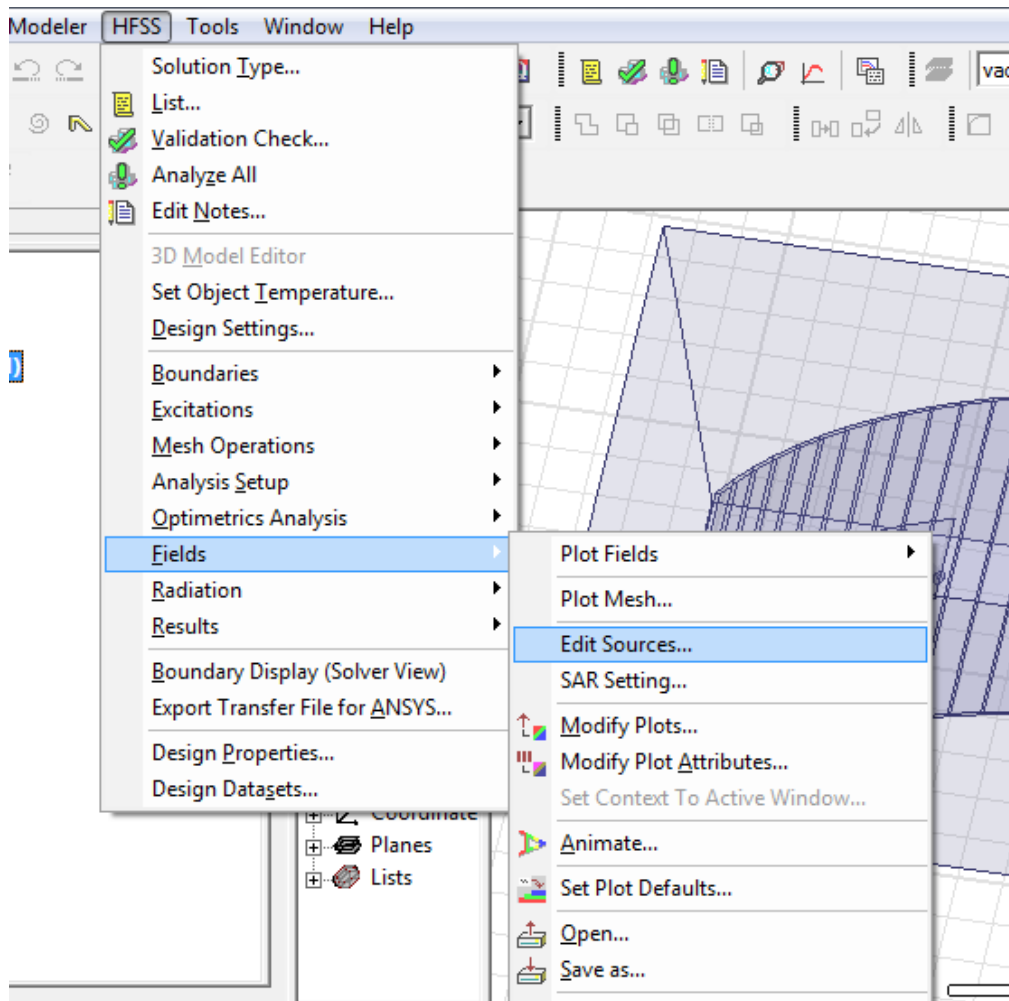


Figure A-56 Edit Sources menu for antenna array

‘Edit Sources’ menu is given in Figure A-57. In this window it is possible to define scaling factor and the offset phase for each element. In this figure antenna pattern is directed to 0° . The amplitude coefficients are selected as unity for all elements in this case.

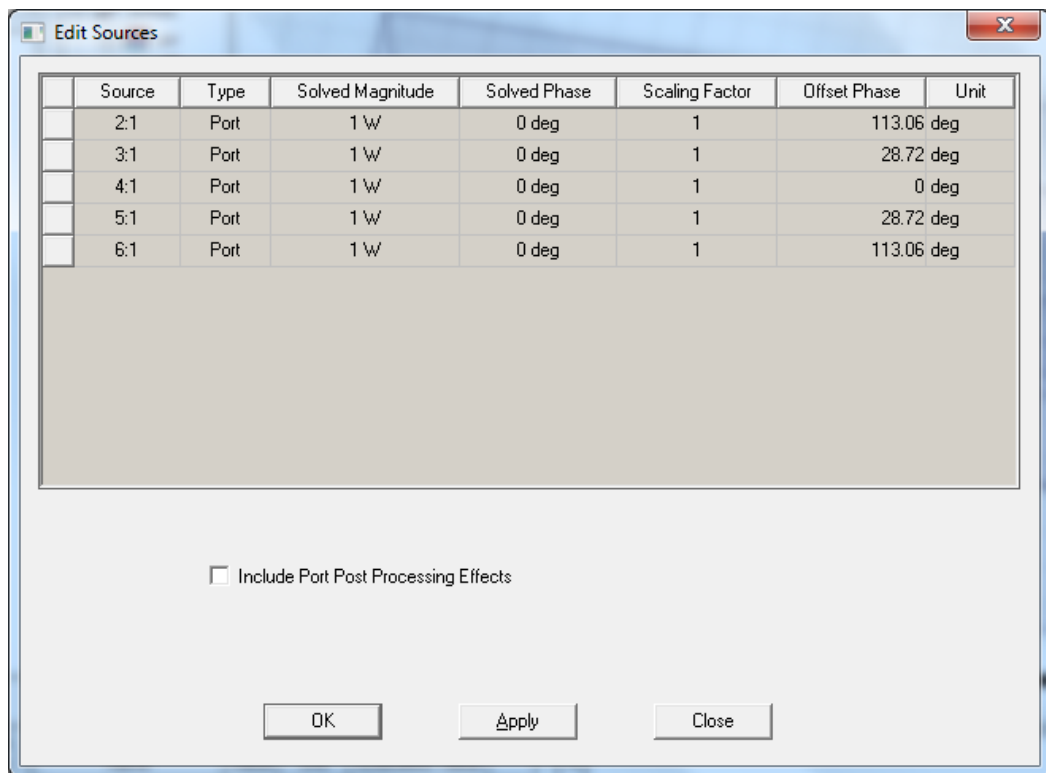


Figure A-57 Edit sources to direct beam to 0°

The solution data can be plotted following Figure A-58, A-59 and A-60. The result report is given in Figure A-61. The complex far field data can also be plotted and exported from the HFSS to use in other numeric calculation programs.

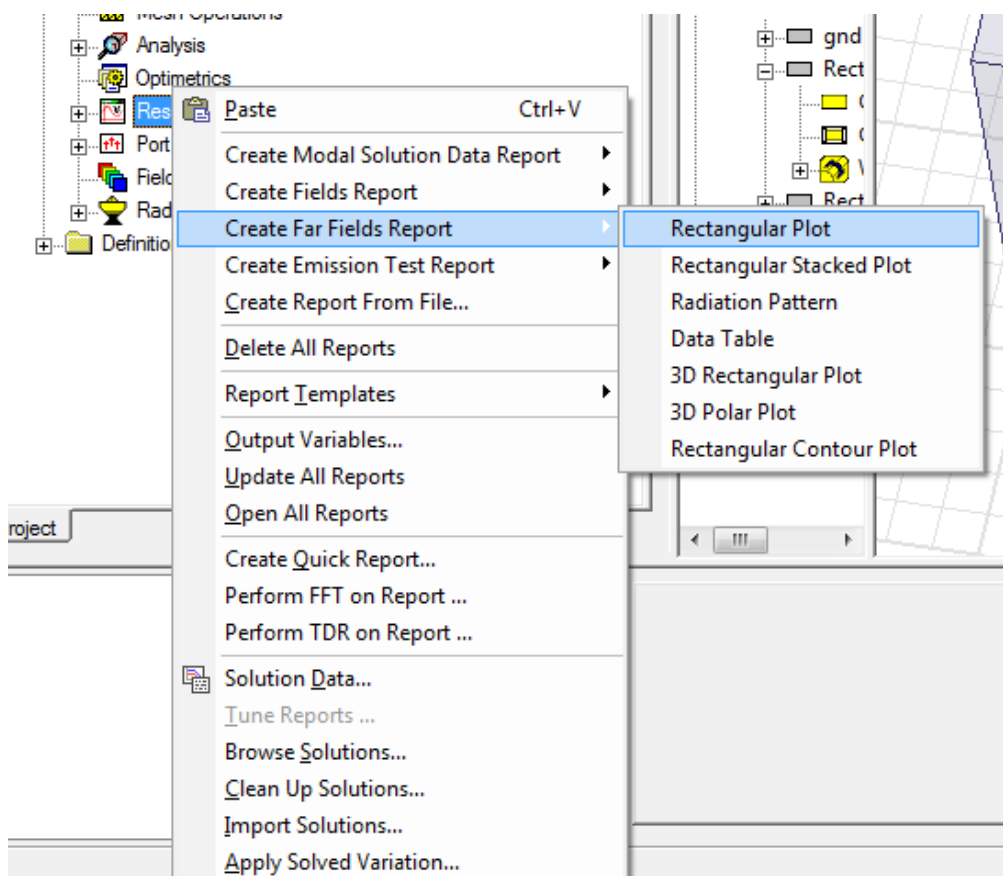


Figure A-58 Create far field data report

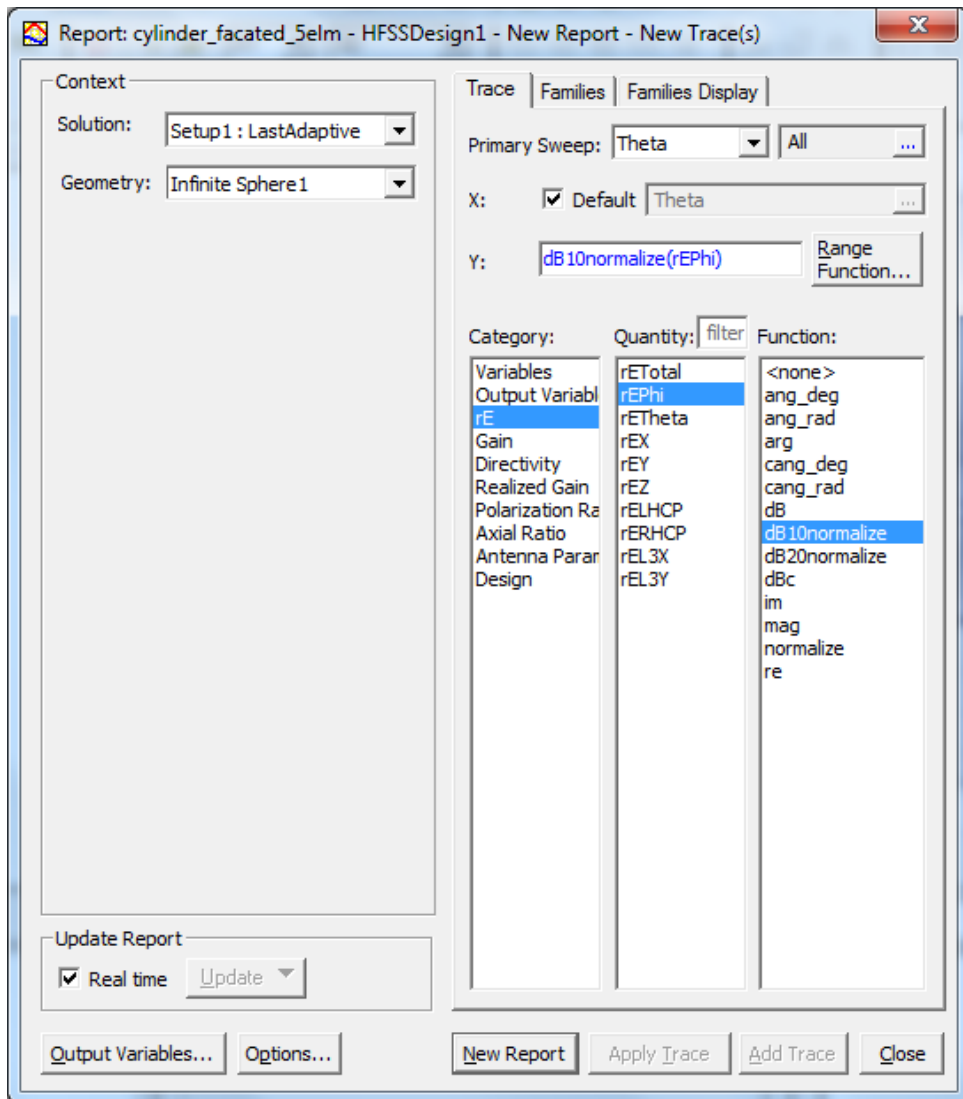


Figure A-59 Select desired plot data type

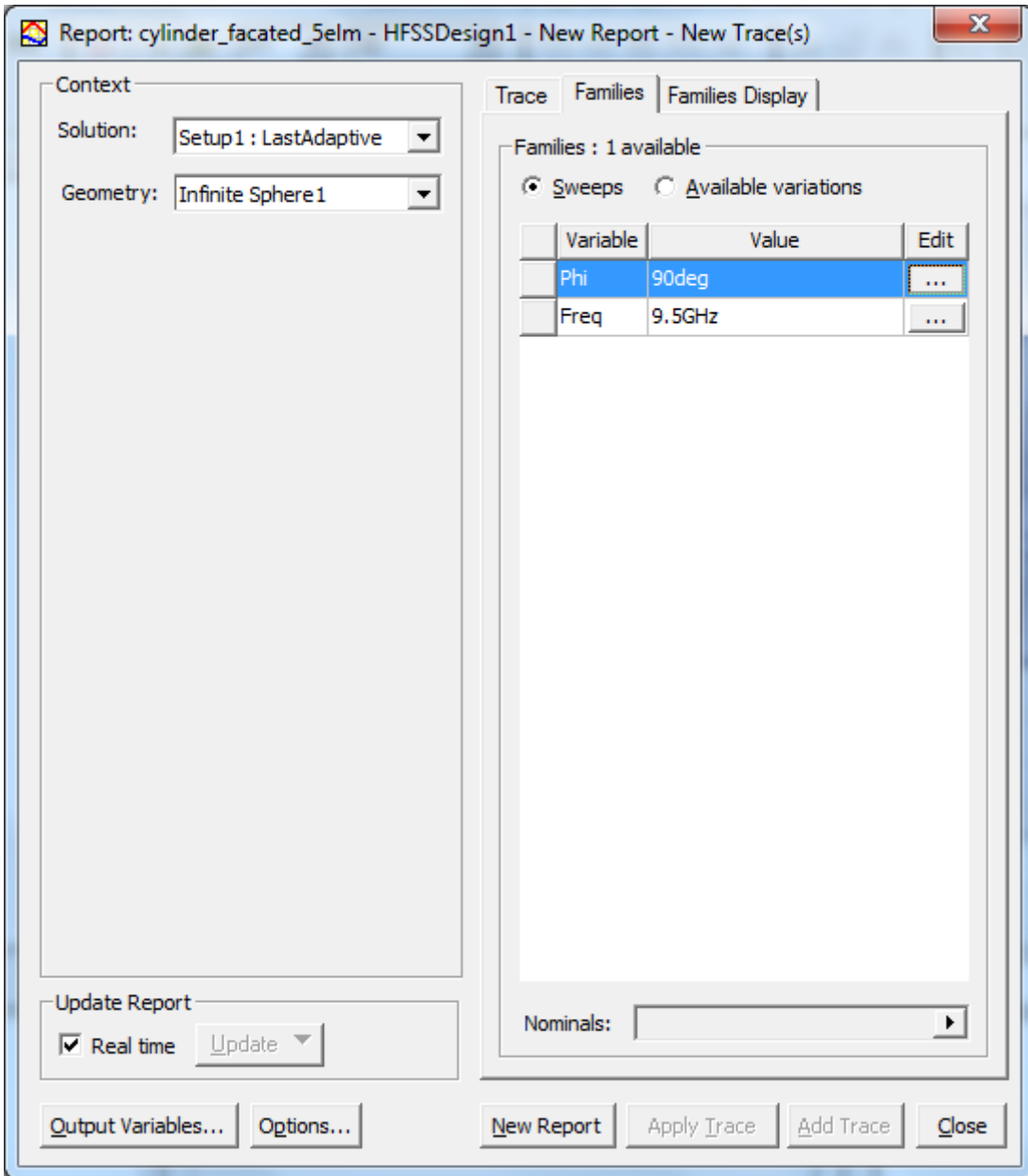


Figure A-60 Select plot axis

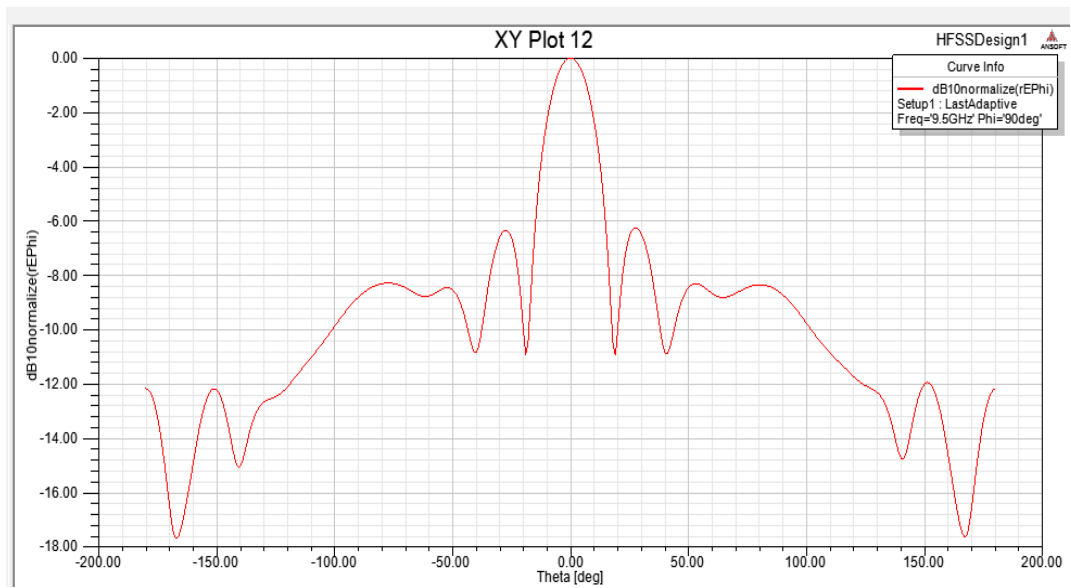


Figure A-61 E_{θ} pattern for the antenna array on $\Theta=90^{\circ}$

Finally, the plotted data can be exported from HFSS like in Figure A-62.

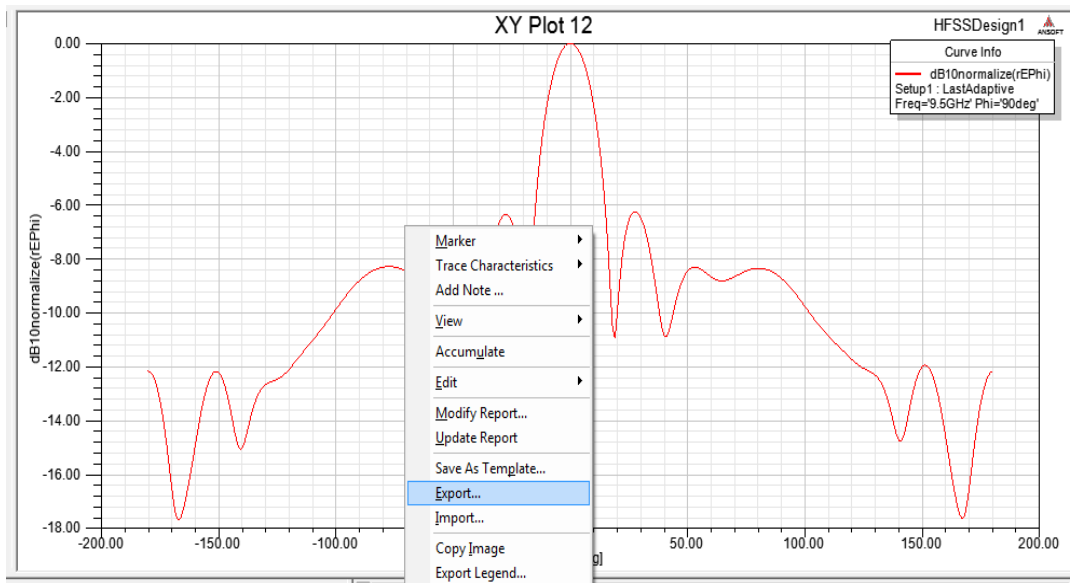


Figure A-62 Export data from HFSS